Diss. ETH Nr. 14352

A GENERAL PROCEDURE FOR THE DESIGN OF CHROMATOGRAPHIC SEPARATIONS

A dissertation submitted to the

SWISS FEDERAL INSTITUTE OF TECHNOLOGY ZÜRICH (ETHZ)

for the degree of

Doctor of Technical Sciences

Presented by

Sebastian Böcker

Diplom-Ingenieur Chemieverfahrenstechnik, Universität Dortmund

born June 17, 1971

Citizen of Germany

Accepted on the recommendation of

Prof. Dr. Massimo Morbidelli, examiner

Prof. Dr. Marco Mazzotti, co-examiner

Zürich 2001

Vorwort

Die vorliegende Arbeit entstand im Rahmen eines Forschungsprojektes zwischen der Novartis Pharma AG und der ETH Zürich zur Untersuchung des Potenzials von chromatographischen Trennverfahren (SMB) für die industrielle Anwendung. Sie wurde am Laboratorium für Technische Chemie der ETH Zürich durchgeführt.

Abstract

The importance of chromatographic separation processes has grown significantly in the last few years, particularly in the pharmaceutical industry. These processes allow to purify or to separate mixtures at different scales, ranging from the few grams of the clinical test phase to the various tons, which may be required at the production scale. Typical example is the separation of racemic mixtures that can be realized using appropriate chiral phases. In order to perform these separation processes efficiently, it is convenient to use continuous chromatography, which in practice is implemented through the relatively new technology of the simulated moving bed (SMB).

In order to reduce the experimental effort and therefore the costs associated with the development of separation processes, simulation models are intensively used. However, due to the high complexity of the phenomena involved in these processes, several parameters appear in these models that cannot be taken from the literature but have to be evaluated specifically for the system under consideration.

One important aspect in this context refers to the adsorption equilibria. In order to achieve high productivities, these processes are typically operated at high concentration values of the mixture to be separated in the feed stream, and therefore in the entire unit. This means that the stationary phase operates close to saturation conditions, where strong interactions among the adsorbed molecules prevail, leading to strong deviations in the adsorption equilibria from the linear or Henry behavior. On the other hand it is known that in order to obtain a reliable model of a chromatographic process, probably the most important condition is that the adsorption equilibrium behavior of the system under consideration should be described accurately enough through a suitable model of the adsorption isotherm. For this we need an adsorption model that on one hand describes the interactions of all components in the mixture and on the other hand takes into account the saturation capacity of the adopted stationary phase. In addition to the adsorption equilibria, the behavior of a chromatographic column is influenced by dissipative phenomena, such as axial dispersion and mass transfer resistances, which lead to a broadening of the concentration profiles along the column. These phenomena have to be carefully accounted for since they are responsible in determining the purities of the produced fractions. This is particularly true for preparative packing materials, which are characterized by large particle diameters so as to allow for large flow-rates industrial operations, with relatively low pressure drops.

The aim of this work is to develop a general procedure to evaluate all the quantities involved in a reliable chromatographic model, which can be used for a fast and reliable optimal design of a separation process at the various scales of its

industrial development. A unique aspect of this analysis is that in developing this general procedure we will account for some constraints, which derive from the industrial practice particularly in the pharmaceutical industry:

1. Only a very little amount of the mixture to be separated is available, and not at all the pure species.
2. All measurements have to be performed on the same packing material, which will be used for the final production process, which is typically of large particle size and therefore exhibit low separation efficiency.
3. The developed procedure has to be general; that is it has to apply to several packing materials as well as to purification and to separation processes.

Under these requirements the classical methods used to measure adsorption equilibria or dispersive parameters cannot be adopted since they require either a high amount of substance to perform the measurements or a high efficiency of the packing material. For example, the classical approach adopted in phase equilibria studies to build a multi-component equilibrium model is based on the idea of first describing the single component equilibria for all the involved chemical species, and then describing the multi-component equilibria by introducing proper interaction parameters among the various components in the same phase. It is clear that such approach cannot be straightforwardly applied here since pure species are typically not available in the early stage of the development of a new drug.

In this work a suitable procedure is developed which satisfies these constraints and is of general validity. In order to validate the procedure, three different separation processes have been considered. These use three different packing materials, and two of them refer to the purification of a drug and one to the separation of a racemic mixture. It is worth mentioning that all the selected examples arise from the industrial practice and have been identified in collaboration with Dr. Schenkel and Dr. Fleury from Novartis, who collaborated to the development of this work.

Zusammenfassung

Chromatographische Trennverfahren haben in den letzten Jahren stetig an Bedeutung gewonnen, insbesondere für die Pharmazeutische Industrie. Derartige Verfahren erlauben es, Stoffsysteme zu trennen oder zu reinigen, die mit herkömmlichen Methoden nicht oder nur schwer aufarbeitet werden können. Zum Beispiel können racematische Gemische, die häufig als Produkt aus Fermentationsprozessen stammen, bei der Verwendung von chiralen Phasen chromatographisch getrennt werden. Um derartige Trennprozesse effizient durchführen zu können, hat sich der SMB- (Simulated Moving Bed) Prozess als ein kontinuierliches Trennverfahren etabliert.

Um den experimentellen und Kosten-Aufwand gering zu halten, werden generell Trennprozesse durch Berechnungen ausgelegt und optimiert. Aufgrund der hohen Komplexität von chromatographischen Trennprozessen, müssen für die Berechnung von solchen Prozessen eine hohe Zahl von Parametern berücksichtigt werden, die nicht oder nur ungenau aus Datenbanken entnommen werden können und stattdessen experimentell ermittelt werden müssen. Aus Produktivitätsgründen wird ein chromatographisches Trennverfahren bei möglichst hohen Konzentrationen des zu trennenden Gemisches im Feed durchgeführt. Gerade in diesem hohen Konzentrationsbereich zeigen die zu trennenden Substanzen häufig nichtlineares Adsorptionsverhalten, d.h. die Adsorption auf der Festphase kann nicht mehr durch den Henrykoeffzienten, der als das Verhältnis der Konzentrationen in der Fest- und Flüssigphase einer Komponente definiert ist, ausreichend genau beschrieben werden, sondern ein Adsorptionsmodell muss angepasst werden, das zum einen die Wechsel-wirkungen aller Komponenten im zu trennenden Gemisch berücksichtigt und zum anderen der Sättigungskonzentration der Adsorptionsstellen auf der Festphase Rechnung trägt. Eine genaue Berechnung von chromatographischen Trennverfahren bei hohen Konzentrationen ist nur möglich, wenn das Adsorptionsverhalten ausreichend genau durch ein geeignetes Adsorptions-isothermenmodell vorhergesagt werden kann. Neben der Adsorption wird das Verhalten auf einer Chromatographiesäule durch dissipative Phänomene, wie axiale Dispersion und Massentransportwiderstände, die zu einer Verbreiterung von Konzentrationsprofilen in der Säule führen, beeinflusst. Speziell auf präparativen Packungsmaterial, das durch weite Partikeldurchmesser charakterisiert ist und das aufgrund des geringen Druckverlustes für Trenn-prozesse im industriellen Massstab zum Einsatz kommt, sind diese Einflüsse stark wirksam.

Chromatographische Trennverfahren können gut berechnet werden, durch die numerische Lösung eines Differentialgleichungssystems, mit dem die Chromato-graphie modelliert werden kann. Die oben genannten Einflussgrössen bilden hierbei die Eingangsparameter für die Simulation eines Trennprozesses.

In dieser Arbeit wird eine generell einsetzbare Auslegungsprozedur vorgestellt, die es erlaubt, schnell und mit geringen Materialverbrauch diese Einflussgrössen systematisch zu bestimmen. Hierbei sind einige Vorgaben von seitens der pharmazeutischen Industrie einzuhalten:

1. Für Experimente steht nur sehr wenig Material des zu trennenden Gemisches und zusätzlich nicht im Reinzustand zur Verfügung, da ein chromatographisches Verfahren zu einem möglichst frühen Zeitpunkt bei der Entwicklung eines neuen pharmazeutischen Wirkstoffes ausgelegt werden soll.

2. Um möglichst reale Daten zu erhalten, werden die Experimente auf dem Originalpackungsmaterial, das für den späteren Produktionsprozess verwendet wird und sich durch eine geringe Effizienz auszeichnet, durchgeführt.

3. Die zu entwickelnde Prozedur soll generell einsetzbar sein, d.h. für verschiedene Packungsmaterialien, als auch für unterschiedliche Trennfälle, von Reingungs- bis Trennprozesse.

Kernpunkt der Auslegungsprozedur ist die Bestimmung der Adsorptionsisothermen des zu trennenden Gemisches.

Durch die oben erwähnten Einschränkungen scheiden generell klassische Messmethoden aus, da sie zum einen eine grosse Substanzmenge und/oder eine hohe Effizienz des Packungsmaterials verlangen. In dieser Arbeit wird die Peak-Fitting-Methode zur Bestimmung der Adsorptionsisothermen verwendet. Diese Methode basiert im wesentlichen auf der Anpassung der freien Parameter eines geeigneten Adsorptionsmodells an überladene Peakprofile, indem diese durch numerische Lösung eines Chromatographiemodells simuliert werden. Diese Peakprofile, die als Antwort auf eine Injektion mit hoher Konzentration und Volumen des zu trennenden Gemisches am Säulenausgang detektiert werden, sind dann aufgrund des nichtlinearen Adsorptionsverhaltens für den Fall eines konvexen Isothermenverlaufes durch ein Fronting und Tailing charakterisiert. Nachdem dissipative Einflussgrössen und die Henrykoeffizienten aller Komponenten im Gemisch bereits im stark verdünnten Bereich gemessen worden sind, kann jetzt das nichtlineare Adsorptionsverhalten bei hohen Konzentrationen genauer durch die Peak-Fitting-Methode untersucht werden.

Die Auslegungsprozedur wurde an konkreten Trennbeispielen aus der pharmazeutischen Industrie entwickelt, um ihre generelle Einsetzbarkeit zu demonstrieren. Diese Beispiele sind in der industruiellen Praxis aufgetreten und in Zusammenarbeit mit Dr.Schenkel und Dr. Fleury von der Novartis Pharma AG ausgewählt worden. Für diese Trennfälle sind häufig verwendete Packungsmaterialien wie Reversed-Phase, Silikagel und Chiralphase eingesetzt worden, zudem unterschiedliche Konstellationen in der Zusammensetzung des zu trennenden Gemisches wie z.B. Reinigungschritte mit einem geringen Anteil der Nebenkomponenten und Trennschritte mit einem hohen Anteil der unerwünschten Komponenten betrachtet worden.

Contents

1. Development of Chromatographic Processes for the Pharmaceutical Industry

1.1 Introduction

The scale-up and optimization of chromatographic separation processes (batch, SMB or recycle) are most conveniently performed through simulations based on suitable mathematical models. These properly account for the nonlinear adsorption equilibria, which determine the inter-phase partitioning of the various mixture components, in addition to the dissipative phenomena due to axial dispersion and mass transfer resistances. The reliability of these models is determined by the accuracy in describing such equilibrium and kinetic processes. In this thesis we develop a general procedure [1] to evaluate the parameters needed to describe such phenomena. Our focus is on systems of interest in the pharmaceutical industry, particularly at the early stage of the development of a new drug. This implies that a few constraints have to be accounted for, in addition to the fact that the procedure has to satisfy convenient compromises between accuracy and time requirement. These include a very limited amount of test material and mostly in the form of a mixture and not pure components, the need of using the same packing material as the industrial chromatographic process, which is in general characterized by a low efficiency, at least compared to analytical packings, and the problem of dealing with multi-component mixtures with widely different adsorptivita and concentration.

We concentrate specifically on the determination of the adsorption isotherms, since these are by far the most important in determining the performance of a chromatographic separation at high concentrations. Several experimental procedures to measure adsorption equilibria are described in the literature [2,3]. The constraints described above prevent the utilization of the classical methods for measuring multi-component equilibria. In this work we use the peak fitting method [4,5], whereby the parameters of a predefined equilibrium isotherm are estimated by fitting directly the composition values at the outlet of an analytical column packed with preparative packing material and fed with a pulse of the mixture to be separated, and operated in the isocratic elution mode. During the first screening phases, a single experiment is sufficient for a first estimation of the adsorption isotherm in a multi-component mixture. By increasing the number of experiments in a later stage of the product development process, the precision of the model can be improved.

The experimental peak profiles are simulated using a detailed column model, which requires the correct knowledge of various parameters, which affect the column behavior. These involve the stationary phase porosities, axial dispersion and mass transfer parameters. Each of these has to be estimated carefully before estimating the equilibrium parameters, since any error in these parameters would lead to a corresponding error in the equilibrium parameters.

We tested the developed general design procedure with three chromatographic separation processes, which cover the various types of situations that may arise in the applications. These include three different stationary phases: silica gel, reversed phase and a chiral phase.

1.2 The general design procedure

The mathematical model of a chromatographic column is constituted of the mass balances of the involved components in the fluid and in the stationary phase. The model used in this work distinguishes between axial dispersion and mass transfer resistances. The first one describes the flow anisotropy outside the particles, whereas the mass transfer coefficient is a "lumped" coefficient, accounting for all the individual resistances between the adsorption sites and the fluid bulk. This so-called pore diffusion model [6] is then given by the following differential equations:

$$\varepsilon_b \frac{\partial c_i}{\partial t} + (1 - \varepsilon_b)\varepsilon_p \frac{\partial c_i^p}{\partial t} + (1 - \varepsilon_b)(1 - \varepsilon_p)\frac{\partial q_i}{\partial t} + u\frac{\partial c_i}{\partial x} = \varepsilon_b D_{ax,i} \frac{\partial^2 c_i}{\partial x^2} \qquad (1.1)$$

$$\varepsilon_p \frac{\partial c_i^p}{\partial t} + (1 - \varepsilon_p)\frac{\partial q_i}{\partial t} = k_{m,i}\left(c_i - c_i^p\right) \qquad (1.2)$$

in which c, c_p and q represent the concentrations in the liquid, pore and solid phase, respectively, D_{ax} is the axial dispersion coefficient and k_m the lumped mass transfer coefficient.

The model is completed by the adsorption equilibrium model, relating the concentrations in the solid and in the pore phase, thus assuming equilibrium conditions between the pore and adsorbed phase at any time and location along the column. The above model equations are solved numerically using the routine DDASSL from the IMSL library [7].

As mentioned above, the key of the success of the developed procedure is the accurate evaluation of all the parameters involved in the model equations above. An effective and systematic procedure for this distinguishes between preliminary measurements at low concentrations, and subsequent overloaded experiments

aimed at the determination of the nonlinear, competitive portion of the adsorption equilibria for all the components of the mixture to be separated. In particular the following steps constituting the general design procedure are identified:

Diluted experiments:

1. Measurement of external and total porosity of the packing.
2. Measurement of the Henry coefficient of each component.
3. Measurement of the van-Deemter plot and evaluation of axial dispersion and mass transfer coefficients.

Overloaded experiments:

4. Development of a series of chromatographic pulse experiments with increasing loading.
5. Estimation of the remaining parameters of the adsorption isotherm through the peak fitting method.

As mentioned above, the developed procedure has to satisfy a number of limitations. In particular, due to the availability of only small amounts of the mixtures to be separated and no pure components, we have to operate with very small amounts of stationary phase, i.e. with analytical columns. Therefore, since we need to operate directly with preparative stationary phases, we perform all the experiments described in the following using columns with analytical dimensions but filled with preparative packing material, identical to that used in the later production process. Such stationary phases are characterized by particle diameters about one order of magnitude larger than those of analytical stationary phases, and therefore exhibit much lower efficiencies. The consequence is that often no complete resolution of the peaks of the various components of the mixture to be separated is obtained, and this poses specific problems to the evaluation of the relevant parameters, which are addressed in the following chapters, where we analyze in detail each of the steps above with reference to typical industrial separation problems. These have been selected in order to cover the entire spectrum of possible situations and include: one separation on silica gel, one on reversed phase, as well as a separation problem of a racemic mixture on a chiral phase.

1.3 Porosity of the packed column

The total porosity is defined as the ratio between the fluid phase volume in the packed column and its total volume and can be estimated from the retention time of an inert tracer as follows:

$$\varepsilon = t_{r,tracer} \, Q \, / \, V \qquad\qquad (1.3)$$

in which Q is the volumetric flow-rate and V the total column volume.

The total porosity can be distinguished in the interparticle, ε_b, and intraparticle, ε_p, porosity, depending on whether the fluid inside or outside the particle pores, respectively, is constituted as fluid volume. These are related to the total porosity through the following equation:

$$\varepsilon = \varepsilon_b + (1\text{-}\varepsilon_b) \, \varepsilon_p \qquad\qquad (1.4)$$

In general, the total porosity can be measured with a small injection of a substance, which does not interact with the adsorption sites, using Eq.1.3. For example, the total porosity of a silica gel packing characterized by a polar surface can be conveniently measured using a non-polar species as tracer, as for example toluene (see chapter 3 section2). The situation is more complicated in the case of reversed phase, where the non-polar ligands do not completely cover the adsorbent surface and therefore leave some SiOH groups free. Accordingly, the surface exhibits portions with polar and portions with non-polar character, which make difficult the selection of a species, which does not adsorb on neither of them. In this case, as discussed in chapter 2, the total porosity can be measured using as a tracer the species to be separated itself, but saturating the column with a more adsorbable eluent. This technique offers the additional advantage of measuring only the volume of the pores, which are accessible to the substance to be separated. On a chiral phase, as reported in a later chapter (see chapter 4), the porosity could be measured by equilibrating first the stationary phase at a composition of the binary eluent system of a mixture with 50/50 v/v% and then by injecting a very small pure amount of the non-polar fraction of the eluent system. As a criterion to check whether or not the tracer adsorbs on the surface of the stationary phase, its retention time can be measured at increasing temperature values, so as to change the adsorption equilibrium and therefore detect the presence of significant tracer adsorption.

Also the interparticle porosity is measured using a pulse tracer technique, but now the tracer should be a chemical species sufficiently large not to enter the pores of the stationary phase. Relatively large non-polar substances such as sugars or polymers are typically used for normal silica gel phases. On the reversed phase the situation is again more difficult, since non-polar species interact with the non-polar portions of the external surface of the particle. In this

case it is convenient to use the "ion exclusion" effect, since ionic substances are excluded from the pores due to the electrostatic interactions.

1.4 Henry coefficients of the main- and the undesired products

The Henry coefficient, H, represents the slope of the adsorption of a pure component at infinite dilution. This can be determined for each component of the mixture to be separated by injecting a very small amount of the mixture in the column and allowing for complete resolution of the peaks of all components i so as to measure the corresponding retention time $t_{r,i}$. The Henry coefficient H_i is then calculated as follows:

$$H_i = \frac{t_{r,i} - t_0}{t_0} \frac{\varepsilon}{1-\varepsilon} \tag{1.5}$$

However, the identification of the single peaks corresponding to each component of the mixture to be separated can be difficult since, as discussed above, in the frame of this procedure we use analytical columns packed with preparative material, which are characterized by poor efficiency and lead to bad resolution of the single peaks. In addition, in purification processes the impurities to be separated are present in such smaller amount with respect to the main products, but exhibit so similar adsorptivity that their chromatographic peaks are completely covered by those of the main products. In this case, while the estimation of the Henry coefficient of the main component is straightforward, that of the impurities becomes impossible.

The sequence of actions to be taken in order to measure the Henry coefficients of all involved components is described in the following, as it can be seen in Fig.1.1.

Decrease flowrate to achieve complete resolution

Complete resolution on the preparative stationary phase?

No

Yes

Complete resolution is achieved?

Estimation of Henry coefficients from the peak retention time

Yes

No

Corresponding analytical stationary phase available?

Yes

No

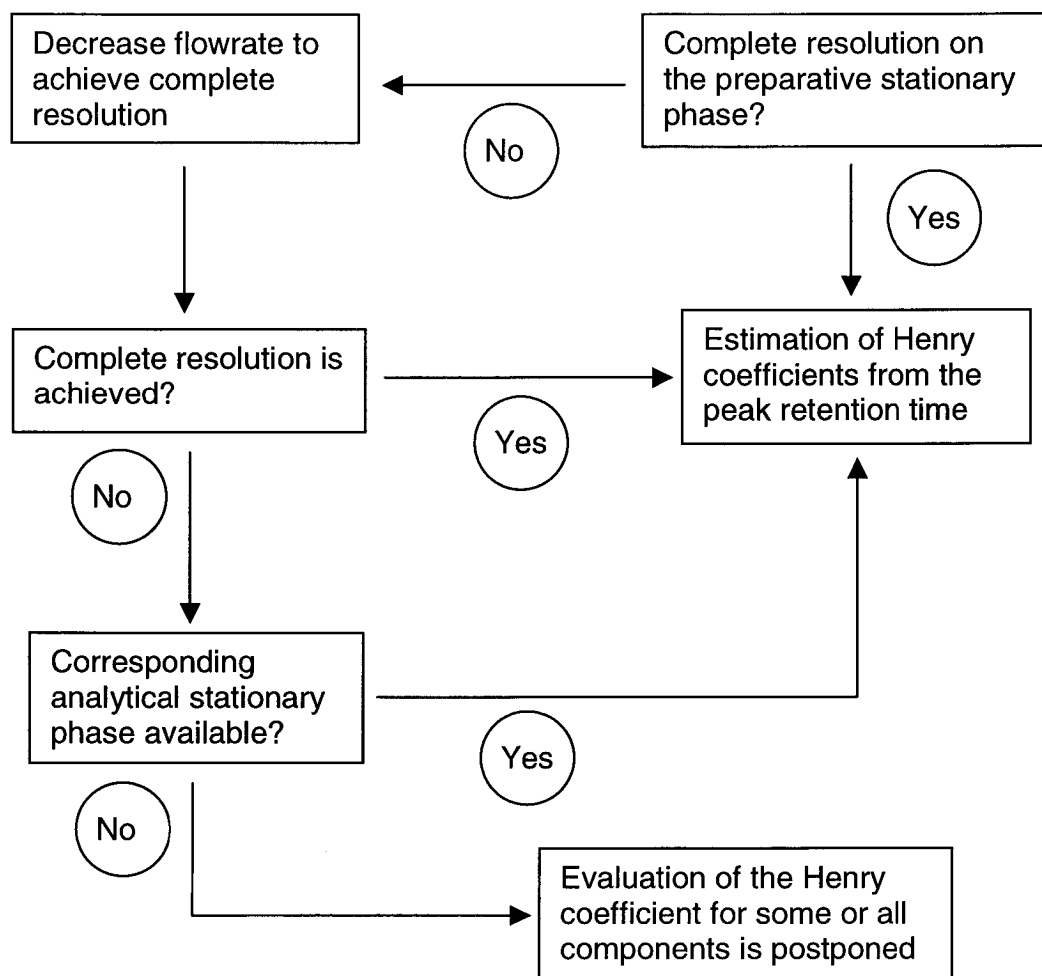Evaluation of the Henry coefficient for some or all components is postponed

Fig. 1.1: Overview scheme for the measurement of the Henry coefficients

In the case where no complete resolution is achieved, the operating conditions of the chromatographic run should be optimized in order to increase the efficiency of the column. For example by properly decreasing the feed flow-rate, it is often possible to increase the number of theoretical plates so that the resolution of all components is achieved.

If this is not sufficient, one can use the corresponding analytical stationary phase, which would definitely allow complete resolution. However, care must be taken in selecting the analytical stationary phase, since this should differ from the preparative one only in the particle size, and therefore in separation efficiency, but not in the chemical composition so as to guarantee that the Henry coefficient is the same. In the case of purification processes mentioned above, a good check can be obtained by comparing the Henry coefficients of the main component measured on the two phases.

If such an analytical phase is not available, then the evaluation of the Henry coefficients has to be postponed to a later step in the general procedure. This is

actually the last step of the procedure indicated in section 2 and corresponds to the determination of the adsorption isotherms through the peak fitting method, where also the Henry coefficients will have to be considered as free parameters to be fitted.

1.5 Dissipative phenomena

As seen from the model equations in section 2, the dissipative phenomena are described in terms of axial dispersion and mass transfer resistance between the bulk and the solid phase. Typically, the axial dispersion coefficient D_{ax} and the mass transfer coefficient k_m are evaluated through the van-Deemter plot [8], which represents the HETP (height equivalent to a theoretical plate) as a function of the superficial velocity:

$$\text{HETP} = \frac{2\varepsilon_b D_{ax}}{u} + \frac{2u}{1-\varepsilon_b}\left[1+\frac{\varepsilon_b}{K_i(1-\varepsilon_b)}\right]^{-2}\frac{1}{k_{m,i}} \tag{1.6}$$

with $K_i=\varepsilon_p+(1-\varepsilon_p)H_i$ and $D_{ax}=\gamma D_m+\beta u d_p$ [9].

The HETP is evaluated from the same outlet concentration profiles obtained by feeding a pulse of the mixture to be separated, that we have used in the previous section to estimate the Henry coefficients, using the following equation [10]:

$$\text{HETP} = L / (5.54 (t_r / w_{0.5})^2) \tag{1.7}$$

in which $w_{0.5}$ is the peak width at half height of the peak concentration and t_r its retention time.

At high flow-rates, which are of industrial interest since imply a high productivity, molecular diffusion can be neglected compared to that of eddy diffusion and the van-Deemter plot reduces to a straight line as in the example shown in Fig.1.2. From a linear regression of these data with Eq.1.6, the axial dispersion coefficient can be calculated from the intercept with the y-axis and the mass transfer coefficient from the slope.
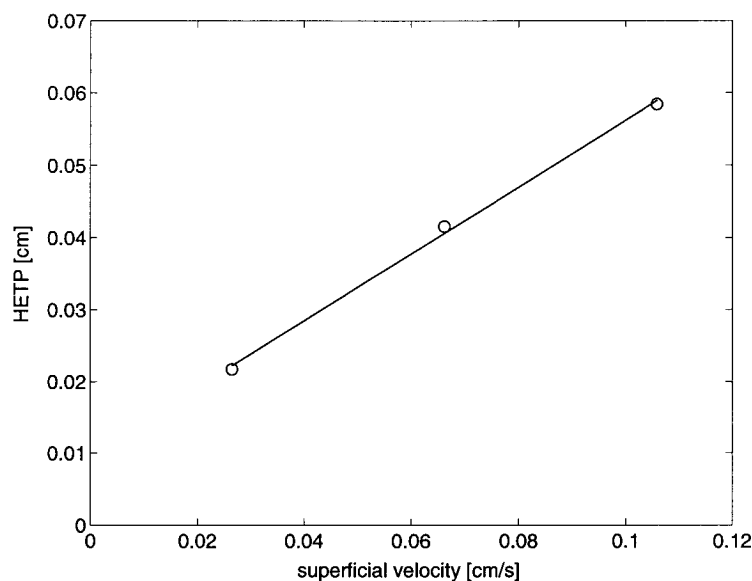
Fig. 1.2: Van-Deemter plot of a pharmaceutical substance on preparative reversed phase.

1.6 Determination of the adsorption isotherms: The peak fitting method

In the frame of the peak fitting method, the free parameters of a pre-defined adsorption isotherm are estimated by fitting directly the experimental peak profiles. In general, the linear portion of the isotherm described through the Henry coefficient has already been measured as described in section 4, at least for the main component, and therefore we can focus here on the nonlinear portion of the isotherm, which is determined by the competitive adsorption of all the species in the mixture. Fig.1.3 shows the linear and non-linear portion of a typical competitive Langmuir isotherm for a two-component system. Here the complete adsorption isotherm can be described by Eq.1.8 for component1:

$$q_1 = \frac{H_1 c_1}{1 + \dfrac{H_1 c_1}{q_1^s} + \dfrac{H_2 c_2}{q_2^s}} \qquad (1.8)$$

With increasing concentration in the fluid phase the adsorption behavior is strongly influenced by the saturation capacity of the stationary phase. In the case of a two-component mixture the two saturation capacities q_1^s and q_2^s are the free parameters to be fitted by the peak fitting method.
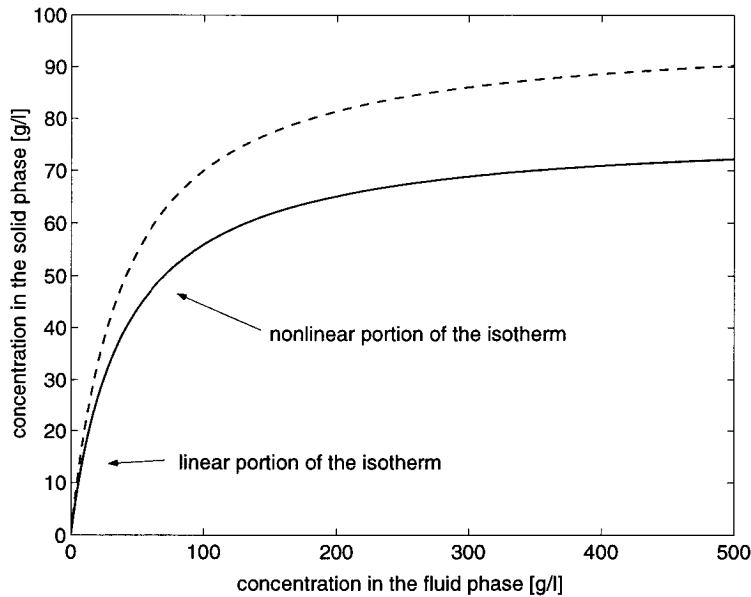
Fig. 1.3: Competitive Langmuir isotherms for a two-component mixture. Henry constants: component1: 2, component2: 2.5, saturation capacity: 175 g/l, isotherms: (—) component1, (--) component2, (..) linear portion of the isotherms, (-·-) non-linear portion of the isotherm

For this we have to feed to the column a sufficiently large pulse with a high concentration of the mixture to be separated, so that the corresponding pulse response at the column outlet exhibits the typical nonlinear adsorption behavior. From the characteristics of such an overloaded peak profile the required information about the adsorption behavior of all components in the mixture are obtained and the adsorption isotherm is estimated.

The chromatographic model used for the simulation of the peak profiles must be sufficiently accurate, since all possible errors eventually reflect on the estimated isotherm. In particular, we use the lumped pore diffusion model described in section 1.2, with parameter values obtained as described in the previous sections of this work.

On the other hand in order to get the experimental outlet peaks we need to measure the concentrations of all components in the mixture as a function of time at the column outlet. Typically this is done using a single online UV-detector, which is part of the HPLC station and measures the total concentration values. Of course this requires that complete resolution of all components is achieved in the column. As already discussed in a previous section, often this is not the case, particularly when using preparative packing material and operating under overloaded conditions. This difficulty can be overcome by collecting many fractions of the overloaded peak profile at the column outlet stream in time and by analyzing them off-line using some suitable analytical technique. Such a fraction collection technique allows to "reconstruct" the peak profiles of all components, including impurities present in low concentrations, with sufficient accuracy and has been applied to all separation cases considered in this work.

2. Design of Chromatographic Separations on Reversed Phase

2.1 The model separation problem

Drug therapy for the major inflammatory skin diseases, which includes atopic dermatitis, psoriasis and allergic contact dermatitis, is often inadequate due to poor efficacy, toxicity, or both. Much research has focused on the macrolactam T cell inhibitors as a promising new class of agents for immunotherapy, and medicinal chemistry efforts to design novel ascomycin analogues have produced clinically promising agents. One example is the ascomycin derivative shown in Fig.2.1, which will be referred to as AD in this work. Several undesired products are formed in the manufacture of AD. In particular, the synthesis of AD produces among others the 9-epimer of AD shown in Fig.2.2 and referred to in the following as 9-EPI. AD and 9-EPI are diastereoisomers, differing only for the inversion of the ethyl-group in position 9. On the other hand two non-polar ascomycin analogues produced in the fermentation process are converted to non-polar structurally closely related homologues of AD, referred to as NP1 and NP2. In the following we illustrate the procedure for the determination of the multicomponent adsorption isotherms with reference to the two chromatographic processes used to separate such undesired products from AD [11,12].
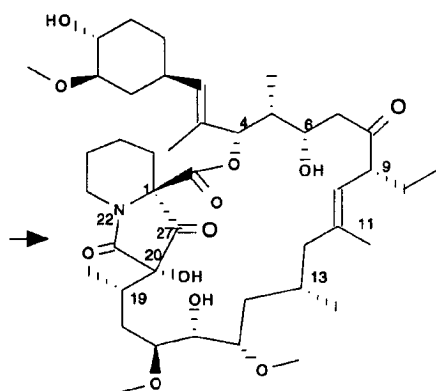

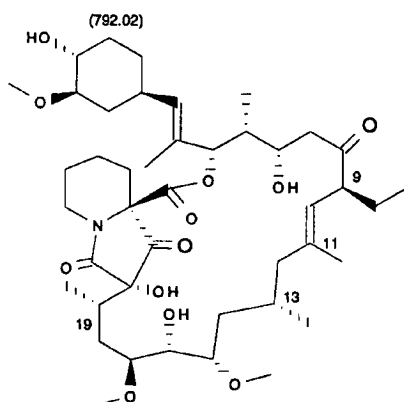Fig. 2.1: Structural formula of AD, $C_{43}H_{69}NO_{12}$, MW=792.02 g/mol

Fig. 2.2: Structural formula of 9-EPI, i.e. the 9-epimer of AD

The first one is actually a purification process involving a ternary mixture, where the mass fraction of AD is 96% while that of NP1 and NP2 is only 2%. The second is a binary separation process since the mass fraction of AD is 70% and that of 9-EPI is 30%. In both processes the reversed phase preparative packing material MN RP C18 (Macherey-Nagel, Germany) has been used. At 25 °C the by-products NP1 and NP2 exhibit a selectivity with respect to AD equal to 1.24 and 1.46, respectively, while for 9-EPI this is equal to 1.14. The packing is characterized by a pore width of 120 Å and a particle diameter of 30 μm. The surface is partially covered with a C18 ligand leaving about 10% of the SiOH groups free. The used column is 250 mm long and has a diameter of 4 mm. All experiments have been carried out on a HP 1090 HPLC station. The eluent is composed of a methanol/water mixture with 80/20 v/v%.

2.2 Total porosity of the packed column

In principle, the porosity is determined as described in section 1.3. Here the problem in practice is to identify an inert tracer, i.e. a chemical species, which does not adsorb on the stationary phase, since even a small adsorptivity would lead to significant errors in the determination of the porosity. It is common practice to select a tracer with opposite polarity as the stationary phase under examination. For example, in the case of normal phase silica gel, the use of non-polar species such as heptane or hexane is appropriate due to their strong repulsion with the SiOH groups covering the adsorbent surface. The situation is more complicated in the case of the reversed phase considered in this work, since the C18 ligands do not cover completely the adsorbent surface thus leaving some free SiOH groups. Therefore, the surface exhibits portions with polar and portions with non-polar character, which make difficult the selection of a species, which does not adsorb in either one of them. Another important aspect in selecting a suitable tracer arises from the complex nature of the intraparticle

porosity structure of the stationary phase, which makes it difficult to determine the smallest pore dimension that should be accounted for in the intraparticle porosity. A practical answer to this question, particularly valuable when considering large molecules such as those typically of interest in the pharmaceutical industry, is that the intraparticle porosity to be considered is the one accessible to the molecules to be separated in the particular system under examination. With this respect the best tracer would obviously be the species to be separated, i.e. AD in the case considered in this work.

Based on the above considerations we can now proceed to consider the pulse tracer experiments, which provide an accurate estimate of the total porosity. According to the solvophobic theory [13,14], the interaction between the ligand and the solute, i. e. the tracer, can be controlled by changing the polar character of the eluent. For example, using an eluent with increasing polarity would increase the adsorptivity of non-polar solutes on non-polar surfaces. Accordingly, by using non-polar solutes and eluents on a reversed phase stationary phase we can minimize the interaction of the solute with the polar portion of the surface. On the other hand, both solute and eluent compete for adsorbing on the non-polar portion. This can be described using the competitive Langmuir isotherm as follows:

$$q_s = \frac{q_s^s K_s c_s}{1 + K_s c_s + K_e c_e} \; ; \; K_i = \frac{H_i}{q_i^s} \qquad (2.1)$$

in which the subscripts s and e refer to the solute and the eluent, respectively, while the superscript s indicates saturation conditions. If we are in the situation where solute and eluent have comparable adsorptivity, since the concentration of the eluent is obviously much larger, it follows that $K_e c_e \gg K_s c_s$, so that Eq.2.1 reduces to:

$$q_s = \frac{q_s^s K_s}{1 + K_e c_e} c_s = H_s^* c_s \qquad (2.2)$$

in which H_s^* is a constant representing the Henry constant of the solute modified by the presence of the eluent. Therefore the solute behaves as in the linear adsorption regime but with a decreased adsorptivity. Accordingly, its retention time is given by:

$$t_{r,s} = t_0 \left(1 + \frac{1-\varepsilon}{\varepsilon} H_s^* \right) \qquad (2.3)$$

From this relation it is seen that if we reduce H_s^* to values well below unity, the measured retention time of the solute approaches that of an ideal tracer. For this,

we need to select an eluent, which exhibits sufficiently larger adsorptivity than that of the solute.

Table 2.1: Measurement of the total porosity ε, through Eq.1.3;
$V=3.14$ml, $Q=0.5$ml/min; $\underline{\varepsilon}$ represents the value of ε estimated without density correction for temperature changes.

Tracer/Eluent	T [°C]	$\underline{\varepsilon}$	ε
Hexane/Pentane	30	0.70	0.70
	35	0.70	0.70
	40	0.69	0.71
AD/Methanol	25	0.73	0.73
	35	0.73	0.74
	45	0.72	0.74
	65	0.70	0.74
	75	0.69	0.73
AD/Ethanol	25	0.69	0.69
	45	0.68	0.69
	65	0.66	0.70
	75	0.66	0.70
	80	0.65	0.70
	85	0.65	0.70
AD/Isopropanol	25	0.68	0.68
	45	0.67	0.68
	65	0.66	0.69
	85	0.64	0.69
AD/2-Butanol	25	0.68	0.68
	45	0.67	0.68
	65	0.65	0.68
	75	0.64	0.68
	85	0.63	0.68

In the first part of Table 2.1 the total porosities are reported measured using pulses of hexane in pentane at three different temperature values. The observed value of $\varepsilon=0.70$ is found to be temperature independent, thus indicating that the effect of hexane adsorption has been eliminated, i.e. $H_s^* \ll 1$ in Eq.2.3. All data in Table 2.1 have been shown to the well reproducible, with an estimated error of about 0.5%.

The porosity measurement obtained above is however not satisfactory, since hexane and AD have quite different molecular size and therefore they most likely access a different network of internal pores. To avoid this problem we have used AD as a tracer and various alcohols as eluents. The porosity values measured

with the different alcohols and at various temperatures are summarized in Table 2.1. Note that two sets of porosity values, $\underline{\varepsilon}$ and ε, are reported in Table 2.1, these have been obtained before and after correcting the volumetric flow-rate for the density change as a function of temperature, respectively. The density has been corrected using the Francis equation [15]. It is seen that this effect is not negligible at all and could lead to misleading conclusions when not properly accounted for.

From the data in Table 2.1 it is seen that the obtained porosity values are temperature independent, but differ depending upon the alcohol used. In particular, larger porosities are estimated using smaller alcohol molecules. This indicates that a residual effect of AD adsorption, which is not sufficiently strong to be detected by changing the temperature, is actually present. This is explained by considering that when decreasing the size of the alcohol molecule its polarity increases. This leads on the one hand to stronger interactions of AD with the solid surface, i.e. larger K_s, and on the other hand to lower values of the eluent adsorptivity on the reversed phase, i.e. lower K_e, which both imply larger values of H_s^* in Eq.2.2. When considering that the porosity values measured with 2-butanol is very close to those measured with isopropanol, we can conclude that 0.68 is the correct value of intraparticle porosity to be used when considering chromatographic processes involving AD. Eluents with polarity lower than 2-butanol cannot be used, since it would then be very difficult to regenerate again the reversed phase stationary phase.

Finally, it is worth noting that the porosity value measured above, i.e. 0.68, is smaller than the value of 0.70 estimated using hexane as a tracer; such a difference is significant, since it is larger than the experimental error. This is consistent with the observation that AD is a much larger molecule and therefore it can access a smaller fraction of the intraparticle porosity.

2.3 Interparticle porosity of the packed column

The interparticle porosity can be measured on reversed phase using again a pulse tracer technique, but now the tracer should be a chemical species that does not enter the pores of the stationary phase. Relatively large non-polar substances such as sugars or polymers are typically used for normal phases. But they cannot be used for reversed phases, because they interact with the non-polar external surface of the particles. In the case of reversed phases it is convenient to use potassium nitrate in an aqueous solution, since ionic substances are excluded from the pores due to electrostatic interactions. For the model system considered in this work an external porosity of 0.41 has been measured using potassium nitrate as a tracer. From the interparticle porosity, ε_b, and the definition of total porosity (Eq.1.4), the intraparticle porosity, ε_p, can be estimated as $\varepsilon_p = 0.46$.

2.4 Henry coefficients of the main- and the undesired products

For the measurement of the Henry coefficients the procedure described in section 4 of chapter 1 has been followed up.

Table 2.2: Henry coefficient and selectivity values with respect to AD

	AD	NP1	NP2	9-EPI
Henry coefficient	1.89	2.42	2.76	2.16
Selectivity	1.00	1.24	1.46	1.14

For the separation systems considered in this chapter the Henry coefficients values reported in Table 2.2 have been measured. For AD, being the main component, the evaluation using the preparative material was straightforward, while for NP1 and NP2 as well as for 9-EPI a significant decrease of the flow-rate in order to increase the column efficiency was required. Fig.2.3 shows a chromatogram of the ternary system AD, NP1 and NP2 obtained at a very low flow-rate of 0.1 ml/min. A complete resolution of the by-products from the main component could be achieved, and the Henry coefficients could be calculated from the retention times of the single peaks using Eq.1.5 in section 1.4.
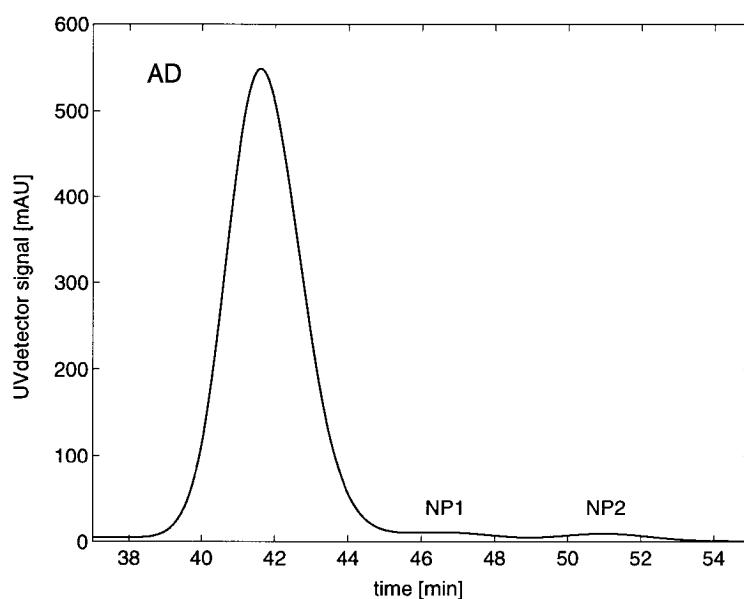
Fig. 2.3: Measurements of the Henry coefficients of AD, NP1 and NP2. Plot of the on-line UV measurement.

2.5 Dissipative phenomena

Dissipative phenomena as the axial dispersion and the mass transfer resistance are typically evaluated through the van-Deemter plot, as described in section 1.5. In the case for the purification process considered in this work, the van-Deemter curve reduces to a straight line, as it can be seen in Fig.2.4. Note that these values have been obtained using directly pulses of the mixtures to be separated and ignoring the presence of NP1 and NP2 due to their low concentration. From the intercept with the y-axis and the slope of the straight line in Fig.2.4, the axial dispersion and the mass transfer coefficient can be estimated as $D_{ax}=9.27 \times 10^{-3}$ u, where u is in cm/s and D_{ax} is obtained in cm^2/s, and $k_m=3.42$ 1/s, respectively.
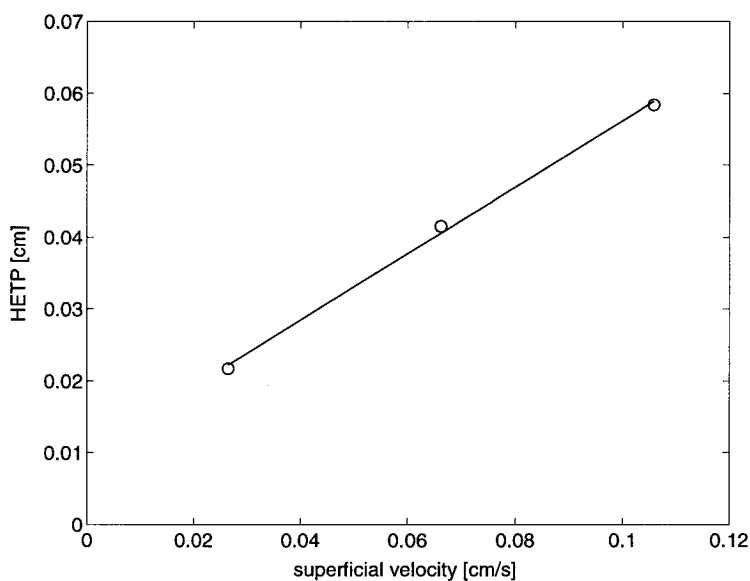

Fig. 2.4: Van-Deemter-plot of AD on MN RP C18 30 μm in MeOH/H2O:80/20 v/v%; (O) experimental data, (—) linear regression

2.6 Estimation of the adsorption isotherms

According to the peak fitting method, the parameters of the adsorption isotherms are estimated by fitting directly the concentration values at the outlet of the chromatographic column, when a sufficiently large pulse of the mixture to be separated has been fed [16]. Actually, since the linear part of the isotherm given by the Henry coefficient has already been estimated in previous steps of this procedure, here we focus on the nonlinear portion of the isotherm, which describes the competition among the different species for adsorption. For this we need to feed to the column a pulse, which is sufficiently large, i.e. to operate the column under overloaded conditions.

In order to successfully apply this procedure it is necessary that the model is sufficiently accurate, since all possible errors eventually reflect on the estimated

isotherms. For this we use the lumped pore diffusion model described in section 1.2, whose parameters have been carefully estimated in the previous sections. In addition, we need to measure the concentration values of all components in the outlet stream as a function of time. Typically chromatographic columns are equipped with a single online detector, and therefore the complete composition of the outlet stream can be measured only if complete resolution of all components is achieved in the column. As discussed above, this is unlikely when using preparative stationary phases in analytical columns, particularly when operating under overloaded conditions. Therefore it is necessary to take samples of the outlet streams in time and to analyze them separately using some other analytical technique. In the following we discuss the application of this procedure separately for the two systems under examination.

2.6.1 Ternary system: AD, NP1 and NP2

A pulse of 250 µl with concentration of 100 g/l of the mixture to be separated (AD 96%, NP1 and NP2 2% each) was eluted at a flow-rate of 0.5 ml/min. Fractions were collected every 30 seconds, and the entire peak was separated in 11 fractions, each with a volume of 250 µl. Each of these fractions was analyzed by HPLC to determine its composition. Fig.2.5 shows the results of the fraction collection method for the overloaded AD peak profile and, as a comparison, the peak profile measured on-line by the UV detector at high wavelength. Symbols indicate the concentration in the collected sample and the corresponding horizontal segment indicates the corresponding sampling interval. Off-line analysis of the samples and on-line UV signal are in good agreement, again due to the negligible concentration level of the impurities NP1 and NP2.
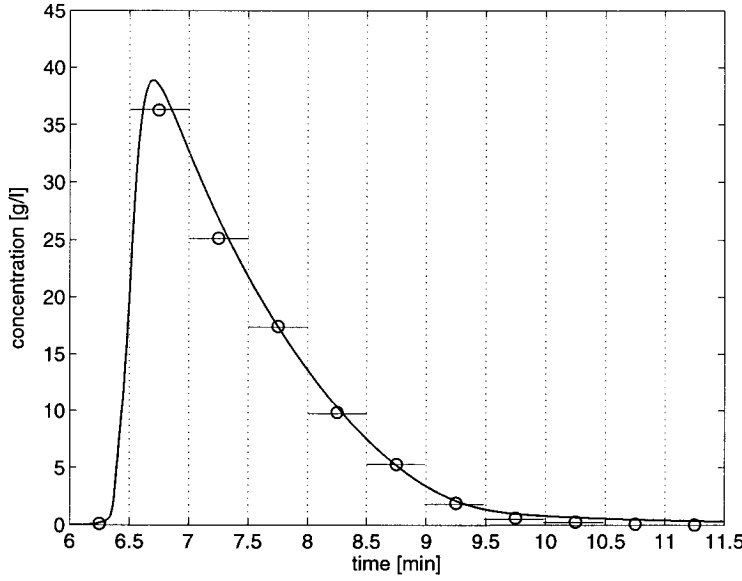
Fig. 2.5: Plot of the calibrated on-line UV signal and the off-line analysis of the fractionated samples of AD; (O) concentration in the fractionated sample, (—) on-line UV measurement

For the system under consideration the adsorption equilibria have been described using the multi-component Langmuir model:

$$q_i = \frac{H_i \cdot c_i}{1 + \dfrac{H_{AD}c_{AD}}{q_{AD}^s} + \dfrac{H_{NP1}c_{NP1}}{q_{NP1}^s} + \dfrac{H_{NP2}c_{NP2}}{q_{NP2}^s}} \qquad (i=AD, NP1, NP2) \qquad (2.4)$$

in which q_i^s represents the adsorbed phase concentration at saturation for the i-th component. As typically happens in purification processes, the concentration of the main component is much larger than that of the impurities, i.e. in this case $c_{AD} \gg c_{NP1}, c_{NP2}$, so that the above relation reduces to:

$$q_i = \frac{H_i c_i}{1 + \dfrac{H_{AD}c_{AD}}{q_{AD}^s}} ; \qquad (i=AD, NP1, NP2) \qquad (2.5)$$

under the reasonable assumption that $q_{AD}^s \cong q_{NP1}^s \cong q_{NP2}^s$ due to the very similar structure of the three molecules.

Although not essential, this observation allows applying the peak fitting procedure first to the main component alone and then to the two impurities, thus reducing the computational effort. In particular, since the value of $H_{AD}=1.89$ has been obtained earlier from experimental data in the diluted region, the only parameter left is the saturation concentration q_{AD}^s. This has been estimated as $q_{AD}^s =175$ g/l by fitting the experimental concentration data as shown in Fig.2.6.
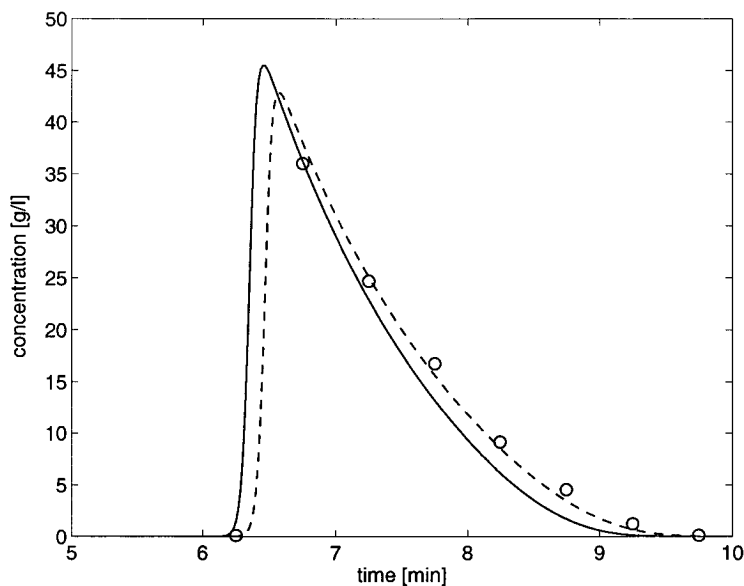
Fig. 2.6: Simulated and experimental peak profile of AD on reversed phase; (O) experimental data; model simulations: (--) H_{AD}=2.03, (—) H_{AD}=1.89

It is seen that the obtained agreement is reasonable, although the concentration values in the tail of the peak are somehow underestimated. A second curve in Fig.2.6 shows that a better agreement with the experimental data could be obtained by slightly changing the Henry coefficient value form 1.89 to 2.03, i.e. by about 7%. This indicates the good sensitivity of the peak profile to the value of the equilibrium parameters, which is very helpful in providing reliable estimates. The above fitting procedure has been repeated using the bi-Langmuir equilibrium isotherm. Since the improvement is only marginal we kept as the final isotherm for AD the Langmuir model with H_{AD}=1.89 and q_{AD}^s=175 g/l.

Let us now apply the peak fitting procedure to the two impurities NP1 and NP2. From the adsorption isotherm in Eq.2.5 it is seen that their behavior is not affected by their own saturation concentration in the adsorbed phase but only by the corresponding Henry constants that have already been measured (see section 2.4 Table 2.2). This is consistent with the fact that these components are present only in small concentrations, and therefore the competition to adsorption comes really only from the main component. Accordingly, there is no free parameter left for these components and we can use the comparison between measured and predicted peak profiles shown in Fig.2.7 as a check of the reliability of the entire procedure.
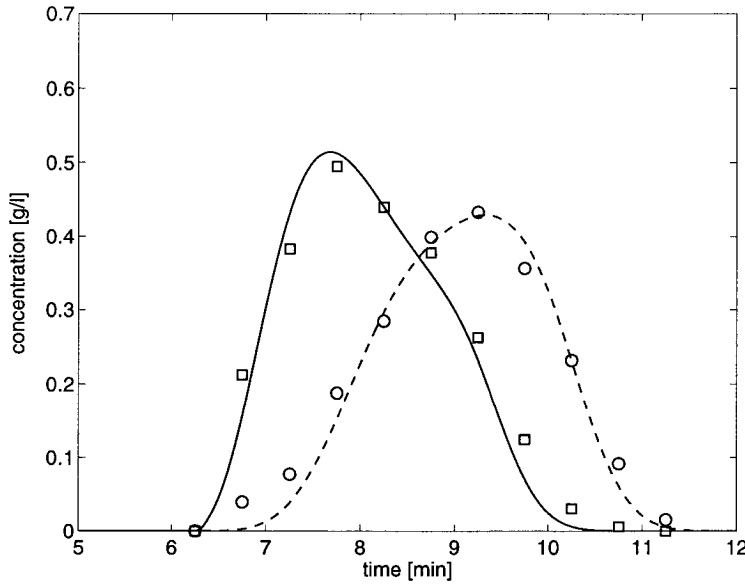
Fig. 2.7: Simulated and experimental peak profiles of the byproducts NP1 and NP2 in an overloaded peak; experimental data: ($\square$) NP1, ($\bigcirc$) NP2; model simulations: (—) NP1, (--) NP2

2.6.2 Binary system: AD and 9-EPI

A pulse of 100 µl of a 100 g/l feed solution (AD 70%, and 9-EPI 30%) was eluted at a flow-rate of 0.5 ml/min. Fractions were collected every 30 seconds, and the peak was fractionated in 10 samples, which have been analyzed separately by HPLC. In this case the peak fitting method is applied using the complete binary Langmuir isotherm:

$$q_i = \frac{H_i c_i}{1 + \dfrac{H_{AD} c_{AD}}{q_{AD}^s} + \dfrac{H_{9-EPI} c_{9-EPI}}{q_{9-EPI}^s}} \qquad (i=AD, 9\text{-}EPI) \qquad (2.6)$$

Since both Henry coefficients were estimated in previous steps of the procedure (i.e. section 2.4), only the two saturation concentrations in the adsorbed phase have been used as adjustable parameters in the fitting procedure, since the value of $q_{AD}^s=175$ g/l from the previous section has been used, only one parameter, i.e. q_{9-EPI}^s, has been varied. As shown in Fig.2.8, it is found that using for both components the same value obtained previously for AD, i.e. $q_{AD}^s=q_{9-EPI}^s=175$ g/l, a rather good agreement between the experimental and calculated concentration values is obtained. In addition, when slightly increasing the Henry coefficient of AD to the value of 2.03, similarly as for the separation system examined above, the quality of the fitting improves further. Note that in this case the Henry coefficient for 9-EPI has also been increased, in order to maintain the same

selectivity of 1.14 measured in the diluted experiments. On the whole, the obtained agreement with the experimental data and the consistence with the data obtained with the separation system considered earlier, indicate the reliability of the developed procedure for estimating the equilibrium parameters.
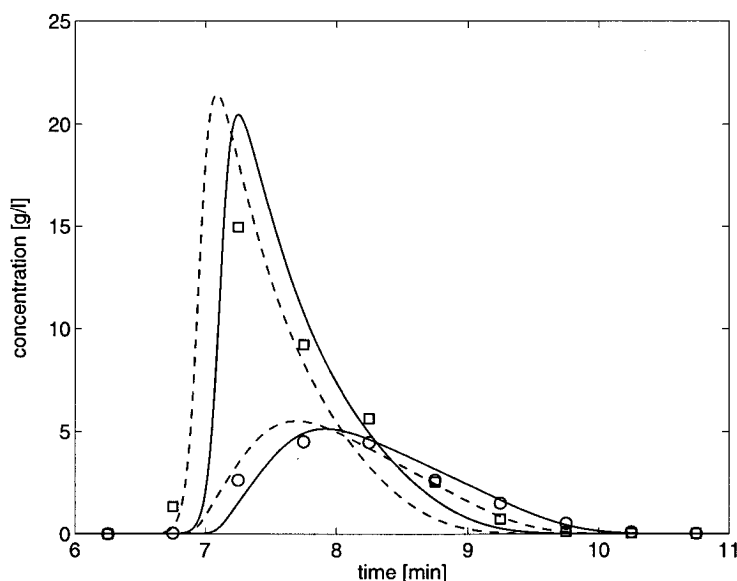

Fig. 2.8: Simulated and experimental peak profiles of AD and 9-EPI; experimental data: ($\square$) AD, (O) 9-EPI; model simulations: (--) $H_{AD}=2.03$ and $H_{9-EPI}=2.31$, (—)$H_{AD}=1.89$ and $H_{9-EPI}=2.16$

2.6.3 Validation of the procedure with independent equilibrium data

In order to further support the developed procedure, the obtained equilibrium isotherms were compared to equilibrium data obtained through a different technique. In particular, the perturbation method [17] was applied to the same purification process considered in section 2.6.1. In the following, we neglect the presence of the two impurities NP1 and NP2 and we concentrate on measuring the equilibrium isotherm of AD. In the frame of the perturbation method various experimental runs were performed using different background values for the concentration of AD ranging from 0 to 80 g/l. In each run the value of the slope of the equilibrum isotherm, i.e. dq_{AD}/dc_{AD}, at the considered background value of C_{AD} is estimated. The obtained values are compared in Fig.2.9 with the curve obtained by derivating the AD isotherm (Eq.2.5), with $H_{AD}=1.89$ and $q_{AD}^{s}=$ 175 g/l, estimated in section 2.6.1 using the peak fitting method. The obtained agreement indicates that the isotherm produced by the peak fitting method is consistent also with the equilibrium data measured with an independent technique, i.e. the perturbation method.
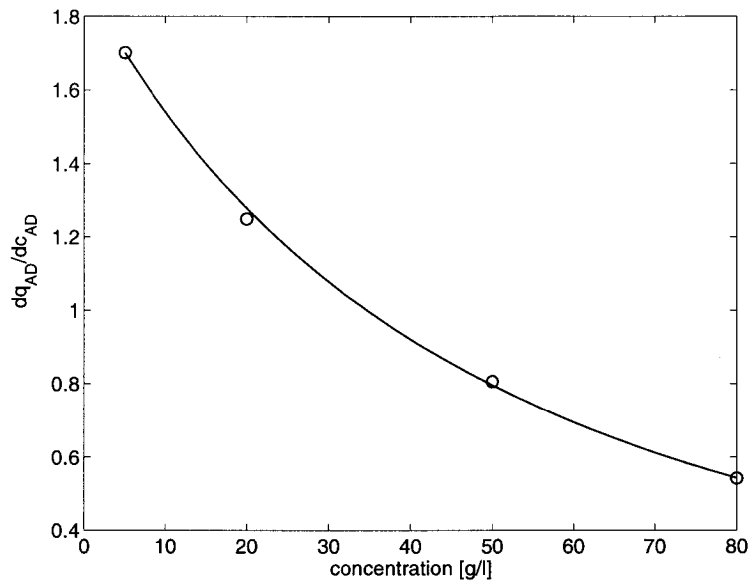
Fig. 2.9: Derivative of the adsorption isotherm of AD. Comparison between data measured using the perturbation method (O), and values computed using the isotherm (Eq.2.5), with the parameters obtained by the peak fitting method, i.e., $H_{AD}=1.89$ and $q_{AD}^s=175$ g/l (—).

3. Design of Chromatographic Separations on Silica Gel

The separation and purification processes of AD, as described in the previous chapter on reversed phase, can also be carried out on silica gel. Here the separation of the homologues NP1 and NP2 from the main component AD is more problematic, since their selectivities are close to one. Due to their shorter retention times, the byproducts NP1 and NP2 are displaced by AD providing an opportunity to separate this mixture. The purification process of the mixture of 9-EPI and AD is comparable with that on reversed phase, since the selectivity is nearly the same on both types of stationary phases.

3.1 The model separation problem

The model separation problem is described in detail in section 2.1. Here again we have used the same separation cases as in chapter 2, where the first one is a purification process, since in this mixture1 the mass fraction of the product AD is 96%, while that of NP1 and NP1 is just 1% and 3%, respectively. The second process is a separation process, in this mixture2 the mass fraction of AD is 70% and that of the byproduct 9-EPI is 30%. In both processes the silica gel packing material YMC Sil (YMC, Japan) has been used. The packing material is characterized by a pore width of 120 Å and a particle diameter of 40 μm. The dimensions of the used column are 250 mm length and 4 mm diameter. The experiments have been carried out on a HPLC station with the designation HP 1090 (Hewlett Packard, USA) at a temperature of 25 °C in the eluent ethylacetate. In this system used the byproducts NP1 and NP2 show a selectivity of 0.92 and 0.94, respectively, to the main product AD, while for 9-EPI this is equal to 1.15.

The possibility of performing the second separation process on a different stationary phase with SMB has been studied by Küsters et al. [12].

3.2 Porosities of the packed column

The total porosity can be measured with a small injection of a substance, which does not interact with the adsorption sites and leaves the column with the column hold-up time. From the retention time of the detected peak at the outlet of the column the total porosity can be calculated by using Eq.1.3 (chapter 1). On silica gel we could measure this quantity with toluene as an inert tracer in the eluent ethylacetate and estimate in our case a total porosity of 0.82. Toluene as a non-polar species does not exhibit any adsorption behavior on the polar surface of the silica gel stationary phase. In principle, the interparticle porosity, ε_b, can be determined by using a tracer substance, which does not interact with the adsorption sites and, in addition, does not enter the pores of the particles, so that from the retention time of the detected peak we can estimate this quantity by using again Eq.1.3. Afterwards, the intraparticle porosity, ε_p, is estimated by using Eq.1.4.

However, the selection of a species for the measurement of the interparticle porosity is difficult taking into consideration the required properties. Relatively large non-polar substances such as sugars or polymers are typically used for normal phases. These species can be detected at the column outlet with a RI-detector (refractive index). The problem here is to find a non-polar substance whose molecules are large enough not to enter the pores and not to large to block the filters at the column in- and outlet. On reversed phase the interparticle porosity could be measured with potassium nitrate using the effect of electrostatic interactions, which leads to the exclusion of this species from the pores. The estimated value of 0.41 for the interparticle porosity in a reversed phase column of the same geometry has been also accepted for the model system considered in this work, assuming that the value of the interparticle porosity on silica gel and on reversed phase is nearly the same, since the particle diameters of 40 µm and 30 µm, respectively, are close to each other and, in addition, the reversed phase is a modification of the silica gel which affects only the intraparticle and not the interparticle porosity. By using Eq.1.4 the intraparticle porositiy, ε_p, can be estimated as $\varepsilon_p = 0.69$.

3.3 Henry coefficients of the main-and the undesired products

In principle, the Henry coefficients have been measured following up the procedure described in section 1.4. However, the identification of the single peaks of all components of the mixture to be separated can be difficult, since it has been used preparative packing material characterized by a low efficiency which leads to bad resolution of the single peaks. In addition, having selectivities of the byproducts to the main product close to 1, the peaks of the byproducts cannot be seen from the detected peak signal and then their Henry coefficients

cannot be measured, while the estimation of the Henry coefficient of the main component is straightforward.

For the system considered in this work the Henry coefficients of the main and the byproducts are reported in Table 3.1. For AD as the main component the evaluation using the preparative packing material was straightforward. The Henry coefficient of 9-EPI could be estimated by decreasing the flow-rate to a very low value in order to increase the efficiency. Then the peak maximum of 9-EPI can be distinguished from the tail of the AD peak profile and a selectivity of AD to 9-EPI of about 1.15 is estimated. This value will be checked again by the peak fitting method, reported in a later section. The Henry coefficients of the byproducts NP1 and NP2 could not be evaluated from the retention times. No resolution of the byproducts has been achieved in the column, since their selectivities are close to 1 and the determination of their Henry coefficients is postponed to a later step.

It has been observed that the Henry coefficients can change significantly depending on the quality of the eluent ethylacetate, which was used for the experiments; on the contrary, the selectivities of the byproducts to the main product kept constant. The reason for this behavior can be probably found in the high sensitivity of the system studied in this work on the presence of small amounts of water in ethylacetate. Since this quantity can change slightly from bottle to bottle, we have determined Henry coefficients of the main product in a range between H=6.1 and 6.7. In the following, the estimation of the adsorption isotherms of the ternary system and of the binary system has to be considered separately. While the experimental part of the peak fitting method has been performed under the same experimental conditions for the same system, same solvent and same Henry coefficients, slightly higher Henry coefficients could be assessed, when the ternary system has been investigated at a later date.

Table 3.1: Henry coefficients and selectivity values with respect to AD

	AD	NP1	NP2	9-EPI
Henry coefficient	1.) 6.18 2.) 6.54	5.69	5.81	7.52
Selectivity	1.00	0.92	0.94	1.15

3.4 Dissipative phenomena

A detailed description of the procedure to evaluate dissipative phenomena as the axial dispersion and the mass transfer resistance is explained in section 1.5. The van-Deemter plot is represented through a straight line as seen in Fig.3.1 for our system. The experimental data has been evaluated only from the peaks of the main component AD, since no resolution of the byproducts NP1 and 2 have been achieved. In the second mixture a resolution of the byproduct 9-EPI could only be achieved at a low superficial velocity and in addition, in the range of such low velocities the peak width of 9-EPI could not be measured, since the resolution of that peak is too poor. Therefore we have also accepted the dissipative parameters, measured only for the main-product AD, as the correct ones for the byproducts. This assumption might be accurately enough, since on the one hand axial dispersion is influenced mainly by the flow-anisotropy and this quantity should be the same for all components in the mixture to be separated, and on the other hand the mass transfer rate is controlled by the pore diffusion as the dominating step which should also be very similar for all components.

From the intercept with the y-axis and the slope of the straight line in Fig.3.1, the axial dispersion and the mass transfer coefficient can be estimated as $D_{ax}=3.32 \times 10^{-2}$ u, where u is in cm/s and D_{ax} is obtained in cm^2/s, and $k_m=3.52$ 1/s, respectively.
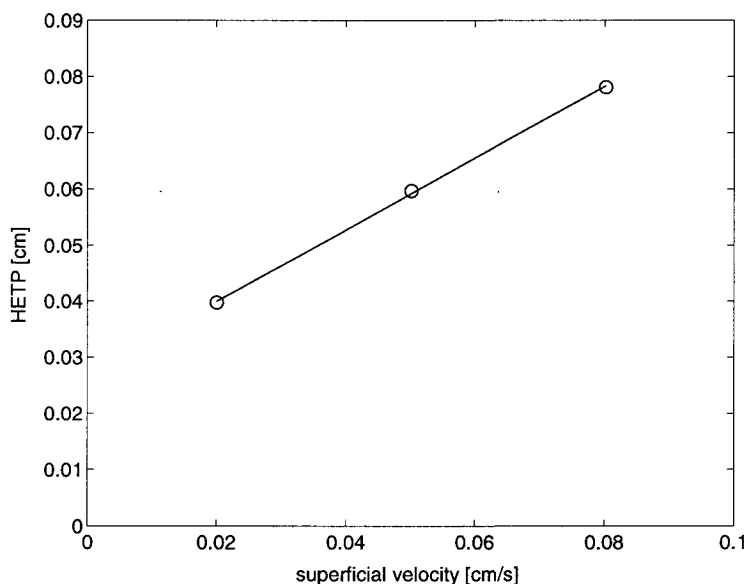

Fig. 3.1: Van-Deemter plot of AD on YMC Sil 40 µm in ethylacetate; (O) Experimental data, (——) linear regression

3.5 Estimation of the adsorption isotherms

As described in a previous chapter, the free parameters of a suitable adsorption model are evaluated by fitting directly the simulated peak profiles to the experimental ones until the best prediction of the experimental band profiles is achieved. For this purpose, we follow up the same procedure as described in section 2.6. Also for the separation and purification processes on silica gel the fraction collection technique have to be carried out on the overloaded peak profiles, in order to achieve the identification of all peaks in the complete composition of the column outlet stream. We discuss now the application of this procedure for the isotherm estimation of the mixture1 and the mixture2 separately.

3.5.1 Ternary system: AD, NP1 and NP2

A pulse of 80 µl with a concentration of 100 g/l of the mixture1 was fed at a flow-rate of 0.5 ml/min and at a temperature of 25 °C. Samples were collected every 30 seconds, and the entire peak was separated in 11 fractions, each with a volume of 250 µl. Fig.3.2 shows a comparison of the fractionated and off-line analyzed peak profile of AD and the detected and calibrated total peak profile of mixture1, neglecting the very low concentrations of NP1 and NP2 in the total peak profile. Symbols indicate the concentration in the collected sample and the corresponding horizontal segment indicates the corresponding sampling interval. Off-line analysis of the samples and on-line UV signal are in excellent agreement, when taking into consideration that for one sample on average only 20 drops were collected and through shifting from vial to the next vial a drop can be lost. Here we can show that the fraction collection can also be successfully applied under analytical conditions and not only for the preparative scale.
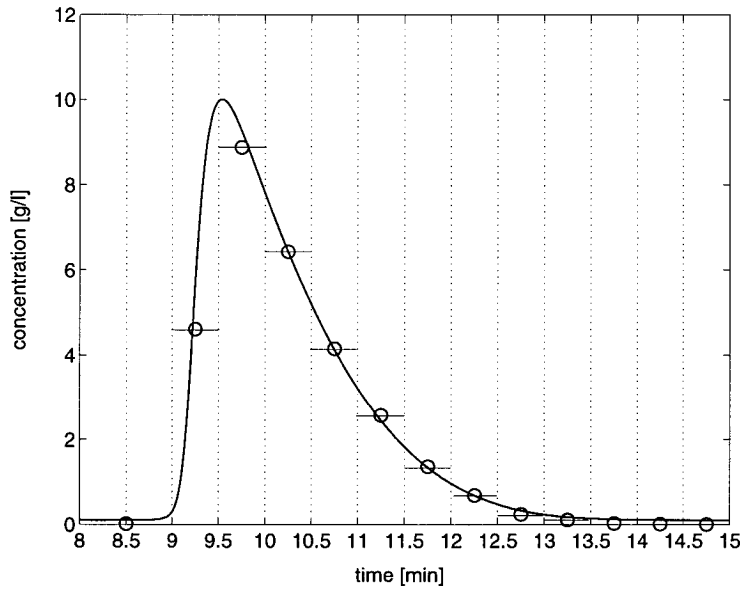
Fig. 3.2: Plot of the calibrated on-line UV signal and the off-line analysis of the fractionated samples of AD; (O) Concentration in the fractionated sample, (—) on-line UV measurement

For the separation process on silica gel, we begin to describe the adsorption behavior of the pharmaceutical mixture using a Langmuir model, neglecting the presence of the impurities due to their very low mass fraction and focusing first on the main product AD. As shown by the broken line in Fig.3.3, the obtained fitting of the overloaded profile of AD is very poor, where only the saturation capacity q_s has been fitted, while the Henry coefficient was already measured under diluted conditions as equal to 6.18. When considering instead the bi-Langmuir model, we have to fit three parameters instead of one, as shown in Eq.3.1, i.e. the saturation capacities of both bi-Langmuir terms and the ratio of the Henry coefficients of the two bi-Langmuir terms, while their sum gives the total Henry coefficient, which has been already measured under diluted conditions as reported above.

$$q_i = \frac{H_{bi1,i}c_i}{1 + \dfrac{H_{bi1,AD}c_{AD}}{q_{AD}^{bi1,s}}} + \frac{H_{bi2,i}c_i}{1 + \dfrac{H_{bi2,AD}c_{AD}}{q_{AD}^{bi2,s}}} \qquad (i=AD, NP1, NP2) \qquad (3.1)$$

in which $H_{AD}=H_{bi1,AD}+H_{bi2,AD}$

In general, the two bi-Langmuir terms describe two different types of adsorption sites, one characterized by a high activation energy and a low number of adsorption sites, and the other one by low activation energy but large number of sites. In particular, the main portion of the overloaded peak profile is determined by the first bi-Langmuir term, while the tailing portion at low concentrations is

substantially determined by the second bi-Langmuir term. As a result, in the fitting procedure it is convenient to focus first on the parameters relative to the first type of adsorption sites, i.e. $H_{bi1,AD}$ and $q_{bi1,s}$. As shown by the broken-dotted curve in Fig.3.3, the experimental data can be much better predicted by using the value $H_{AD}=5.5$ and $q_{bi1,s}=255$ g/l.
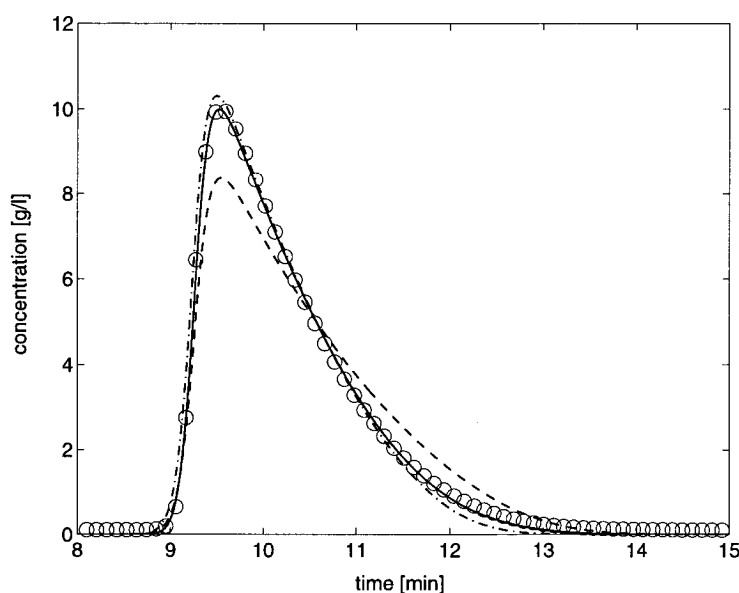

Fig. 3.3: Experimental peak profile of the mixture1 on silica gel, and simulated ones by using a bi-Langmuir and Langmuir model; Injection volume: 80 µl, injection concentration: 100 g/l; Main component AD: (O) experimental data; model simulations: (—) $H_{bi1,AD}=5.5$, $H_{bi2,AD}=0.68$, $q_{bi1,s}=255$ g/l, $q_{bi2,s}=0.5$ g/l, (--) $H_{AD}=6.18$, $q_s=180$ g/l, (-—·) $H_{AD}=5.5$, $q_s=255$ g/l

However, the tailing portion of the peak is not got satisfactorily reproduced. For this we consider the second type of adsorption sites and fit the parameter $q_{bi2,s}$, while the corresponding Henry coefficient is fixed at $H_{bi2,AD}=0.68$, since the sum of the Henry coefficients of both terms must give the value 6.18 as indicated above. The obtained solid curve shown Fig.3.3, which corresponds to the fitted value $q_{bi2,s}=0.5$ g/l, exhibits another accurate reproduction of the overloaded peak profile.

In order to show that the parameters fitted following the procedure described above are correctly evaluated, simulations of a parametric analysis has been performed where the influence of the single parameters were analyzed in detail. The influence of the ratio of the Henry coefficients of the two bi-Langmuir terms has been studied, while the saturation capacity of the first term was fitted to the peak maximum and that of the second one was kept constant. The results of that study are seen in Fig.3.4 and show that only with the ratio found with the procedure described above the experimental peak profile can be predicted accurately enough.
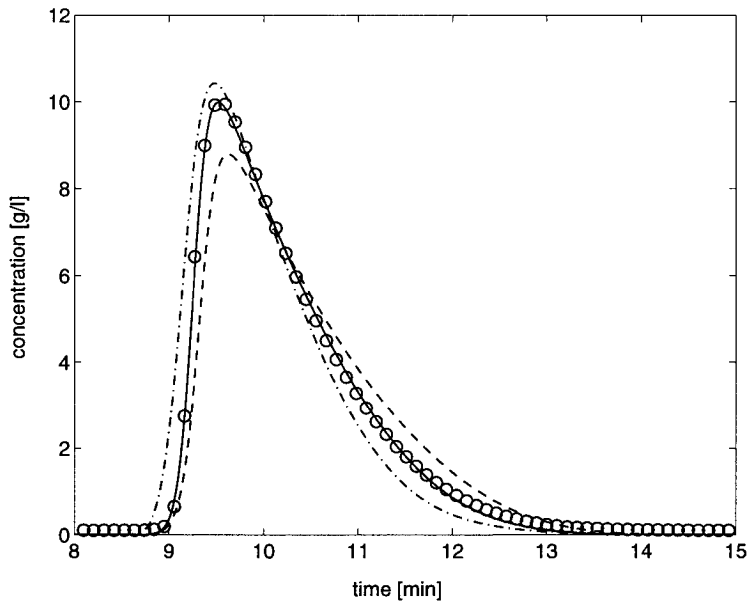
Fig. 3.4: Parametric analysis of the influence of the ratio of the Henry coefficients of the bi-Langmuir terms on the peak shape. (O) Experimental data, see caption of Fig.3.3, model simulations: (—) $H_{bi1,AD}=5.5$, $H_{bi2,AD}=0.68$, $q_{bi1,s}=255$ g/l, $q_{bi2,s}=0.5$ g/l, (--) $H_{bi1,AD}=5.8$, $H_{bi2,AD}=0.38$, $q_{bi1,s}=210$ g/l, $q_{bi2,s}=0.5$ g/l, (·—·) $H_{bi1,AD}=5.0$, $H_{bi2,AD}=1.18$, $q_{bi1,s}=320$ g/l, $q_{bi2,s}=0.5$ g/l.
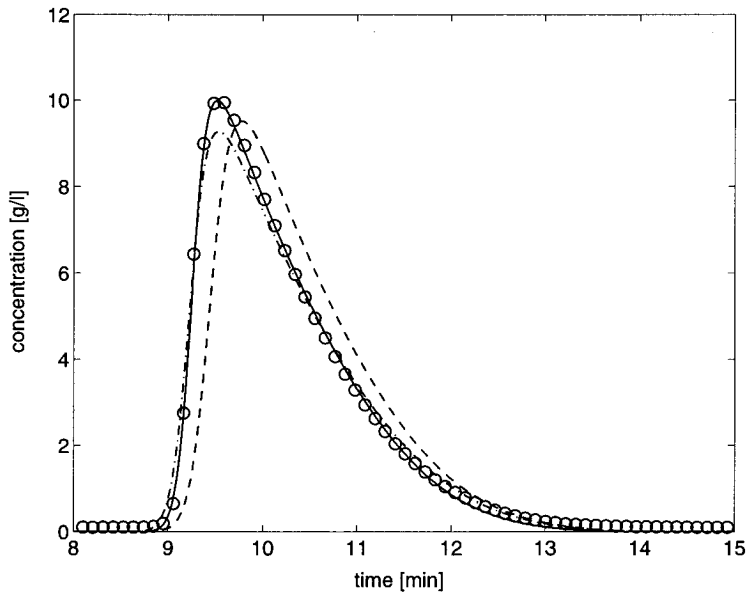

Fig. 3.5: Parametric analysis of the influence of the saturation capacity of the first bi-Langmuir term on the peak shape. (O) Experimental data, see caption of Fig.3.3, model simulations: (—) $H_{bi1,AD}=5.5$, $H_{bi2,AD}=0.68$, $q_{bi1,s}=255$ g/l, $q_{bi2,s}=0.5$ g/l, (--) $H_{bi1,AD}=5.5$, $H_{bi2,AD}=0.68$, $q_{bi1,s}=280$ g/l, $q_{bi2,s}=0.5$ g/l, (·—·) $H_{bi1,AD}=5.5$, $H_{bi2,AD}=0.68$, $q_{bi1,s}=230$ g/l, $q_{bi2,s}=0.5$ g/l.

A second study demonstrates the influence of the saturation capacity on the peak shape, in particular on the position of the shock front and of the peak maximum as shown in Fig.3.5. By increasing and decreasing that parameter those characteristics of a peak profile move to longer and shorter retention times, respectively.
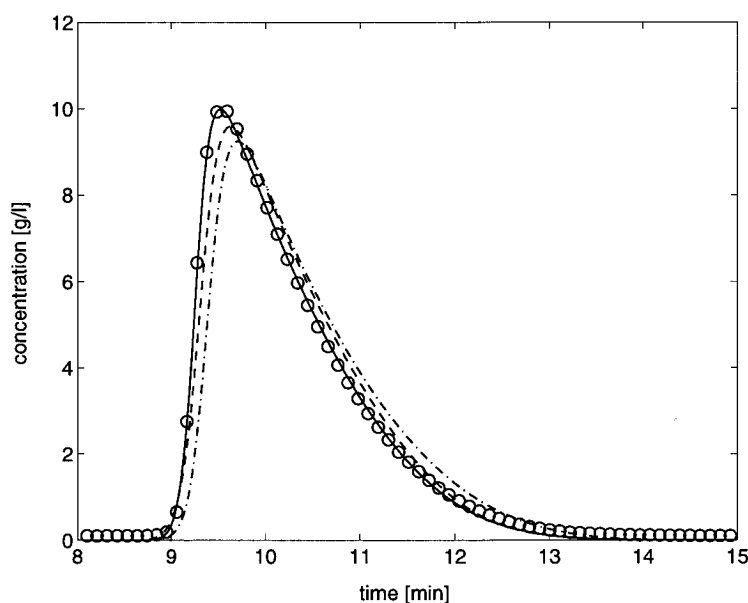

Fig. 3.6: Parametric analysis of the influence of the saturation capacity of the second bi-Langmuir term on the peak shape. ($\bigcirc$) Experimental data, see caption of Fig.3.3, model simulations: (——) $H_{bi1,AD}=5.5$, $H_{bi2,AD}=0.68$, $q_{bi1,s}=255$ g/l, $q_{bi2,s}=0.5$ g/l, (--) $H_{bi1,AD}=5.5$, $H_{bi2,AD}=0.68$, $q_{bi1,s}=280$ g/l, $q_{bi2,s}=0.1$ g/l, (·——·) $H_{bi1,AD}=5.5$, $H_{bi2,AD}=0.68$, $q_{bi1,s}=230$ g/l, $q_{bi2,s}=1$ g/l.

It is also shown in Fig.3.6 that a low saturation capacity of the second bi-Langmuir term leads to a shifting especially of the shock front to shorter retention times, while a high value of that parameter leads to less steeper fronts and stronger tailing.

Let us now apply the peak fitting procedure to characterize the adsorption behavior of the impurities NP1 and NP2. Again their behavior is not affected by their own saturation concentration due to their low mass fractions. However, in this case the Henry coefficients of the impurities could not be measured with the diluted experiments, since complete resolution of the corresponding peaks could not be achieved. Therefore, their determination has been postponed at this step of the general procedure. Accordingly, the peak profiles of NP1 and NP2 have been fitted using the bi-Langmuir isotherm Eq.3.1, and the following Henry coefficients values have been estimated $H_{NP1}=5.69$ and $H_{NP2}=5.81$, which indicate selectivities equal to $\alpha_{NP1/AD}=0.92$ and $\alpha_{NP2/AD}=0.94$. The results of the peak fitting method applied to the byproducts NP1 and NP2 can be seen in Fig.3.7.
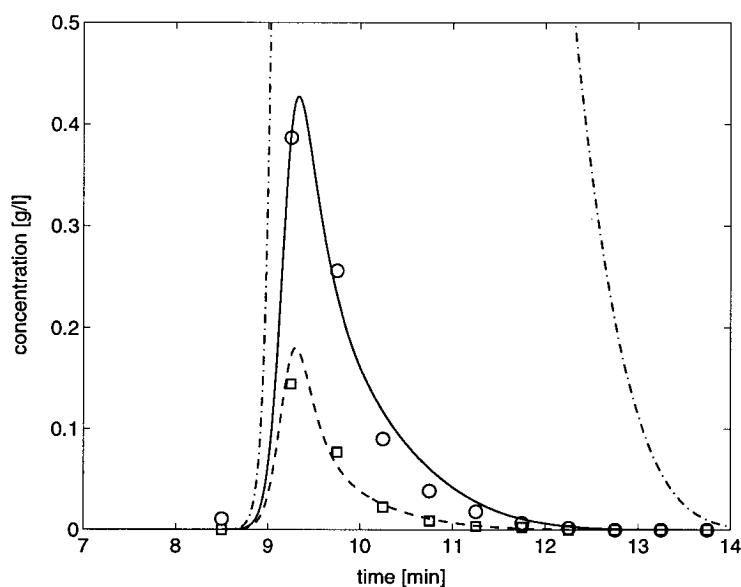
Fig. 3.7: Experimental peak profile of the mixture1 on silica gel, and simulated ones by using a bi-Langmuir and Langmuir model; Injection volume: 80 µl, injection concentration: 100 g/l; Impurities NP1 and NP2, experimental data: (□) NP1, (O) NP2; model simulations with best bi-Langmuir isotherm (see caption of Fig.3.3): (--) NP1, $\alpha_{NP1/AD}$=0.92, (—) NP2, $\alpha_{NP2/AD}$=0.94, (·—·) AD

The robustness of the fitting procedure for the selectivity of the byproducts is shown in Fig.3.8 for NP2, where this quantity was varied in a range between 0.9 and 0.96. Increasing the selectivity strengthens the displacement effect, decreasing that quantity leads to a weaker effect, so that the entire peak shape has to be used for the fitting procedure, not only the retention time at the peak maximum.
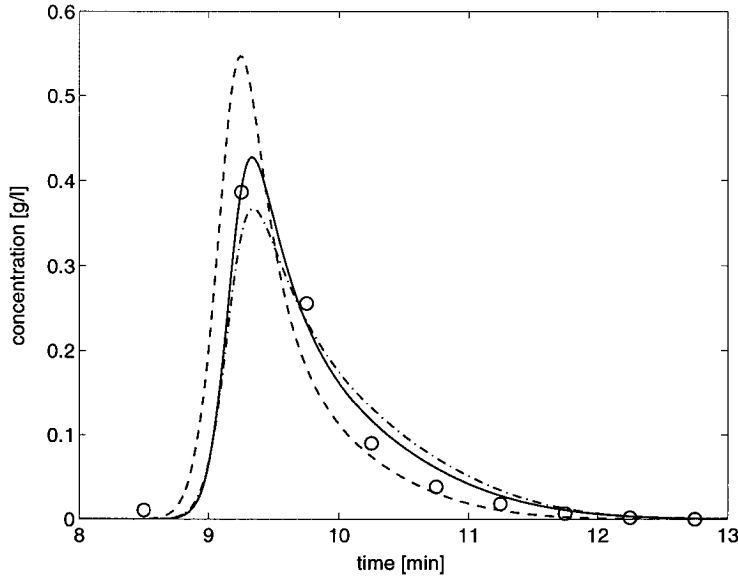
Fig. 3.8: Parametric analysis of the influence of the selectivity of NP2 on the peak shape. (O) Experimental data, see caption of Fig.3.3, model simulations with best bi-Langmuir isotherm (see caption of Fig.3.3): (—) $\alpha_{NP2/AD}$=0.94, (--) $\alpha_{NP2/AD}$=0.9, ($\cdot$—$\cdot$) $\alpha_{NP2/AD}$=0.96,

3.5.2 Binary system: AD and 9-EPI

A pulse of 100 μl of a 100 g/l feed solution of mixture2 was eluted at a flow-rate of 0.5 ml/min. Fractions were collected every 30 seconds, and the peak was fractionated in 13 samples, which have been analyzed separately by HPLC. For this system the peak fitting method has been applied using the complete, competitive bi-Langmuir isotherm for a two-component system, since the fraction of the byproduct 9-EPI is large and accordingly, a significant influence of that component on the adsorption behavior of the main component is to be expected. The complete bi-Langmuir isotherm for the two-component system is given by the following equation:

$$q_i = \frac{H_{bi1,i} c_i}{1 + \dfrac{H_{bi1,AD} c_{AD}}{q_{AD}^{bi1,s}} + \dfrac{H_{bi1,9-EPI} c_{9-EPI}}{q_{9-EPI}^{bi1,s}}} + \frac{H_{bi2,i} c_i}{1 + \dfrac{H_{bi2,AD} c_{AD}}{q_{AD}^{bi2,s}} + \dfrac{H_{bi2,9-EPI} c_{9-EPI}}{q_{9-EPI}^{bi2,s}}} \qquad (3.2)$$

(i=AD, 9-EPI)

For the system described in this section a Henry coefficient of 6.54 in the very diluted region was measured for the main component AD, thus significantly larger than that measured for the system in the previous section, for reasons discussed in section 3.3. Again the parameters to be fitted are the ratio of the Henry coefficients of the two Langmuir terms and the saturation capacities of the

two classes of adsorption sites, for each of the two components, i.e. six in all. For the sake of simplicity, we first assume that the saturation capacities are the same for both components, since the main product AD and the byproduct 9-EPI have very similar structural formulas. Moreover, we assume that the ratio of the Henry coefficients of the two Langmuir terms is the same for both components, and this is the one already found for the byproducts NP1 and NP2 as described in the previous section.

As shown in Fig.3.9, the experimental and calculated concentration profiles for the main component are in good agreement when using a saturation capacity for the first bi-Langmuir term of 290 g/l instead of 255 g/l fitted for the system described in the previous section.
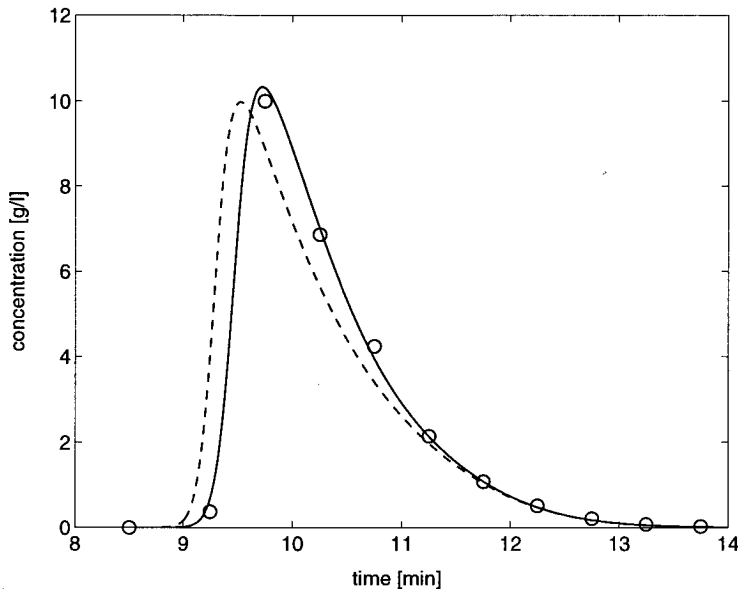

Fig. 3.9: Experimental peak profile of the mixture2 on silica gel, and simulated ones by using a bi-Langmuir model; Injection volume: 100 μl, injection concentration: 100 g/l; Main component AD: (O) experimental data; model simulations: (—) $H_{bi1,AD}=5.86$, $H_{bi2,AD}=0.68$, $q_{bi1,s}=290$ g/l, $q_{bi2,s}=0.5$ g/l, $\alpha_{9EPI/AD}=1.18$, (--) $H_{bi1,AD}=5.86$, $H_{bi2,AD}=0.68$, $q_{bi1,s}=255$ g/l, $q_{bi2,s}=0.5$ g/l, $\alpha_{9EPI/AD}=1.18$.

As seen in Fig.3.10, the experimental peak profile of 9-EPI cannot be predicted in such a good way as the one of AD. By increasing the selectivity from 1.15 to 1.18, the quality of the fitting can be improved slightly. By leaving the assumptions given above and varying all parameters in the bi-Langmuir model (Eq.3.2), a prediction of the experimental peak profile of a quality of that of the main product AD cannot be achieved. The simulated peak profiles show a stronger peak broadening effect than the experimental one, indicating that in the case of 9-EPI the efficiency could be higher. Note that the axial dispersion and mass transfer coefficient, estimated only for the main product AD, have been used for all byproducts. This assumption should be correct for the axial dispersion, since the flow anisotropy must be the same for all components. The

mass transfer is a more complex process including all resistances from the outside part of the particles to the adsorption sites in the inner part of the particles and vice versa, namely film and pore diffusion and the adsorption/desorption kinetic. As reported in the literature for separations on chiral phases, the adsorption/desorption kinetic can be different for the two adsorption sites. While for one adsorption site being infinitely fast, as normally assumed, the adsorption/desorption kinetic can be significant slower on the other site affecting the lumped mass transfer coefficient. If we assume now in the case of 9-EPI that this is fact for the type of adsorption site described through the second term of the bi-Langmuir isotherm and we set the saturation capacity of this term to zero, the experimental peak profile of 9-EPI is much better described by using a mass transfer coefficient which is twice as high as that of the main product AD, as it is seen in Fig.3.10. This result indicates that the adsorption/desorption kinetic of the adsorption site described through the second bi-Langmuir term is not infinitely fast and influences significantly the total mass transfer rate. However, this phenomenum should be determined more in detail to get more reliable data, but it could be demonstrated that the results of the peak fitting method can offer more information than only the adsorption isotherm.
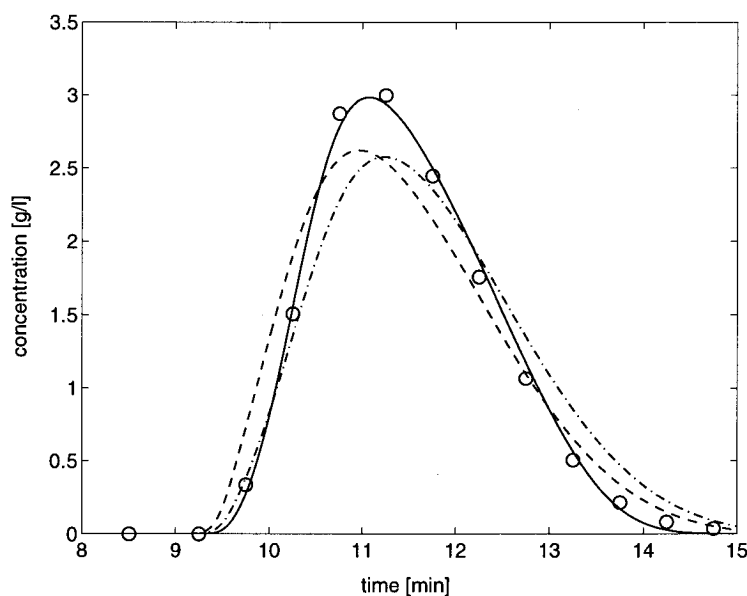

Fig. 3.10: Experimental peak profile of the mixture2 on silica gel, and simulated ones by using a bi-Langmuir model; Injection volume: $100\mu l$, injection concentration: 100 g/l; Byproduct 9-EPI: (O) experimental data; model simulations with best bi-Langmuir isotherm (see caption of Fig.3.9): (—) $\alpha_{9EPI/AD}=1.18$, $k_{m,9\text{-}EPI}=2*k_{m,AD}$, (--) $\alpha_{9EPI/AD}=1.15$, (·—·) $\alpha_{9EPI/AD}=1.18$.

3.6 Validation of the procedure with independent equilibrium data

In order to further support the developed procedure, the obtained equilibrium isotherms were compared to equilibrium data obtained through a different technique. In particular, this is the adsorption/desorption method, which was applied to the same purification process considered in section 3.5.2. For the comparison, we only focus on the adsorption isotherm of the main product AD. Performing the adsorption/desorption procedure, five equilibrium points have been measured for the concentration of AD ranging from 5 to 100 g/l. At each run the stationary phase was equilibrated at a given AD concentration. Then the whole amount of AD was eluted from the column and collected, and then off-line analyzed to evaluate the amount of AD, which was adsorbed on the stationary phase. The obtained values are compared in Fig.3.11 with the curve calculated through Eq.3.1 by using the parameters, which were evaluated by the peak fitting method for this system. The obtained agreement indicates that the isotherm estimated through the peak fitting method is consistent also with the equilibrium data measured with an independent technique, i.e. the adsorption/desorption method.
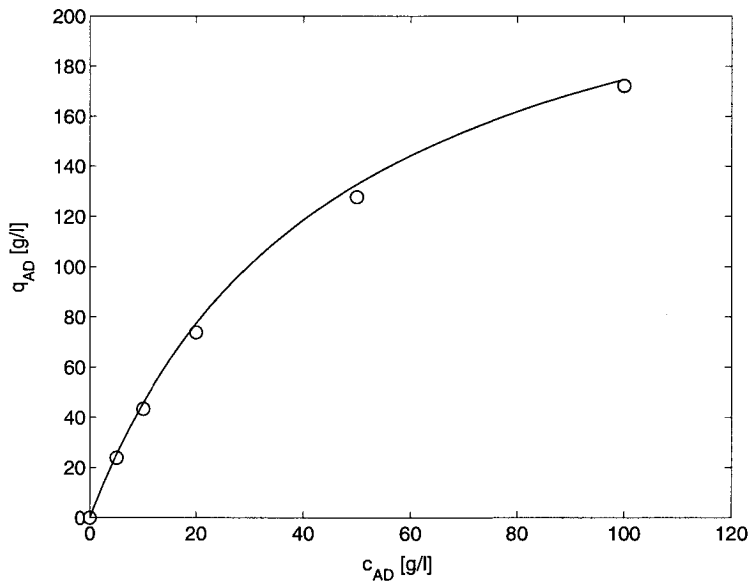

Fig. 3.11: Adsorption isotherm of AD. Comparison between data measured using the adsorption/desorption method (O), and values computed using the isotherm (Eq.3.1), with parameters obtained by the peak fitting method (—), i.e. $H_{bi1,AD}=5.5$, $H_{bi2,AD}=0.68$, $q_{bi1,s}=255$ g/l, $q_{bi2,s}=0.5$ g/l.

4. Design of Chromatographic Separations on a Chiral Phase

In this chapter we discuss in detail the application of the developed design procedure to the chromatographic separation of a model racemic mixture of industrial interest [18]. In particular, we will first estimate the adsorption isotherms using the peak fitting method, and then design a SMB (simulated moving bed) process with a production rate of 50 t/a of the separated racemic mixture.

4.1 The model separation problem

The model separation problem is a racemic mixture of two alcohols containing two aromatic centers. In the following the mixture to be separated is referred as the racemate and its two components as Enantiomer1 and Enantiomer2, respectively. In the separation process a Chiralcel AD (Daicel, Japan) stationary phase has been used. The packing is characterized by a particle diameter of 10 µm. The dimensions of the column are 250 mm length and 4.6 mm diameter. The experiments have been carried out on a HPLC station with the designation HP 1090 (Hewlett Packard, USA) at a temperature of 25 °C. The eluent is a 75/25 v/v% mixture of hexane/iso-propylalcohol. In this system Enantiomer2 exhibits a selectivity with respect to Enantiomer1 at infinite dilution of 1.26.

4.2 Porosities of the packed column

The porosity can be determined principally as described in section 1.3. Again an inert tracer has to be identified. This tracer must not adsorb on the stationary phases and has to be characterized by an opposite polarity to the chosen stationary phase. As already described in section 2.2 for the reversed phase, the situation on a chiral phase is similarly complicated, since the adsorbent surface exhibits polar and non-polar groups.
Based on the considerations described in section 2.2, the total porosity of the Chiralcel AD phase could be measured with a small amount of hexane fed to the column, equilibrated with a hexane/iso-propylalcohol mixture of 50/50 v/v%. The measured porosity is 0.66. This value is temperature independent, which

indicates that the effect of hexane adsorption has been eliminated. It could be determined that a hexane/iso-propylalcohol mixture of 50/50 v/v% has the optimal composition for a complete saturation of the polar and non-polar adsorption sites, so that a small perturbation of pure hexane does not show any interactions with the adsorption sites.

No measurement of the interparticle porosity has been done. This porosity quantity has been estimated at 0.39, taking into account the measured values of comparable packings with spherical particles. By using Eq.1.4 the intraparticle porosity, ε_p, can be estimated as $\varepsilon_p=0.44$.

4.3 Henry coefficients of the main- and the undesired products

The Henry coefficients have been measured following the procedure described in section 1.4. A sufficient resolution of the peaks of both components could be achieved to identify the single peaks and to calculate the Henry coefficients from the retention times using Eq.1.5. The Henry coefficient values and the selectivity for the separation system considered in this chapter are reported in Table 4.1.

Table 4.1: Henry coefficient and selectivity values with respect to Enantiomer1

	Enantiomer1	Enantiomer2
Henry coefficient	1.15	1.45
Selectivity	1.00	1.26

4.4 Dissipative phenomena

The axial dispersion and mass transfer coefficients are usually measured with the help of a van-Deemter-plot as described in section 1.5. In order to predict the experimental peak profiles as accurately as possible using the peak fitting method, these coefficients have been determined separately for the two enantiomers. Enantiomer1 shows a weaker adsorption behavior and therefore has a lower Henry constant. Using an eluent constituted of a hexane/iso-propylalcohol mixture with 75/25 v/v% a complete resolution of the two enantiomers could be reached only at a very low flow-rate (<0.1 ml/min). This low flow-rate is sufficient for the measurement of the peak width at half height in order to calculate the HETP value only for Enantiomer1. For a sufficient resolution of Enantiomer2 to measure the peak width at half height, as shown in

Fig.4.1, it was necessary to use a mixture of hexane/iso-propylalcohol with 85/15 v/v% instead of 75/25 v/v%. Accordingly the following strategy has been adopted. First, we investigated the van-Deemter plot of the racemate using the eluent mixture with a composition of 85/15 v/v%, where both enantiomers can be resolved. The aim is to check by direct measurement if the axial dispersion and the mass transfer coefficient for the two enantiomers are equal or different. Next, we investigated the cases with 75/25 v/v% eluent composition where only Enantiomer1 is sufficiently resolved to measure the half height width and therefore build a van-Deemter plot.
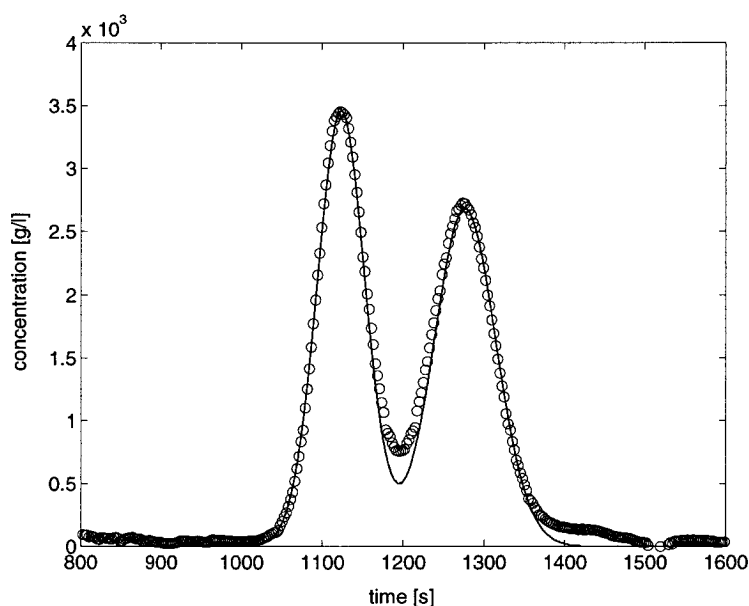

Fig. 4.1: Experimental peak profile (O) of the racemate and simulated one (—) under analytical conditions in a hexane/iso-propylalcohol: 85/15 v/v% mixture; flow: 0.3 ml/min, injection volume: 5 μl, injection concentration: 0.5 g/l

The van-Deemter-plot for the 85/15 v/v% eluent system is shown in Fig.4.2. It is seen that the mass transfer coefficients are 4.45 1/s and 3.39 1/s for Enantiomer1 and Enatiomer2, respectively, while the axial dispersion coefficient is equal to $9*10^{-3}$ cm*u for both components. As a result, the mass transfer coefficient of Enantiomer2 is about 30% lower than the corresponding one of Enantiomer1.
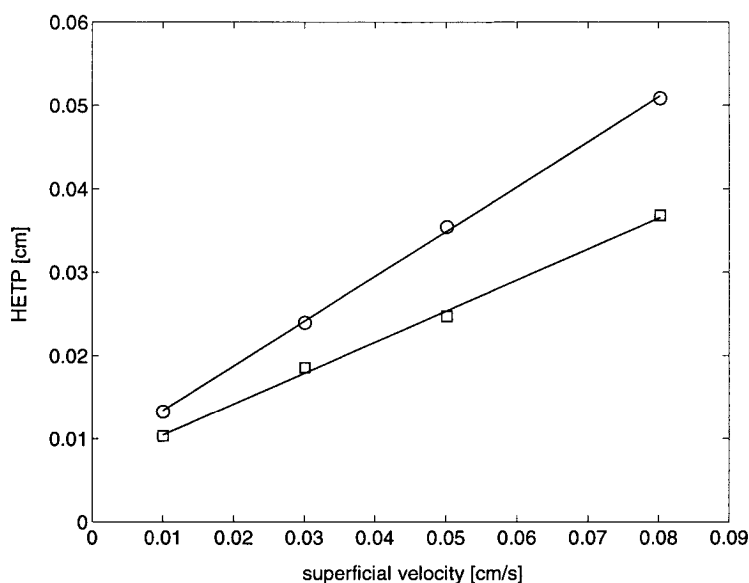
Fig. 4.2: Van-Deemter-plot of the racemate measured in a hexane/iso-propylalcohol: 85/15 v/v% mixture at a temperature of 25 °C

The accuracy of the measurement of mass transfer and axial dispersion coefficients with the help of a van-Deemter plot could be demonstrated by predicting the analytical peak profile, shown in Fig.4.1. At this low concentration the knowledge of the isotherm at high concentrations is not necessary. The Henry constants had already been measured in a previous step as described in the previous section and band broadening effects are described only through axial dispersion and mass transfer coefficient.

Let us consider the eluent composition of 75/25 v/v%. We can now safely assume that the axial dispersion coefficient is the same for both components. For Enantiomer1 the axial dispersion coefficient and the k_{m1}-value could be measured using the measured van-Deemter plot, shown in Fig.4.3. These values are of $D_{ax}=8*10^{-3}$ cm*u and $k_{m1}=3.73$ 1/s, respectively. Based on the results above we can safely assume that Enantiomer2 has the same axial dispersion coefficient. The mass transfer coefficient, k_{m2}, has been instead estimated by directly fitting the Racemate peak profiles, although only partially resolved, as shown in Fig.4.4.
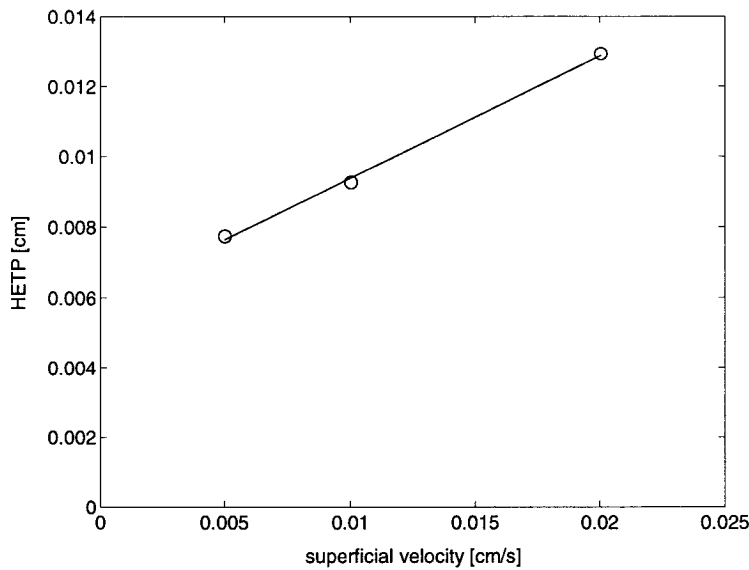
Fig. 4.3: Van-Deemter-plot of the Enantiomer1 measured in a hexane/iso-propylalcohol: 75/25 v/v% mixture at a temperature of 25°C

Following this fitting procedure, a mass transfer coefficient of $k_{m2}=2.9$ 1/sec could be determined in the 75/25 v/v% hexane/iso-propylalcohol mixture. Note that the nice agreement with the experimental values in Fig.4.4 provides further support to the values of the mass transfer and the axial dispersion coefficient of Enantiomer1 estimated from the van-Deemter plot in Fig.4.3.
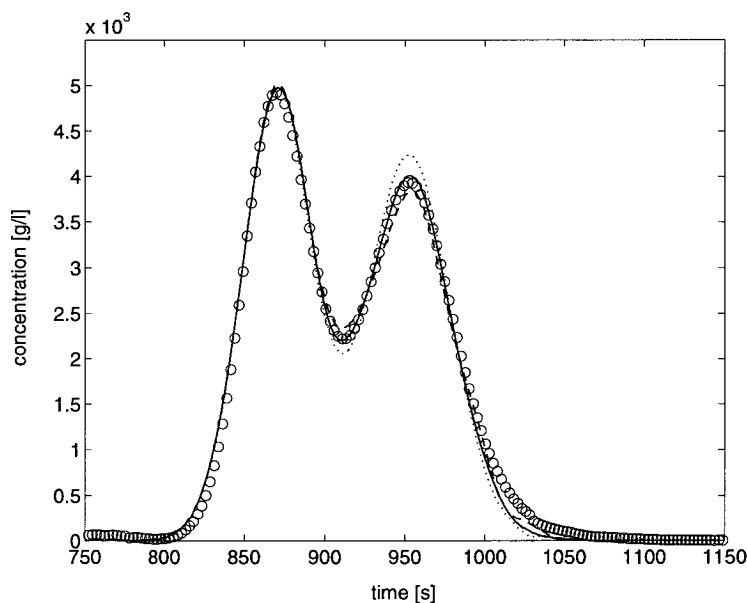

Fig. 4.4: Experimental peak profile of the Racemate and simulated ones under analytical conditions in a hexane/iso-propylalcohol: 75/25 v/v% mixture; flow: 0.3 ml/min, injection volume: 5 µl, injection concentration: 0.5g/l; (O) experimental peak profile; model simulations: (—) $k_{m2}=2.9$ 1/sec, (--) $k_{m2}=2.5$ 1/sec, (..) $k_{m2}=3.5$ 1/sec

4.5 Estimation of the adsorption isotherms

In order to characterize the adsorption behavior of the racemate by using the peak fitting method, overloaded peak profiles have to be measured at high concentrations. To avoid a super-saturation of the UV-detector and because the racemate is a strong UV-absorbing substance, such peak profiles have to be detected at high wave lengths. Beside Enantiomer1 and 2, the racemate mixture contains another substance with a very low mass fraction, but which is absorbing very strongly particularly in the UV region of high wave lengths. In addition to this problem, the UV-absorption of the racemate is nonlinear and a complete resolution could not be achieved under these overload conditions.

Therefore, in order to avoid the problems mentioned above and to identify the concentration peaks of both enantiomers, the fraction collection method had to be used. The various fractions have been analyzed off-line at a low wave length (<230 nm) after proper dilution. The peak fitting method has been carried out for two overloaded peak profiles with an injection volume of 250 µl and a concentration of 33 g/l and 51.6 g/l, respectively. Due to the low solubility of the racemate in the eluent system, the final production process will be performed at the relatively low feed concentration of 30 g/l. The higher concentrated racemate solution of 51.6 g/l could only be reached by a combination of heating and ultrasonic mixing. The solution was then immediately injected to investigate the adsorption behavior at concentrations as high as possible.

Since the concentrations of the racemate in the injected samples were relatively low, the band broadening of the overloaded peak profiles were modest and therefore we could collect only 5 to 6 fractions, each separated by about 30 seconds. Using time intervals lower than 30 seconds, the fraction collection method becomes not sufficiently accurate. Therefore the shape of the overloaded peak profile is reconstructed only poorly through the analyzed fractions, in opposition to the overloaded peak profiles on reversed phase and on silica gel, as it can be seen in the Figs.2.5 and 3.2.

In order to fit the experimental data with the model results, the simulated peaks have also been divided into the same time intervals and the mean concentration values in each time interval have been calculated. The simulated data points obtained in this way have been compared with the experimental ones and the free parameters of the adsorption isotherm have been estimated so as to obtain the best agreement. Note that in this case we could not use the frontal part of the overloaded peak profiles, because the number of samples was too low to reconstruct this region sufficiently enough, as it can be seen in Fig.4.6. The results of the peak fitting method, shown in the Figs.4.5 and 4.6 for the two overloaded peak profiles, indicate that actually the fraction collection method can also be used as a robust technique for peak profiles characterized in the presence of a relatively low band broadening.

For the system under consideration the adsorption equilibria of the racemate have been described using the competitive Langmuir model. The Henry coefficients were already measured under diluted conditions as described earlier in this chapter:

$$q_i = \frac{H_i c_i}{1 + \dfrac{H_1 c_1}{q_1^s} + \dfrac{H_2 c_2}{q_2^s}} \qquad \text{(i=Enantiomer1, Enantiomer2)} \qquad (4.1)$$

The axial dispersion and mass transfer coefficients, which were determined using the van-Deemter plot, describe sufficiently well the peak broadening effects at high concentrations. By applying the peak fitting method to the two overloaded peak profiles, a saturation capacity for both components of about 175 g/l could be estimated.
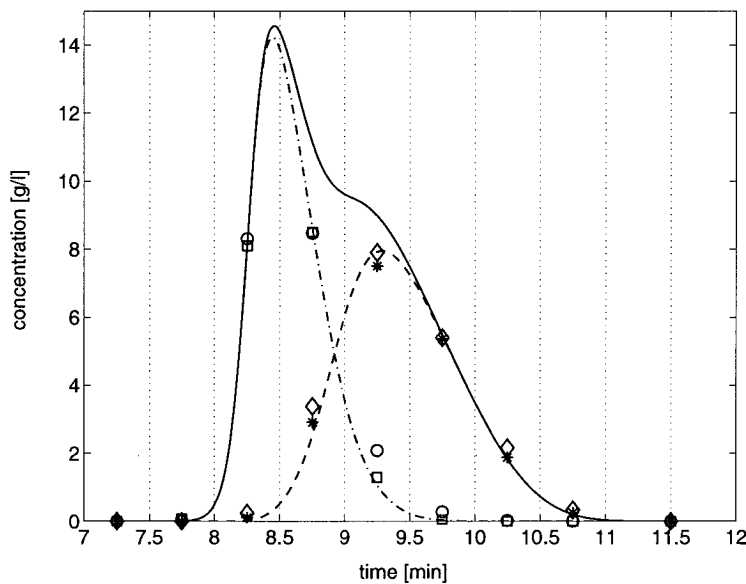

Fig. 4.5: Experimental peak profile of the racemate and simulated ones; flow: 0.5 ml/min, injection volume: 250 µl, injection concentration: 33 g/l; Experimental data: (O) Enantiomer1, (◊) Enantiomer2; model simulations: (□) Enantiomer1, (*) Enantiomer2, (—) peak profile of the Enantiomer2, (·—·) peak profile of Enantiomer1, (--) peak profile of Enantiomer2
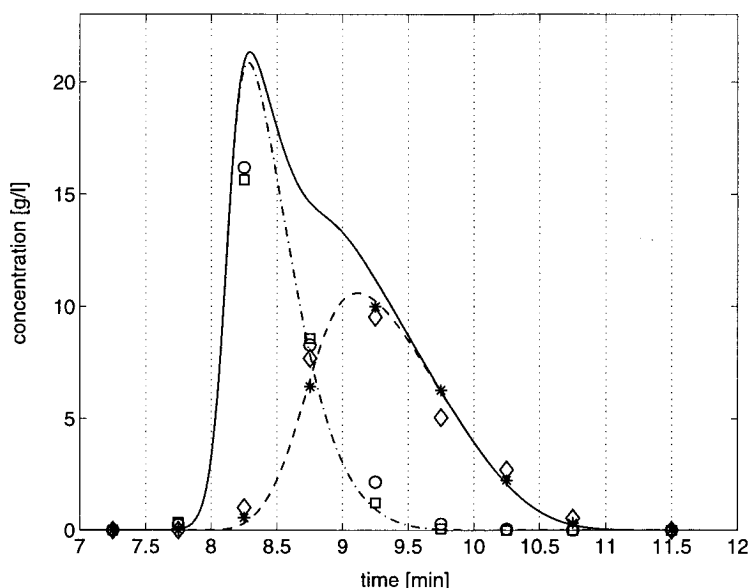
Fig. 4.6: Experimental peak profile of the Racemate and simulated ones; flow: 0.5 ml/min, injection volume: 250 µl, injection concentration: 51.6 g/l; Experimental data: (O) Enantiomer1, (◊) Enantiomer2; model simulations: (□) Enantiomer1, (*) Enantiomer2, (—) peak profile of the Enantiomer2, (·—·) peak profile of Enantiomer1, (--) peak profile of Enantiomer2

4.6 Design of the SMB separation of the racemate

The objective is to design a continuous SMB process [19,20] for the separation of 50 t/a of the racemate. The design is based on the adsorption isotherms measured above, and on additional information that will be discussed below. The process specifications established by the pharmaceutical industry are the following: minimum purity in extract and raffinate must be 99.5%; maximum pressure drop over the whole SMB plant must be 64 bar; a preparative stationary phase with particle size of 20 µm must be used instead of the 10 µm of the analytical column; the maximum concentration in the feed must be 30 g/l.

4.6.1 Complete separation region in the m3/m2-diagram

Based on the adsorption isotherms discussed above the complete separation region in the m3/m2-diagram can be calculated. The definition of m_i is given by the following equation:

$$m_i = \frac{Q_i \cdot t^* - \varepsilon V}{(1 - \varepsilon)V} \tag{4.2}$$

This is given by explicit relationships in terms of the overall feed concentration. Three regions, corresponding to three different values of the overall feed

concentration, namely 1, 10, and 30 g/l, are drawn in Fig.4.7. The optimal operating point in terms of productivity and solvent consumption is the vertex of each triangle-shaped region. Operating points within the complete separation region allow to achieve complete separation in the frame of the so-called Equilibrium Theory [20].
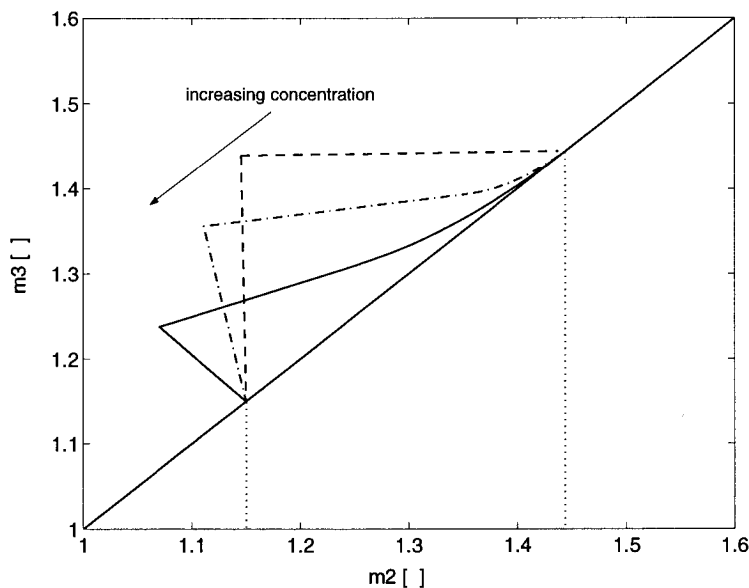

Fig. 4.7: m3/m2-diagram for different feed concentrations of the racemate. Feed concentrations of the racemate (Enantiomer1 and 2): (--) 1 g/l, (·—·) 10 g/l, (—) 30 g/l

4.6.2 Pressure drop and column efficiency

In the design of a SMB process, one of the key process constraints refers to the pressure drop in the unit, which is upper bounded to avoid damage of the column packing. The fluid velocity and the column length are ultimately determined by this constraint, together with the purity specifications. For the system under examination pressure drop has been measured as a function of the fluid velocity in the analytical column packed with a 10 μm stationary phase yielding the data shown in Fig.4.8. These can be linearly regressed in a rather accurate way, as illustrated in the same Fig.4.8. In the following, to describe pressure drop as a function of column length, fluid velocity, and packing characteristics, we will use the Ergun equation:

$$\Delta p = \frac{K_p \cdot L \cdot u}{d_p^2} \tag{4.3}$$

The parameter K_p has been estimated from the experimental data in Fig.4.8, and its value is equal to $8.32*10^{-6}$ bar*cm. Using the Ergun equation, the pressure

drop behavior of columns packed with the same material of a different average particle size can be predicted.
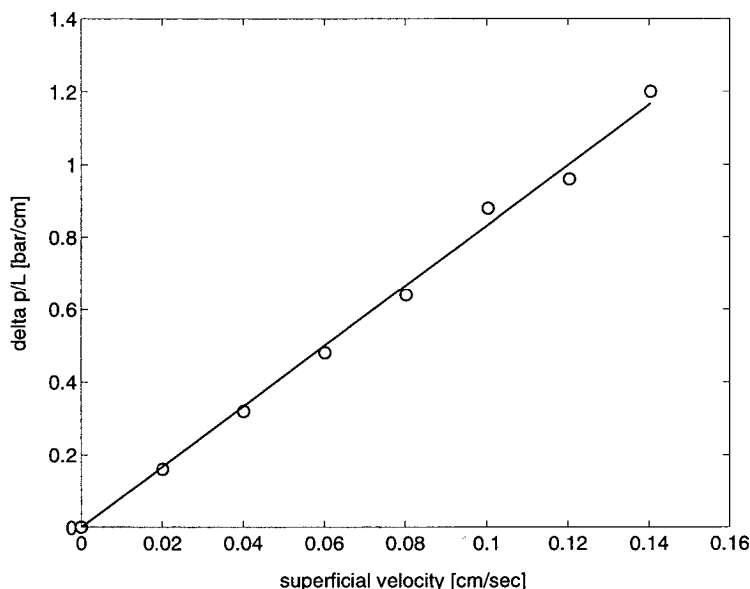

Fig. 4.8: Measurement of the pressure drop for a 250x4.6 mm AD column and 10 μm particles.

As discussed with reference to Figs 4.2 and 4.3, column efficiency can be quantified in terms of HETP, which in turn can be expressed in terms of fluid velocity using the van-Deemter equation and in terms of the particle size using the Chung and Wen equation, thus yielding the relationship that will be used in the following:

$$HETP=dp/0.2+C*u*dp^2 \tag{4.4}$$

4.6.3 Design of a SMB unit for the separation of 50 t/a of the racemate

The approach we follow to design an optimal SMB unit for the desired separation consists of two steps. First, an optimization routine [21] based on a true moving bed (TMB) model is used. This allows to define optimal dimensions of the unit and operating conditions for the separation. Optimal conditions mean in this context that the highest productivity can be achieved for the given purities in the extract and in the raffinate and the given process specifications. Subsequently a simulated moving bed (SMB) model is used to check that the same performance achieved in the TMB unit can be achieved also in the equivalent SMB unit. If this happens, then the design is complete; if not, a new optimization using directly the SMB model has to be carried out. Both the SMB and the TMB model account for the same physical phenomena, including axial dispersion and mass transfer resistance

The input information for the optimization routine are as follows:

1. Purity specification in the extract and raffinate
2. Pressure drop relationship (Ergun equation, eq. (4.3))
3. Maximum pressure drop
4. HETP relationship (Van-Deemter equation, eq. (4.4))
5. Adsorption isotherms
6. Feed composition
7. Particle size
8. Unit configuration (number of columns per section)
9. Unit capacity

The results obtained using the optimization routine are summarized in Fig. 4.9. As it can be observed, a column length of 18 cm has been determined and from the given production rate a column diameter of 104 cm has been calculated. The value of the productivity, defined as the yearly production rate per unit volume of the SMB unit, is of 41 t/m^3/a.

Table. 4.2: Overview scheme for the separation of a SMB plant with 8 columns

Design of a SMB plant

Criteria:		Unit:	Descriptions:
Maxim. pressure dop			
of the SMB plant:	64	[bar]	
Production per year:	50	[t/a]	300 working days per year
Particle diameter:	0.002	[cm]	
Feed concentration:	30	[g/l]	Racemate 1 und 2

The following quantities are set to the values at the beginning:

m1 (zone1):	1.89	H_A*S1 (S1=1.3,H_A=1.44)
m4 (zone4):	0.92	H_B*S2 (S2=0.8,H_B=1.15)
Number of columns:	8	
in zone 1 und 4:	2	
in zone 2 und 3:	2	

Optimized quantities:

Length of a column:	18	[cm]
Lengths of all columns:	143	[cm]
m2 (zone2):	1.11	
m3 (zone3):	1.245	

Calculated quantity
Maxim. flow velocity

in zone1:	0.216	[cm/sec]

Quantity to be fitted:

Column diameter:	104	[cm]

Data for the design of a SMB plant:

Cross sectional area:	8.4E+03	[cm^2]	
Volume of a column:	1.5E+05	[cm^3]	
Total SMB volume:	1.2E+06	[cm^3]	
Eluent stream in zone1:	1.1E+05	[ml/min]	Maxim. eluent stream
Switching time:	1.79	[min]	
Eluent stream in zone2:	8.7E+04	[ml/min]	
Eluent stream in zone3:	9.1E+04	[ml/min]	
Eluent stream in zone4:	8.2E+04	[ml/min]	

Outlet and inlet streams:

Extract stream:	2.2E+04	[ml/min]
Raffinate stream:	9.3E+03	[ml/min]
Feed stream	3.9E+03	[ml/min]

Productivity:	41	[t/m^3/a]

Running a SMB simulation using the data calculated for the equivalent TMB unit and reported in Fig.4.9 yields purity values of 99.8% and 99.3% in the raffinate and in the extract, respectively. This is considered acceptable, and the design is complete. Using the detailed SMB model further information about the start-up of the process can be achieved, as well as about the concentration profiles in the unit. These are illustrated in Figs 4.9 and 4.10, respectively. In Fig. 4.9, it can be observed that the steady-state of this SMB process is reached after about 250 switches, which means 31 cycles. Note that the concentration of the undesired

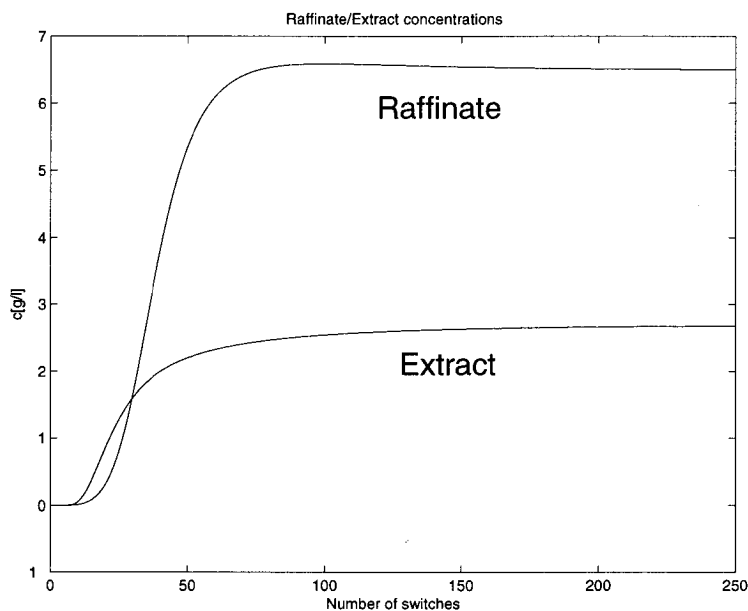enantiomer in the two product streams is so small that it cannot be seen in this scale.

Fig. 4.9: Concentration in the extract and in the raffinate as a function of the number of switches for the SMB design in Table 4.2

Fig.4.10 shows the concentration profile of Enantiomer1 and 2 after 250 switches and immediately before the next switch for the SMB process.
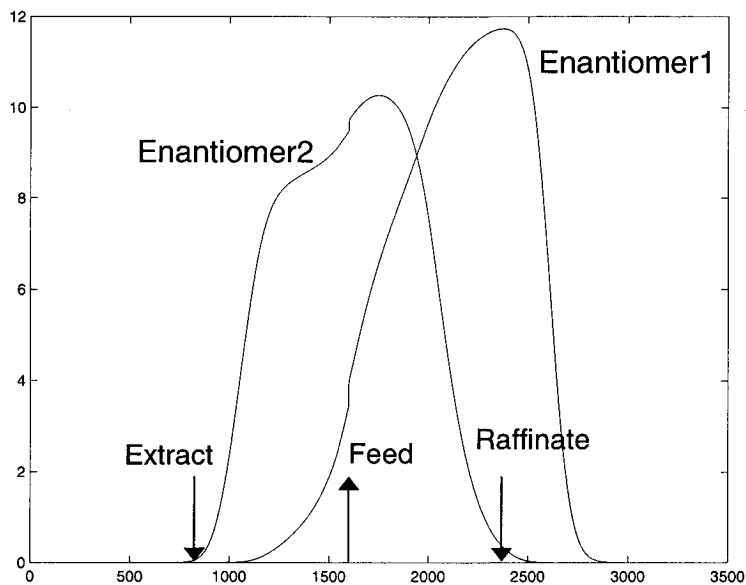

Fig. 4.10: Profiles of Racemate 1 and 2 in the SMB plant for the SMB process based on the data given in Table 4.2. X-axis: Grid points, y-axis: concentration [g/l]

It is instructive to verify the validity of the design criteria based on the dimensionless groups m_j, where column size, flow rates, and switch time are

brought together in a single scalable quantity. We have done this, by checking a different SMB unit configuration where the number of columns has been reduced from 8 to 6, so that only one column is left in sections 1 and 4. In order to keep the same m_j values, the column length is increased from 18 to 24 cm and accordingly the switching time is increased from 1.79 min to 2.44 min, while all the other design data are kept constant. Actually, it is found that the same high purities can be achieved as where 8 columns are used.

It is also interesting to compare the operating conditions calculated using the detailed model and the optimization routine, and those predicted through the equilibrium theory approach. Fig.4.11 shows the calculated complete separation triangle (30 g/l overall feed concentration) in the m3/m2-diagram, together with the operating point corresponding to the calculated optimal operating conditions (point 3, circle). As expected, this operating point is shifted to the right with respect to the vertex of the triangle , i.e. the theoretical optimal point where the highest productivity is to be expected. If points closer to the vertex of the triangle are considered, i.e. point 2 (box) and point 1 (diamond) it is expected that productivity increases, whereas purities decrease. This can be checked using the detailed SMB model. In point 1, the productivity can be increased of about +12%, whereas the purity in the extract is only 98.6%, and the purity in the raffinate is still at 99.8%. In the case of the operating point 2 we obtain an increase of the productivity of about +6%, a purity in the extract of 99.1%, and a purity in the raffinate of 99.8%. It can be concluded that the optimal operating conditions are more robust in terms of raffinate purity than in terms of extract purity.
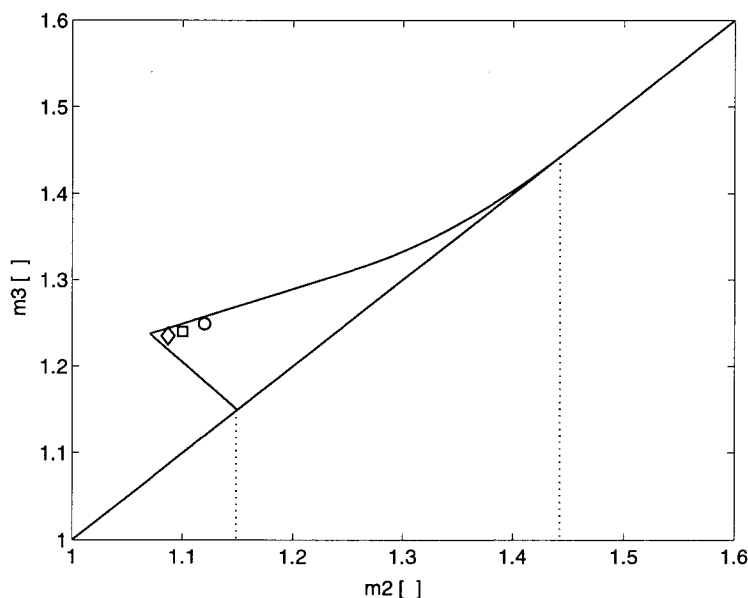

Fig. 4.11: m3/m2-diagram for the Racemate at a total concentration in the feed of 30g/l and three combinations of m3/m2-values indicated by symbols. (◊) 1. m3/m2: 1.087/1.235, (□) 2. m3/m2: 1.1/1.24, (O) 3. m3/m2: 1.11/.1245 (calculated by the optimization routine)

Finally, Table 4.3 summarizes the design parameters of the optimal SMB calculated in this chapter.

Table 4.3: Design data of a SMB unit for the separation of 50 t/a Racemate

Maximum pressure drop in the SMB plant [bar]	64
Particle diameter [μm]	20
Number of columns in the SMB plant	6
Diameter of the columns [cm]	104
Length of a column [cm]	24
Volume of the SMB plant [m^3]	1.25
Production rate of the Racemate mixture [t/a]	50
Eluent consumption per production of the Racemate mixture [l/g]	0.273
Productivity [t/m^3/a]	41
Purity of Enantiomer1 in the Raffinate [%]	99.8
Purity of Enantiomer2 in the Extrakct [%]	99.3
Yield of Enantiomer1 [%]	99.4
Yield of Enantiomer2 [%]	99.7

5. Deviations between Experimental and Simulated Elution Profiles on RP

In this chapter we reconsider some details of the results discussed in the previous three chapters that may lead to some interesting conclusions of some fundamental nature. We refer to the deviations between experimental and simulated concentrations in the eluted streams under overloaded conditions, that have been observed in section 2.6, in the case of reversed phase chromatography, which contrast with the excellent agreement between the calculated and experimental data obtained when using either silica gel or a chiral stationary phase (chapter 3 and 4). In particular, in the case of overloaded pulses on reversed phase the experimental curve shows a significant stronger tailing and a lower peak height than the simulated one. Although, the same procedure and the same accuracy was used for this study, as in the case where silica gel or the chiral phase were used, it was not possible to improve the quality of the agreement between model calculations and experimental data. We deep this analysis in the following by considering in detail all possible sources of such an error: the presence of impurities, dead volume effects, model inaccuracies and finally the dependence of mass transfer coefficients on the mixture composition.

5.1 The role of impurities on elution profiles

In the adopted mixture AD is the main component and has a mass fraction of about 96%, while each of the byproducts (NP1 and NP2) has a mass fraction of about 2%. These two components exit the column on the tail of the chromatography pulse, and therefore could be responsible for the stronger tailing measured experimentally. The model in fact assumes that the pulse fed to the column contains only AD. In order to investigate this point, in Fig.5.1 the calibrated on-line UV-signal measured at the column outlet is compared with the concentration values obtained off-line by analyzing fractionated samples of the outlet stream. In particular, the circles represent the concentration of AD alone, while the squares that of AD and the two impurities NP1 and NP2 together. It is seen that the presence of the two impurities does not really affect the tail of the measured peak profile. This conclusion can also be confirmed through simulations using the model developed in chapter 1 of an overloaded peak profile. In Fig.5.2, the simulation performed assuming only a single component, i.e. AD, present in the feed and the simulation performed assuming AD, NP1 and

NP2 in the feed, but with the same total concentration, being 0.98, 0.02 and 0.02 the percentage composition, are compared. Since again only a small difference has been evidenced we can conclude that the fact that in the simulation NP1 and NP2 were assimilated to AD cannot be taken as a justification for the mismatch between simulations and experimental data observed in the tails of the overloaded peak profiles.
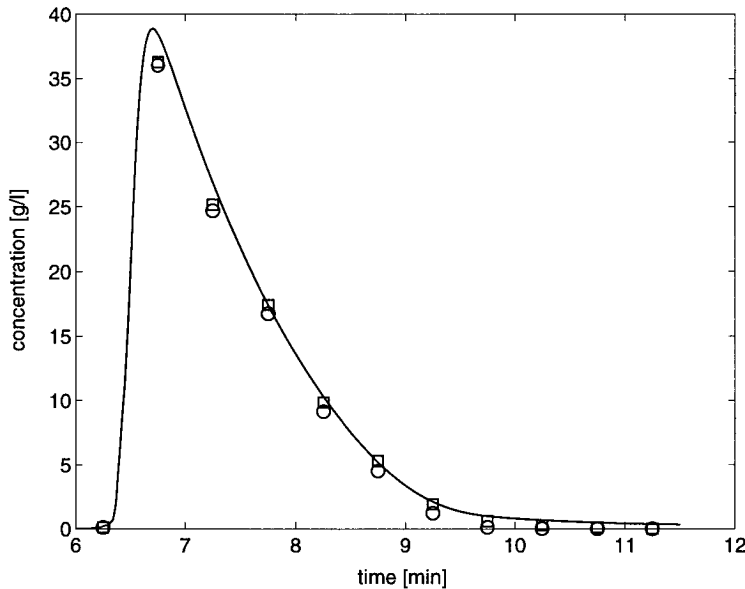
Fig. 5.1: Plot of the calibrated on-line UV signal and of the results of the off-line analysis of the fractionated samples; (O) concentration of AD alone, (□) total concentration of AD, NP1 and NP2.
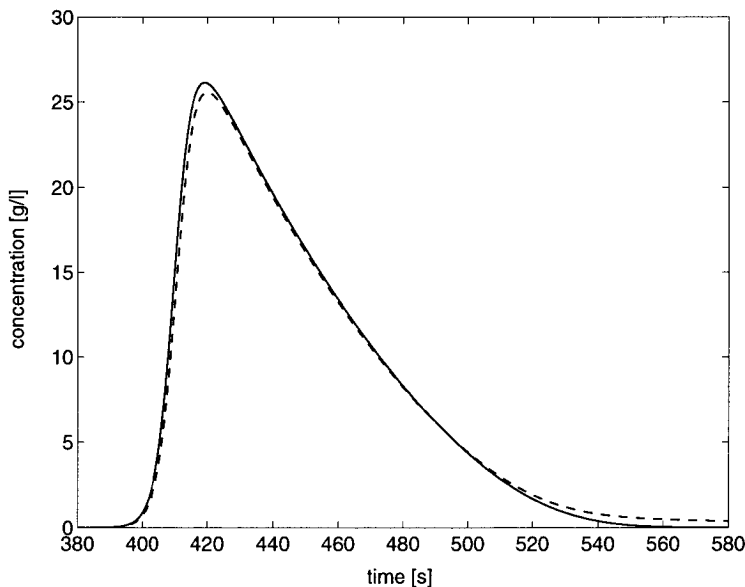
Fig. 5.2: Simulations of an overloaded peak profile of AD. Injected amount: 250 μl, (—) single component AD, injected concentration: 50 g/l, (--) ternary system: injected concentration of AD, NP1 and NP2=48, 1, 1 g/l.

Another aspect worth considering is the possible presence of other impurities, particularly of ionic nature. As mentioned above, in the overloaded pulse experiments the UV signal was detected at large wave lengths (320 nm) in order to avoid a saturation of the detector by AD. However, at such high wavelengths, impurities as ionic substances can strongly affect the sample response due to their strong UV absorption. In other words, such impurities are present in very small amounts in the mixture and thus cannot be detected at low UV wavelengths. However, their presence may affect significantly the overall UV signal at high wavelengths. Fig.5.3 shows the calibrated on-line UV-signal of the outlet stream at the high wavelength. It is seen that in front of the overloaded peak profile at lower retention times appear some impurities indicated by a small peak in the UV signal. In this case the impurities are well separated from the peak profile of AD, but obviously in the case of the frontal analysis shown for example in the Figs.5.18-5.20, where the signals due to the add to that due to AD, thus are introducing some errors in the experimental evaluation of the AD concentration profile by ignoring the presence of such impurities.
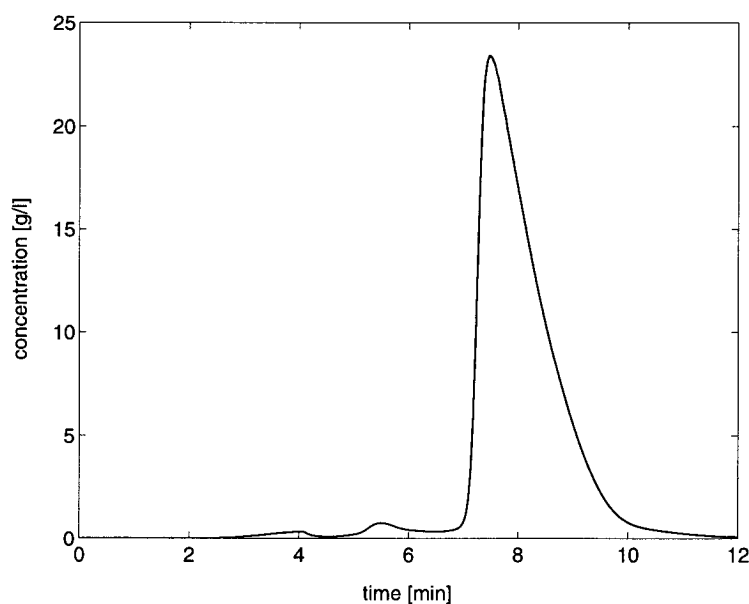

Fig. 5.3: Plot of a calibrated on-line UV signal of AD at a high wavelength of 320 nm.

That is, since the on-line UV signal at the plateau of the frontal analysis is the sum of the UV absorption of AD and of the impurities, a calibration of this signal, which attributes this value to AD alone, leads to a falsified shape of the breakthrough curve. To analyze such effect more in detail, we consider the UV signal at the column outlet shown in Fig.5.4, and assume that the dotted line represent the contribution of the impurity. This value has been subtracted from the original signal and the obtained values have been calibrated using the concentration of 50 g/l for the plateau of the signal. The so obtained corrected values (squares) have been compared in Fig.5.4 with the original ones (circles). It

is seen that this correction does not significantly affect the shape of the breakthrough curves. As a conclusion, in the following we are entitled on the one hand to assimilate the impurities NP1 and NP2 to AD, and on the other, when considering the breakthrough profiles measured by frontal analysis, to ignore the impurities affecting the first part of the breakthrough curve.
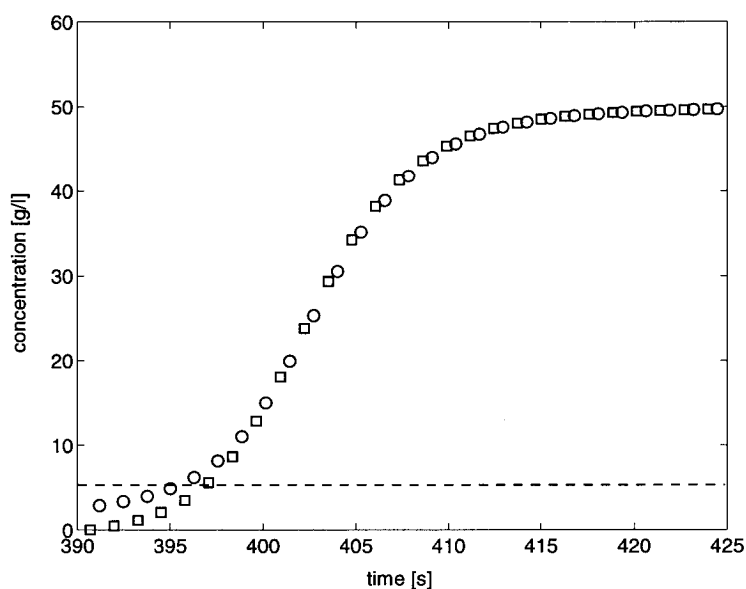

Fig. 5.4: Breakthrough curves of AD at a concentration of 50 g/l, see Fig.5.18. (O) Original calibrated UV-detector signal, (□) UV-detector signal calibrated after correcting the UV-signal by the presence of impurities, indicated through the horizontal dotted line.

5.2 Influence of "extra-column" effects on the elution profile

Parts in the HPLC station such as valves, tubes and connections upstream of the column as well as the detector cell downstream of the column can have a significant effect on the elution profiles. Remixing-effects caused by such parts are in fact equivalent to a decrease of the column efficiency. The influence of such parts for the HPLC station used in this work can be demonstrated by injecting a sample after having removed the column. Fig.5.5 shows the on-line UV-detector signal corresponding to an injection of a 250 μl-sample with a low concentration of AD. The injected sample leaves the HPLC system after a retention time due entirely to the parts of the HPLC station mentioned above. As a comparison, in Fig.5.5 the rectangular injection signal is indicated through the dotted lines. It is apparent that these accessory parts of the HPLC station are also responsible for a significant broadening of the rear part of the band profile, which clearly indicates significant remixing effects.
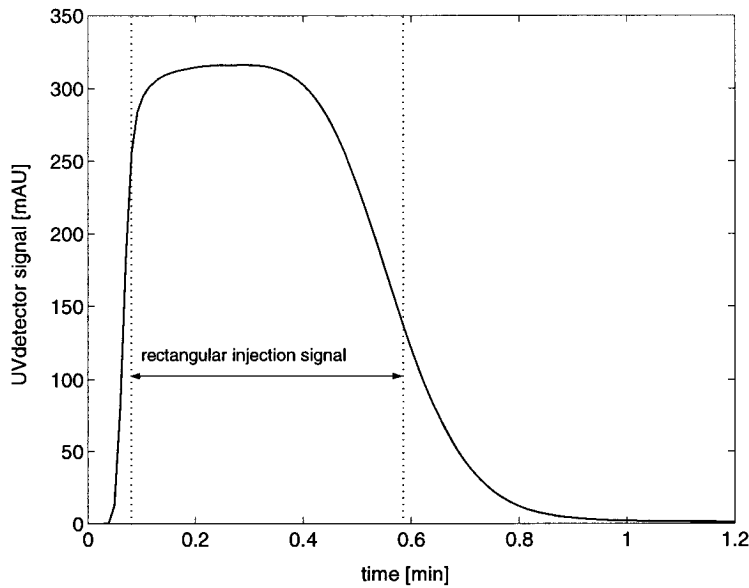
Fig. 5.5: On-line UV-detector signal of a 250 μl injection of an AD sample at low concentration, when the column is removed. Flow-rate: 0.5 ml/min, hold-up volume of the HPLC station: 40 μl

Such remixing-effects can be conveniently simulated introducing two CSTs, (continuous stirred tank), one up- and the other downstream of the column:

$$\frac{dc_i}{dt_i} = \frac{Q}{V_{CSTR}}\left(c_{in,i} - c_{out,i}\right)$$

(5.1)

Fig.5.6 shows a comparison of the simulation results for an overloaded peak profile, obtained using the chromatographic model described in section 2 of chapter1 with and without the two CSTs up- and downstream of the column. It is seen that the use of CSTs in the chromatographic model has two effects: 1. the peaks are shifted to longer retention times to an extent equal to the total residence time in the CSTs. 2. the overloaded peaks show a less steep front and a stronger tailing, which corresponds to a lower efficiency

One typical way to account for these extra-column effects is to measure the van-Deemter plots in the presence of the column and then to introduce an overall axial dispersion coefficient in the model. In order to verify the reliability of this approach we compare the elution peaks calculated by two models: one accounting for the two CSTs, and the other for the increased axial dispersion coefficients (with properly corrected retention times). For this the realistic parameter values reported in the caption of Fig.5.6 have been used, and two pulse experiments have been simulated. One is an overloaded pulse with an injection volume of 500 μl and an injection concentration of 50 g/l, and the other is a diluted pulse 20 μl and 1 g/l, respectively. The obtained comparison is shown in Fig.5.6 and 5.7. As it can be seen in Fig.5.7, in the case of a diluted pulse the

additional band broadening caused by the CSTs can be well described through an increase of the axial dispersion coefficient. In particular, the value of the axial dispersion coefficient has been increased from $1.4*10^{-2}$ to $2.25*10^{-2}$ cm*u.
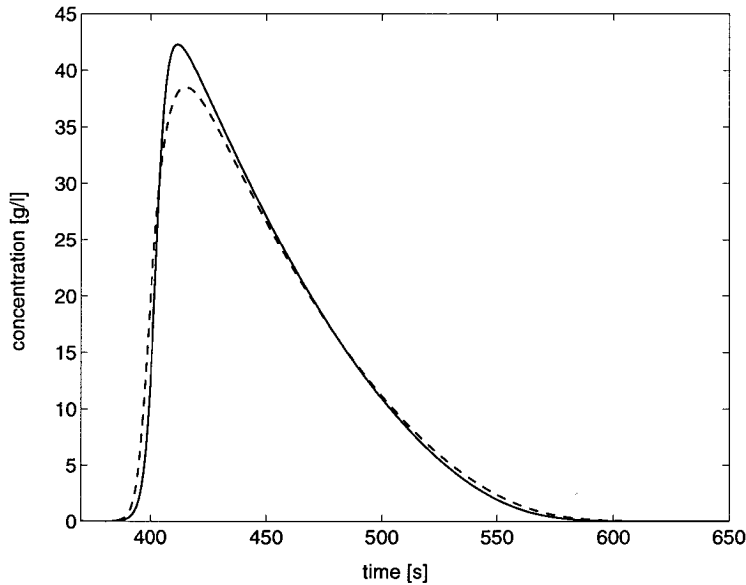

Fig. 5.6: Effect of CSTs and D_{ax} on peak broadening for an overloaded pulse. (—) Simulation without CSTs and modified axial dispersion coefficient of $D_{ax}=2.25*10^{-2}$ cm*u, (--) simulation with a CSTR up- and downsteam, $V_{CST1,2}=0.2$ µl
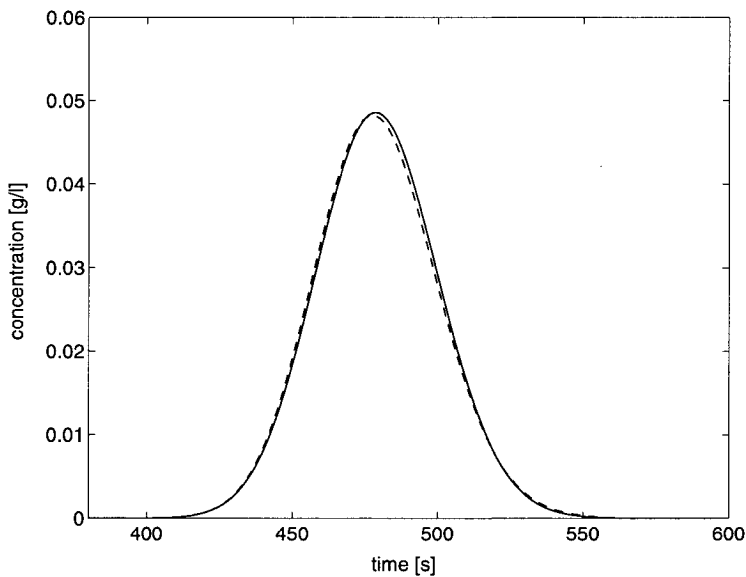

Fig. 5.7: Effect of CSTs and D_{ax} on peak broadening for a diluted pulse. (—) Simulation without CSTs and modified axial dispersion coefficient of $D_{ax}=2.25*10^{-2}$ cm*u, (--) Simulation with a CSTR up- and downstream, $V_{CST1,2}=0.2$ µl and original $D_{ax}=1.4*10^{-2}$ cm*u.

In the case of an overloaded pulse, as shown in Fig.5.6 the calculated peak profiles move from each other, and the CSTs cause a stronger tailing than what can be described through an increased axial dispersion coefficient. Therefore we conclude that under overloaded conditions the influence of significant extra column dead volumes cannot be taken into account correctly by using an increased axial dispersion coefficient.

In order to better investigate the role of extra column remixing-effects on peak profiles, we can change the feed system to the column. In practice, instead of using the injection loop, the second pump (pump B) of the HPLC station, schematically represented in Fig.5.8, can be employed to feed a sample to the column. This can be done by switching from pump A to pump B for the duration of the sample feed, being the eluent fed by pump A and the sample by pump B. While the hold-up volume of the HPLC station is only 40 µl when the injection loop feed system is used, this value becomes about 800 µl when using the pump switching feed system due to much longer connecting tubes and a third, high-pressure pump (pump C in Fig.5.8) with additional hold-up volume (from the T-connector to column inlet). As a result, a sample, which is injected employing the pump switching feed system, takes a much longer way to the column inlet, passing the T-connector and being broadened by the pump C. Figs.5.9 and 5.10 show the influence of these parts of the HPLC station on overloaded peak profiles, for the silica gel and for the reversed phase system as described in chapters 2 and 3. Two overloaded peak profiles were measured for each of both stationary phase systems, one by using the injection loop feed system and the other using the pump switching feed system. To get a clear comparison of the influence of both injection systems on the broadening of the overloaded peak profiles, the time values for the data obtained with the pump switching system have been corrected for the larger average hold-up time.
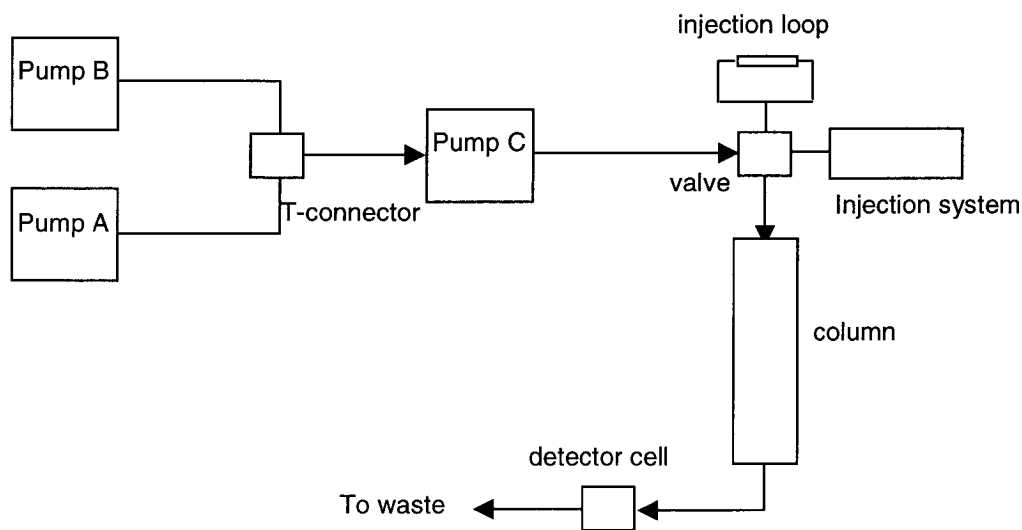

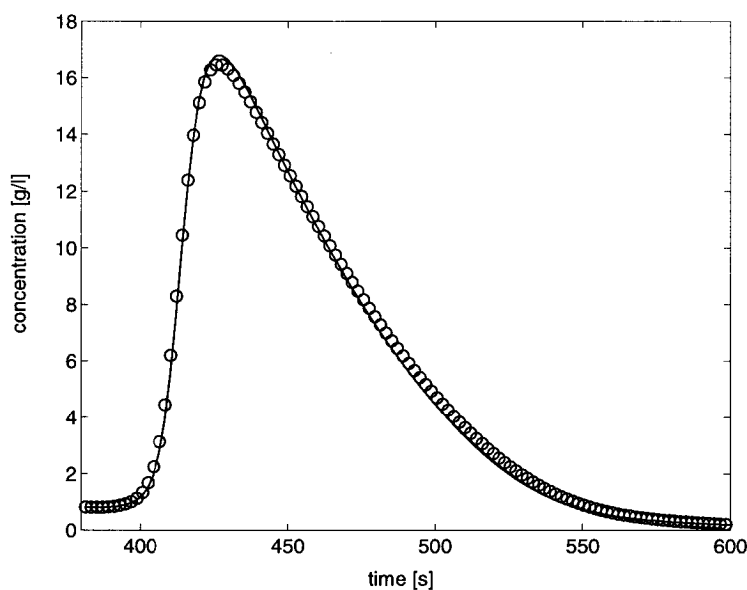Fig. 5.8: Schematic representation of the HPLC experimental station

Fig. 5.9: Experimental peak profiles of AD on RP C18 30 μm in MeOH/H$_2$O: 80/20 v/v%. Injected concentration: 50 g/l, injected amount: 200 μl, flow-rate: 0.5 ml/min; (—) injection loop feed system, (○) pump switching feed system.
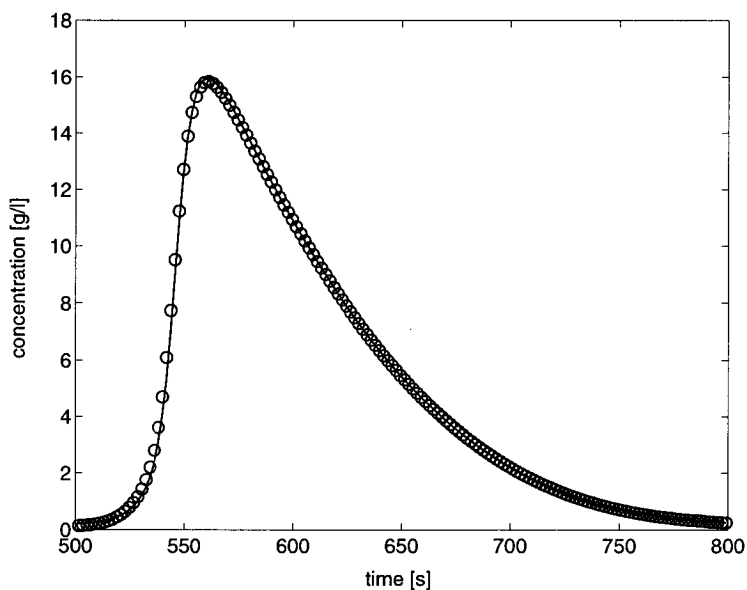

Fig. 5.10: Experimental peak profiles of AD on Sil YMC 40 μm in ethylacetate. Injected concentration: 50 g/l, injected amount: 200 μl, flow-rate: 0.5 ml/min; (—) injection loop feed system, (○) pump switching feed system.

It is evident from Figs.5.9 and 5.10 that the parts of the HPLC station upstream of the column do not have a strong influence on the peak shapes. No difference can be observed for the peak profiles on silica gel, while a slight deviation on reversed phase is visible. All things considered, possible remixing-effects and additional band broadening effects on overloaded peak profiles, due to extra-column dead volumes upstream the column, can be neglected. Remixing effects

in the detector cell downstream of the column are also insignificant, as seen from Fig.2.5 in chapter 2: here the off-line analysis of the fractionated samples, which bypassed the detector cell, and the on-line UV signal are in excellent agreement.

In addition to the investigations described above, we checked the influence of the column inlet and outlet frits on the peak shapes, these frits operate like a filter. For this purpose, a part of the frit system of the RP column (see chapter 2), which is constituted of several layers of thin filters, has been removed. This has the effect of a significant decrease of the pressure drop, since the frit system was used for a long time and was partly plugged up. Fig.5.11 shows an overloaded peak profile measured by utilizing the total frit system compared to that measured after the removal of parts of the frit system. It is apparent from Fig.5.11 that the frit system, located at the column inlet and outlet, does not have a significant influence on the shape of the peak profiles.

We can come to the conclusion that for the experimental station and the operating conditions used in this work the shape of the peak profiles is mainly influenced through "inner-column" effects, namely adsorption, kinetics and dissipative phenomena.
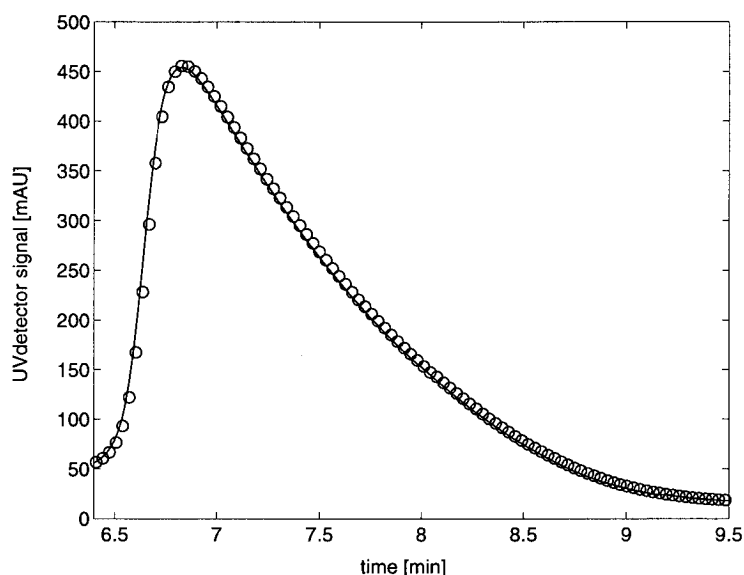

Fig. 5.11: Overloaded peak profiles on MN RP C18 30 μm column, (—) total frit system, (--) frit system partly removed.

5.3 Role of the accuracy of the chromatographic model

As described in section 1.2, we have used the so-called lumped pore diffusion (POR) model to describe mass transfer in the chromatographic column. In this model an average pore concentration is assumed, which is assumed in equilibrium with the adsorbed phase. The difference between this average pore concentration and the liquid bulk concentration is the driving force for the mass transfer process. The corresponding lumped mass transfer coefficient includes film and pore diffusion. In the following, we discuss several possible refinements of this model in order to assess its reliability.

5.3.1 The pore diffusion model

The most serious approximation in the adopted pore diffusion model is the linear driving force assumption for mass transfer. In order to test the reliability of the predictions of this model a comparison has been made with a refined version of the same model where an additional space variable, i.e. the particle radius, has been introduced [22]. Accordingly, the entire concentration profile inside the packing material has been computed. Considered the non-linearity of the adsorption equilibria under consideration and the relatively large particle size of the adopted preparative packing material, such a refinement of the model could lead to a more accurate prediction of the elution profiles. The pore diffusion model is constituted of a set of mass balance equations, where Eq.5.2 is the overall mass balance along the column axis, Eq.5.3 represents the inter-phase between the bulk and the pore phases, while Eq.5.4 describes the mass balance inside the pores.

$$\varepsilon_b \frac{\partial c_i}{\partial t} + (1 - \varepsilon_b) \frac{\partial \overline{q}_i}{\partial t} + u \frac{\partial c_i}{\partial x} = \varepsilon_b D_{ax,i} \frac{\partial^2 c_i}{\partial x^2} \tag{5.2}$$

$$\frac{\partial \overline{q}_i}{\partial t} = \frac{3}{R_p} \varepsilon_p D_p \left. \frac{\partial c_i^p}{\partial r} \right|_{R_p} = \frac{3}{R_p} k_f \left(c_i - c_i^p \big|_{R_p} \right) \tag{5.3}$$

$$\varepsilon_p \frac{\partial c_i^p}{\partial t} + (1 - \varepsilon_p) \frac{\partial q_i}{\partial t} = \varepsilon_p \frac{D_p}{r^2} \frac{\partial}{\partial r} \left(r^2 \frac{\partial c_i^p}{\partial r} \right) \tag{5.4}$$

In this model the overall mass transfer resistance is described by the film mass transfer coefficient k_f and the pore diffusion D_p, which operates in series. The

lumped mass transfer coefficient k_m of the linear driving force approximated model, which also appears in the HETP-equation (Eq.1.6, chapter 1), is related to the parameters above as follows:

$$\frac{1}{k_m} = \frac{R_p}{3k_f} + \frac{R_p^2}{15\varepsilon_p D_p}$$

(5.5)

Since in all considered simulations the contribution of the film resistance to the overall mass transfer resistance is negligible, and the pore diffusion coefficient can be calculated from the lumped mass transfer coefficient, estimated from the van-Deemter plot, as follows:

$$D_p = \frac{R_p^2 k_m}{15\varepsilon_p}$$

(5.6)

The simulations of an overloaded peak profile using the two models are compared in Fig.5.12. It is seen that both models lead to nearly the same elution profiles. This has been confirmed for large varieties of the input parameter values, leading to the conclusion that the lumped linear driving force approximation is sufficiently accurate for the situations here examined.
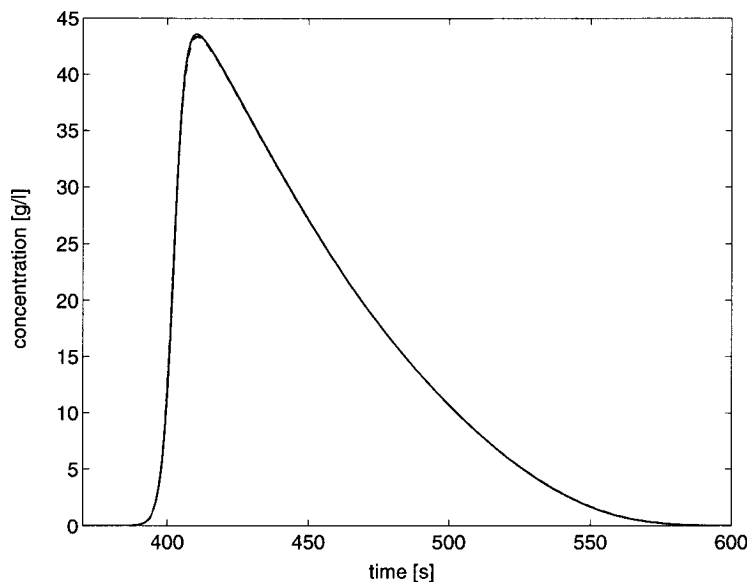

Fig. 5.12: Comparison of the pore diffusion and lumped pore diffusion model with the help of the simulation of an overloaded peak profile. (—) Lumped pore diffusion model, (--) pore diffusion model; Input parameter for the simulations: Injected concentration: 50 g/l, injected amount: 500 µl, flow-rate: 0.5 ml/min, Langmuir isotherm: H=1.84, q_s=175 g/l, k_m=3.5 1/s, D_{ax}=1.4*10^{-2} cm*u, column dimension: 250x4 mm.

5.3.2 The parallel diffusion model

A second improvement of the adopted lumped pore diffusion model is to account also for surface diffusion [23], which means to use the parallel diffusion model [24]. The surface diffusion describes a process, in which a molecule interacting with an adsorption site diffuses directly to the next free adsorption site without taking the step of pore diffusion. This process can be seen as a "creeping" or "hopping" mechanism and can be observed often for macromolecules. A complete expression of the lumped mass transfer coefficient, k_m, is given by Eq.5.7:

$$\frac{1}{k_m} = \frac{R_p}{3k_f} + \frac{R_p^2}{15\left(\varepsilon_p D_p + \left(1-\varepsilon_p\right)D_s \dfrac{dq}{dc_i^p}\right)} + \frac{1-\varepsilon_p}{K_a}\frac{H^2}{\left(\dfrac{dq}{dc_i^p}\right)^2} \tag{5.7}$$

The first term on the rhs of Eq.5.7 describes the mass transfer resistance by film diffusion at the surface of the particle, the second one takes into account the contribution of pore and surface diffusion and the third the resistance due to the adsorption kinetics. Usually the adsorption/desorption kinetics is a very fast process and the third term in Eq.5.7 can be neglected. Likewise, as mentioned above, negligible the influence of the film diffusion on the overall mass transfer resistance with the result that only the second term of Eq.5.7 is relevant. The surface diffusion is both temperature and concentration dependent, as given by the following relation in the case of a Langmuir isotherm:

$$D_s = \frac{D_s^0}{1-\theta} = \frac{D_s^0}{1-\dfrac{q}{q_s}} \tag{5.8}$$

$$\Rightarrow D_s = D_s^0\left(1+\frac{H}{q_s}c\right) \quad \text{(Langmuir mod el)}$$

which substituted in Eq.5.7 leads to:

$$\frac{1}{k_m} = \frac{R_p^2}{15\varepsilon_p D_p + 15\left(1-\varepsilon_p\right)D_s^0 \dfrac{H}{1+\dfrac{H}{q_s}c}} \tag{5.9}$$

In contrast to the lumped pore diffusion and to the pore diffusion model, the parallel diffusion model takes into account the non-linearity effects at high concentrations, which in the case of a Langmuir isotherm lead to a decrease of k_m and then of the column efficiency. In order to compare the prediction of the

difference between the lumped pore diffusion model and the parallel diffusion model, we have to fix realistic values for the pore diffusion D_p and for the surface diffusion D^0_s. For this we took $D_p=9*10^{-8}$ cm^2/s and estimated D^0_s so as to reproduce under diluted conditions, i.e. c=0, the experimental value of $k_m=3.5$ 1/s. A value of $4.7*10^{-7}$ cm^2/s for the surface diffusion has been found. For these calculations we have used the Langmuir parameter as given in section 2.6.3. The results of the parallel diffusion model are compared with those of the lumped pore model with $k_m=3.5$ 1/s in Fig.5.13. From the simulated overloaded peak profiles it is seen that also the introduction of the contribution of surface diffusion does not significantly affect the lumped pore model predictions.
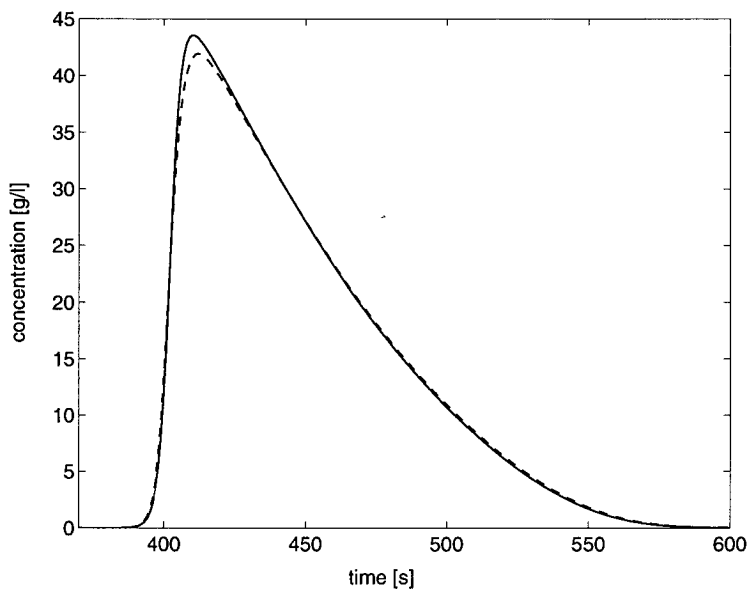

Fig. 5.13: Comparison between the parallel diffusion (--) and the lumped pore diffusion model (—); Input parameter see caption of Fig.5.12, $D_p=8.9*10^{-8}$ cm^2/s, $D^0_s=4.7*10^{-7}$ cm^2/s

5.3.3 The kinetic model

For completeness, also the case where the adsorption/desorption kinetics are the rate determining step has been investigated [25]. In this case mass transfer resistances can be neglected and the chromatographic model reduces as follows:

$$\varepsilon \frac{\partial c_i}{\partial t} + (1-\varepsilon)\frac{\partial q_i}{\partial t} + u \frac{\partial c_i}{\partial x} = D_{ax,i}\frac{\partial^2 c_i}{\partial x^2} \tag{5.10}$$

$$\frac{\partial q_i}{\partial t} = k_{ads,i} c_i \left(q_i^s - q_i\right) - k_{des,i} q_i \tag{5.11}$$

where $k_{ads,i}$ and $k_{des,i}$ represent the adsorption and desorption rate, respectively, of component i. At equilibrium, Eq.5.11 leads to:

$$\frac{c_i \left(q_i^s - q_i\right)}{q_i} = \frac{k_{des,i}}{k_{ads,i}} = K_i \tag{5.12}$$

where K_i represents the equilibrium constant of component i.
Under diluted conditions, $q_i \ll q_i^s$, Eq.5.12 can be further simplified to:

$$K_i = \frac{c_i \, q_i^s}{q_i} \quad \Rightarrow \quad c_i = \frac{q_i K_i}{q_i^s} = H_i q_i \tag{5.13}$$

So the Henry constant is given by $H_i = K_i/q_i^s$ and its value determines the ratio of the desorption and adsorption rate constants, i.e. $k_{des}/k_{ads} = q_i^s H_i$. On the other hand, the absolute values of the desorption and adsorption rate constants control the kinetics of the process: if k_{des} and k_{ads} are increased, both adsorption and desorption become faster. This is the role of the lumped mass transfer coefficient in the lumped pore diffusion model. As it can be seen in Fig.5.14, an analytical peak can be predicted in the same way by using the lumped pore diffusion model as well as the kinetic model, using the parameter values as given in the caption of Fig.5.14 in addition to $k_{ads}=0.0148$ and $k_{des}=1.4076$ for the kinetic model. When extrapolating the same conditions to an overloaded pulse the results shown in Fig.5.15 are obtained. It is concluded that also in this case the differences in the model results are marginal.

We can then conclude that the mismatch between experimental and modeling results mentioned above cannot be attributed to model errors. Accordingly, due to its simplicity, the lumped pore diffusion model is used in the following.
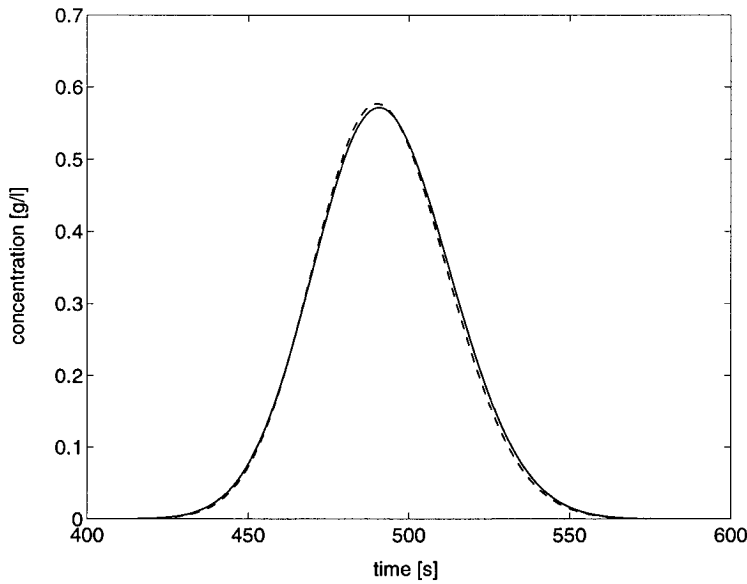
Fig. 5.14: Simulation of an analytical peak. (—) Lumped pore diffusion model, (--) kinetic model, k_{ads}=1.4076, k_{ads}=0.0148. Input parameter for the simulations: injected concentration: 1g/l, injected amount: 250 μl, flow-rate: 0.5 ml/min, Langmuir isotherm: H=1.84, q_s=175 g/l, k_m=3.5 1/s, D_{ax}=1.4*10^{-2} cm*u, column dimension: 250x4 mm.
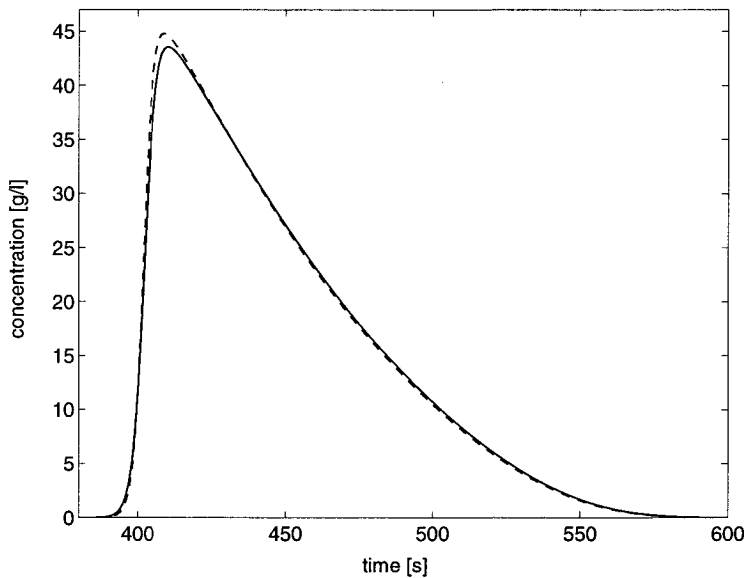

Fig. 5.15: Comparison of the lumped pore diffusion model and the kinetic model with the help of the simulation of an overloaded peak profile. (—) Lumped pore diffusion model, (--) kinetic model k_{ads}=1.4076, k_{ads}=0.0148; Input parameter for the simulations as given in caption of Fig.5.12 with the exception of: Injected concentration: 50 g/l, injected amount: 500 μl.

5.4 Determination of the mass transfer kinetic on reversed-phase

In this section we examine the feasibility of describing the mismatches mentioned above by considering the possible dependence of the mass transfer rate constant on concentration. For the simulations of overloaded peak profiles described in chapter 2, in fact the lumped pore diffusion model has been used with a constant mass transfer coefficient evaluated under diluted conditions. However, in the literature several references [26,27,28,29] indicate a possible concentration dependence of the mass transfer rate constants. In this chapter we use frontal analysis and the perturbation method, in order to see if the mass transfer coefficient changes with concentration.

5.4.1 Description of the procedure to investigate the mass transfer kinetics

As discussed in chapter 1, in the adopted chromatographic model the dissipative phenomena are taken into account through an axial dispersion and a mass transfer coefficient. In the frame of the developed general procedure, these are measured at very low concentrations using the classical method of the van-Deemter plot. In this chapter, in order to determine a possible concentration dependence of the mass transfer coefficient, we use both the frontal analysis [3] and the perturbation method [17]. In the first one a rough estimate of the mass transfer coefficient can be obtained fitting the mean region of the breakthrough curve [30], and attributing it to the half of the concentration value of the plateau. In the perturbation method, the column equilibrated at a certain concentration is disturbed with a very low amount of the pure eluent and the mass transfer coefficient is fitted to the negative peak measured at the column outlet. The perturbation method has the advantage to estimate the mass transfer coefficient at a constant solute concentration, but the disadvantage of a difficult reproducibility, since the width of the perturbation peaks is difficult to measure due to the very low amount injected. The frontal analysis is a more robust method to determine the mass transfer coefficients, but here the entire range of solute concentration values, from zero to the plateau value are involved in determining the rate of mass transfer kinetics during the experimental run. Therefore in this case a continuous dependence of the mass transfer coefficient on local concentrations has to be postulated in order to reconstruct correctly the measured breakthrough curves. In the following, we apply both methods to reliably determine the mass transfer constant and its dependence on the solute concentration.

5.4.2 Description of the experimental work

The experimental part of this work has been performed under the same conditions described in chapter 2 section 1. The same mixture of AD, where this component has a mass fraction of about 96%, has been used in all experiments. The flow-rate was fixed to 0.5 ml/min. In the perturbation experiments, a volume of 20 µl of pure eluent was fed to the column, which had previously been equilibrated at different concentrations. This was done using the injection loop feed system of the HPLC station, where the maximum possible injection volume is 250 µl. In the frontal analysis experiments a larger amount of solute has to be fed to saturate the column. Therefore for these experiments, the pump switching feed system, shown in Fig.5.8, has been used, which allows feeding an arbitrary large amount of solute to the column. As described in section 1 of this chapter, when using this feeding system instead of the injection loop, the hold-up volume of the HPLC station is larger, i.e. 800 µl, which has a significant effect on the retention time and on the band broadening, as illustrated in Fig.5.16.
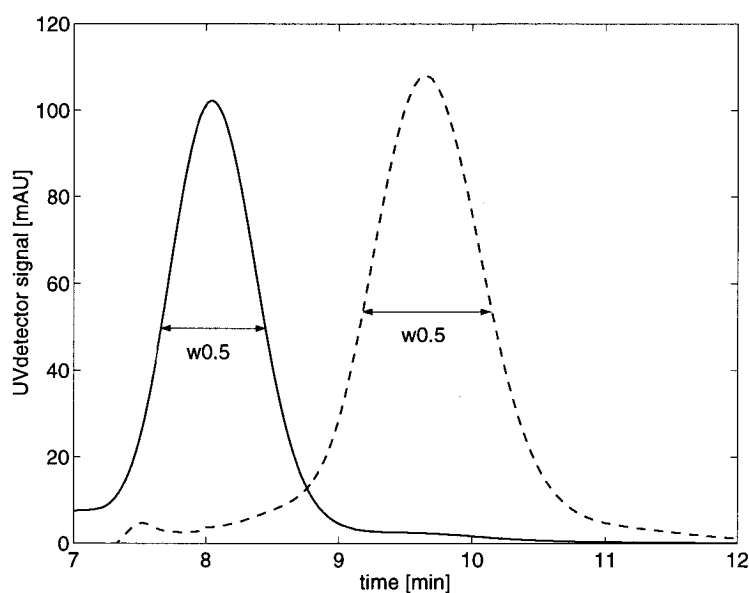

Fig. 5.16: Comparison of an analytical peak measured using the injection loop feed system, (—), and the pump switching feed system, (--), at a flow-rate of 0.5 ml/min.

It is seen that the peak width of the analytical peak obtained with the pump switching feed system is significantly larger than that of the peak obtained using the injection loop system. The additional band broadening is mainly due to pump C in the HPLC station illustrated in Fig.5.8. Since mass transfer and axial dispersion coefficients are ultimately estimated from the broadening of the elution profiles obtained in various types of experiments, it is clear that in order to achieve a reliable measurement of the mass transfer kinetics, this effect has to be carefully taken into account.

The procedure to determine the dissipative phenomena for both injection systems is as follows. First, a van-Deemter plot is measured under diluted conditions using the injection loop feed system and the mass transfer coefficient as well as the axial dispersion coefficient are evaluated, as described in section 1.5. In this way, a value of 3.38 1/s for the mass transfer coefficient and a value of $1.26*10^{-2}$ cm*u for the axial dispersion coefficient have been obtained. Next the analytical peak, shown in Fig.5.16, has been measured using the pump switching feed system. This is first corrected by subtracting the hold-up time of the HPLC station as shown in section 5.2. From the obtained peak widths a new van Deemter plot can be constructed as shown in Fig.5.17.
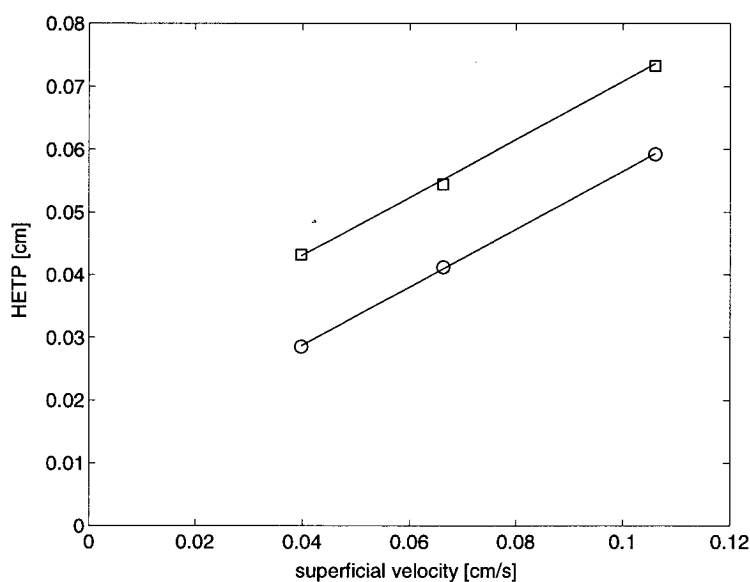

Fig. 5.17: Van Deemter plot of AD obtained with the loop switching system (O), and with the pump switching feed system (□) after correction by subtracting the hold-up time of the HPLC station, (—) linear regression.

When comparing it with the one obtained with the loop switching system, it is seen that while the same value for the mass transfer coefficient is obtained, the axial dispersion coefficient is increased. This leads to the value of $3*10^{-2}$ cm*u, which is obviously an effective value accounting also for the extra-column dead volumes associated with the pump switching feed system. In the following, we simulate the outlet elution profiles using these two different values of the axial dispersion coefficient depending on whether the injection loop or the pump switching feed system has been used.

5.4.3 Results of frontal analysis and perturbation method

The frontal analysis experiments had been performed using feed concentrations of 25, 50 and 80 g/l and a value of the mass transfer coefficient has been estimated by fitting to the mean part of the experimental breakthrough curves, as shown in the Figs.5.18, 5.19 and 5.20. Here the model prediction obtained using the mass transfer coefficient value estimated under diluted conditions as described in the previous section is also shown for a comparison.
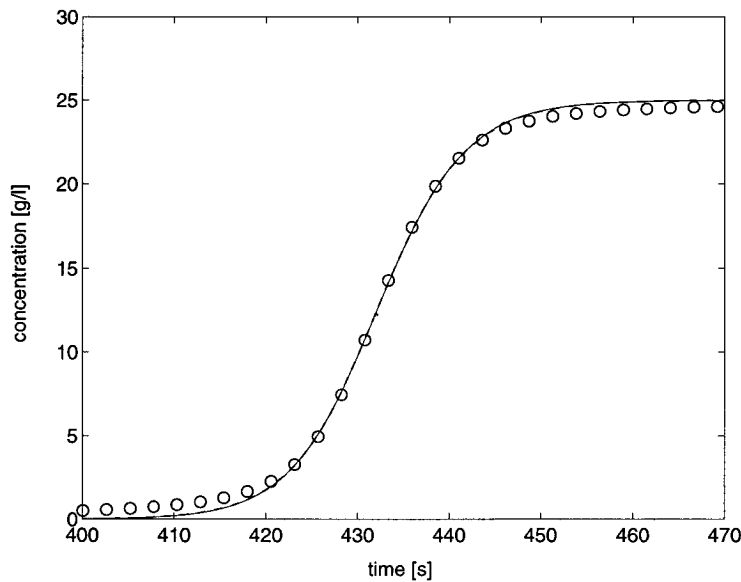

Fig. 5.18: Experimental and simulated breakthrough curves for a plateau concentration of 25 g/l. Experimental data (O); model simulations: (—) k_m=3.38 1/s, (--) k_m= f(c), given by Eq.5.14.
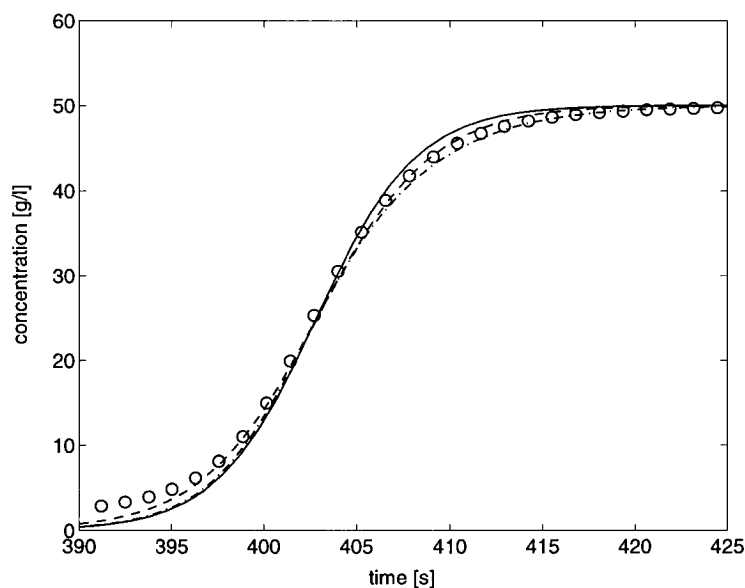
Fig. 5.19: Experimental and simulated breakthrough curves for a plateau concentration of 50 g/l. Experimental data (O); model simulations: (—) k_m=3.38 1/s, (--) k_m=2.7 1/s, (·—·) k_m=f(c), given by Eq.5.14.
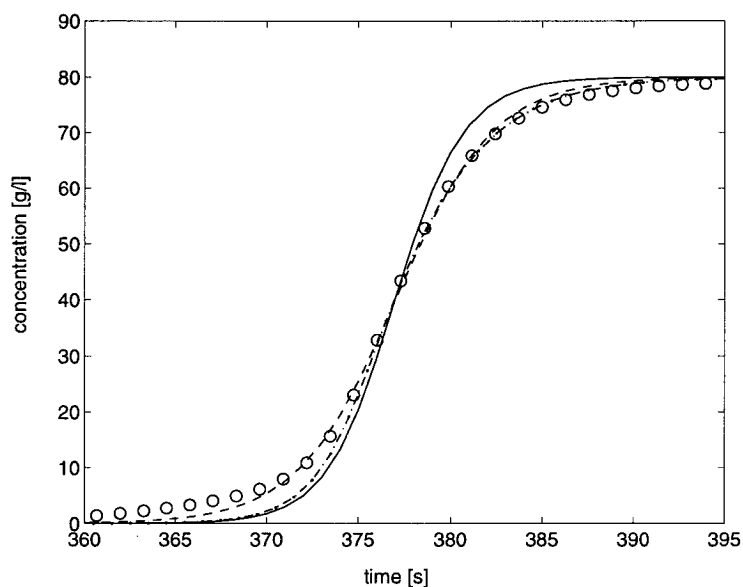

Fig. 5.20: Experimental and simulated breakthrough curve for a plateau concentration of 80 g/l. Experimental data (O); model simulations: (—) k_m=3.38 1/s, (--) k_m=1.9 1/s, (·—·) k_m=f(c), given by Eq.5.14.

The data in Figs.5.18-5.20 show clearly that the value of the mass transfer coefficient has to be decreased as larger solute concentrations are involved in the experiments in order to achieve a good representation of the experimental curves. In order to investigate this point more precisely, three perturbation experiments have been performed at feed concentrations of 25, 50 and 80 g/l. Since the column equilibrated at these concentrations is only very slightly disturbed, with

these experiments it is possible to measure the mass transfer kinetic exactly at three different solute concentration values. The experimental data and the simulation results, obtained using both the best-fitted mass transfer coefficient and the one estimated at diluted conditions, are shown in Figs.5.21-5.23.

Fig. 5.21: Experimental perturbation curve and simulated results for a saturation concentration of 25 g/l. Experimental data (O); model simulations: (——) k_m=3.38 1/s, (--) k_m=2.7 1/s.

Fig. 5.22: Experimental perturbation curve and simulated results for a saturation concentration of 50 g/l. Experimental data (O); model simulations: (——) k_m=3.38 1/s, (--) k_m=1.7 1/s.
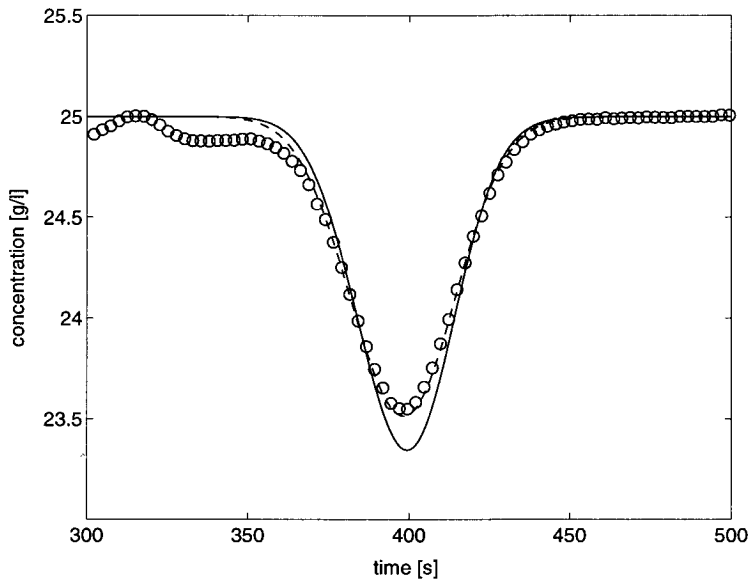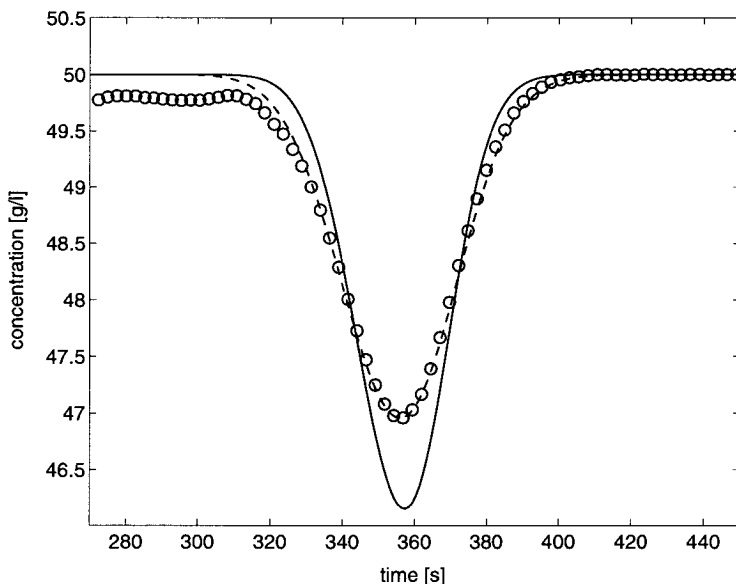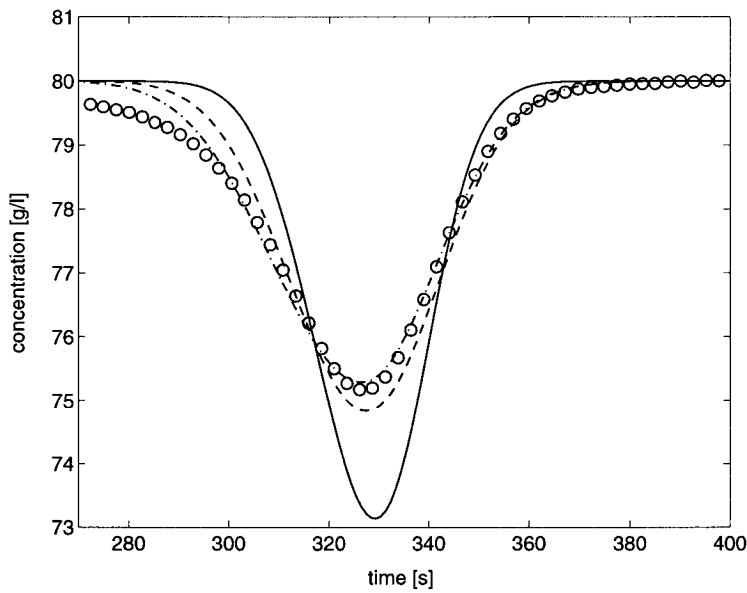
Fig. 5.23: Experimental perturbation curve and simulated results for a saturation concentration of 80 g/l. Experimental data (O); model simulations: (——) k_m=3.38 1/s, (--) k_m=1.4 1/s, (—·) $k_{m,ads}$=1.4 1/s, $k_{m,des}$=1 1/s.

The so estimated values of the mass transfer coefficient are plotted as a function of the solute concentration in Fig.5.24. A continuous well behaved trend has been evidenced which has been fitted the following empirical function:

Fig. 5.24: Mass transfer coefficient as a function of the solute concentration, estimated through the perturbation method. (O) Experimental data, (——) data calculated with Eq.5.14.

$$k_m = k_{m,anal} - \frac{Ac + Bc^2 + Cc^3}{1 + Dc + Ec^2 + Fc^3}$$
(5.14)

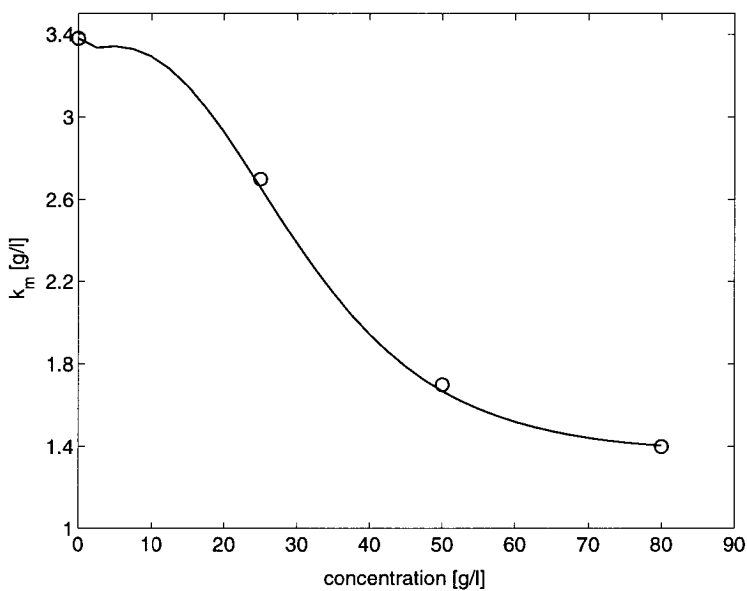where $k_{m,anal}$ is the mass transfer coefficient determined under diluted conditions using the van-Deemter plot in the previous section, and the following values have been obtained for the adjustable parameters: A=5.6, B=-1, C=0.12, D=81.6, E=-2.13, F=0.067.

To verify the validity of the obtained function the breakthrough curves consider above have been simulated using the mass transfer coefficient given by Eq.5.14. The obtained results shown in Figs.5.18-5.20, agree well with the experimental data. This indicates that the experimental data obtained with different methods and the model results are all consistent with the concentration dependence of the mass transfer coefficient shown in Fig.5.24. Eq.5.14 can be regarded as a good tool to reproduce the experimental elution profiles although its nature is fully empirical and not related, at the moment, to a physical interpretation of the diffusion process in reversed phase.

Let us now see if the decrease of the mass transfer coefficient with solute concentration in the fluid phase, given by Eq.5.14, can explain the deviations between the experimental overloaded peak profiles and those calculated using a constant mass transfer coefficient evaluated under diluted conditions. For this in Figs.5.25 and 5.26 two overloaded peak profiles of AD have been compared with the simulation results obtained using both a constant mass transfer coefficient as estimated under diluted conditions and one given by Eq.5.14. It is seen that a slight improvement is obtained using the concentration dependent mass transfer coefficient, but the deviations between model and experiments, particularly in the tailing region of the eluted peaks remain significant.

The next step taken in order to reconcile the shape of these eluted peaks with a model simulation is to assume different values for the mass transfer coefficient depending on whether the diffusion process is directed from the bulk fluid phase to the solid phase or vice versa. A physical justification of the peculiar behavior is not offered here, although it would have to be related to the complexity of reverse stationary phases and to their complex multiple interactions with large molecules such as AD. Considering that Eq.5.14 gives a good representation of the frontal analysis data, where only the adsorption process occurs, i.e. transport from fluid to solid phase, in the following we have focused on the reverse process, i.e. transport from solid to fluid phase. For this we performed desorption experiments of chromatographic columns saturated with different solute concentrations, where the shape of the elution profiles is entirely controlled by the desorption process. The experimental profiles obtained for initial saturation concentrations of 5, 30 and 50 g/l are compared in Figs.5.27-5.29 with the simulated profiles, obtained with constant but different values of the mass transfer coefficient, estimated so as to best fit the experimental data.

Fig. 5.25: Experimental and simulated overload peak profiles of AD; injected amount: 100 µl, injected concentration: 100 g/l, flow-rate: 0.5 ml/min. Experimental data (O); model simulations: (—) $k_{m,anal}$=3.38 1/s, (--) k_m=f(c), given by Eq.5.14.
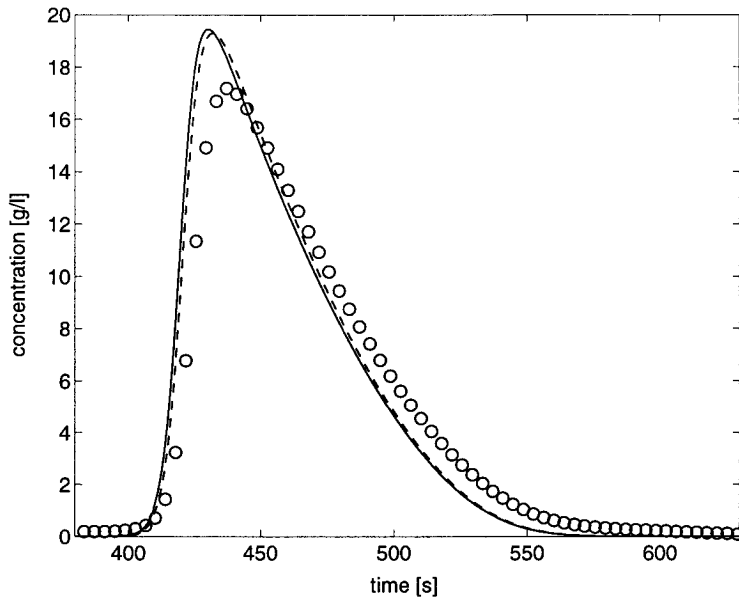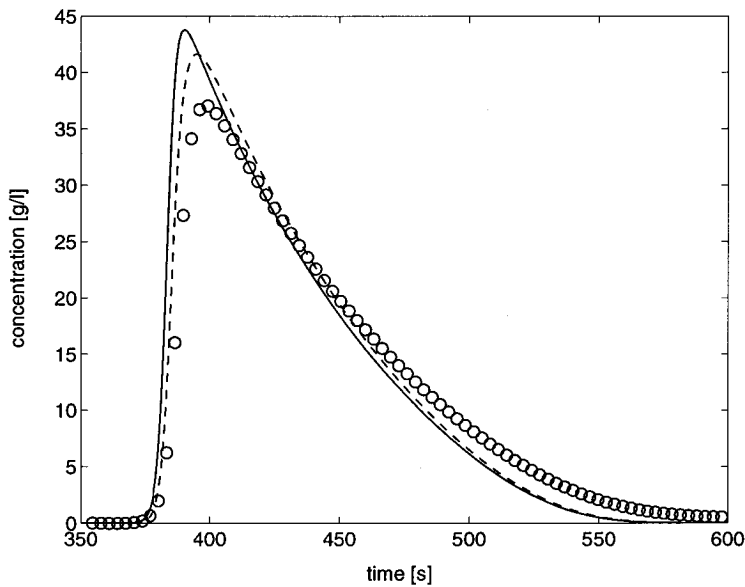

Fig. 5.26: Experimental and simulated overload peak profiles of AD; injected amount: 250 µl, injected concentration: 100 g/l, flow-rate: 0.5 ml/min. Experimental data (O); model simulations: (—) $k_{m,anal}$=3.38 1/s, (--) k_m=f(c), given by Eq.5.14.
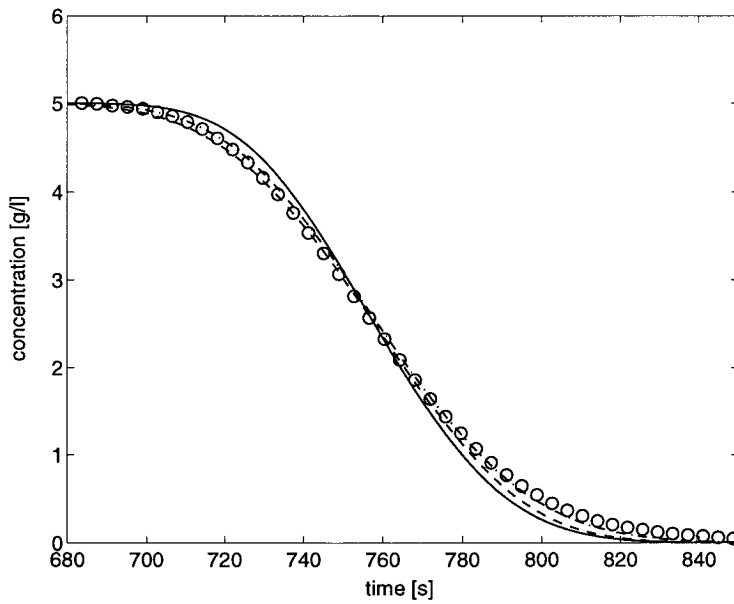
Fig. 5.27: Experimental and simulated desorption curves for an initial saturation concentration of 5 g/l. (O) Experimental data; model simulations: (—) $k_{m,des}$=3.38 1/s, (·—·) $k_{m,des}$=2.0 1/s,) (--) $k_{m,des}$=f(c), given by Eq.5.15.

Fig. 5.28: Experimental and simulated desorption curves for an initial saturation concentration of 30 g/l. (O) Experimental data; model simulations: (—) $k_{m,des}$=3.38 1/s, (·—·) $k_{m,des}$=0.8 1/s, (--) $k_{m,des}$=f(c), given by Eq.5.15.

Fig. 5.29: Experimental and simulated desorption curves for an initial concentration of 50 g/l. (O) Experimental data; model simulations: (—) $k_{m,des}$=3.38 1/s, (--) $k_{m,des}$=0.6 1/s, (·—·) $k_{m,des}$=f(c), given by Eq.5.15.
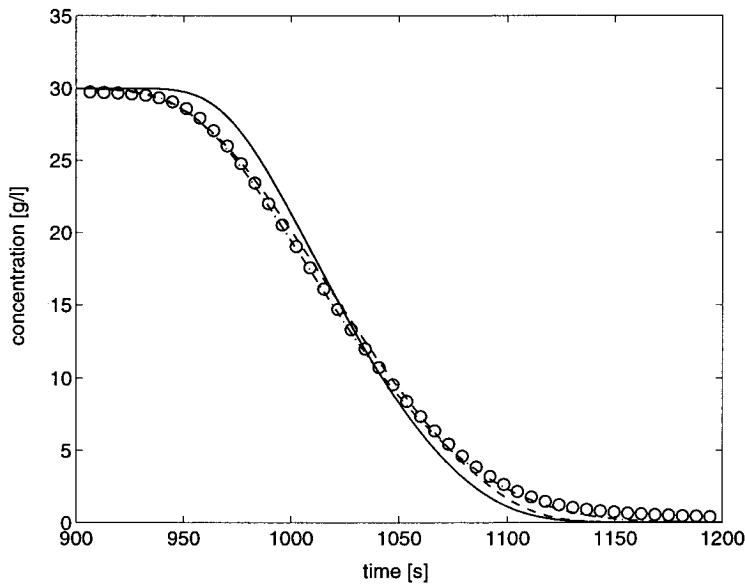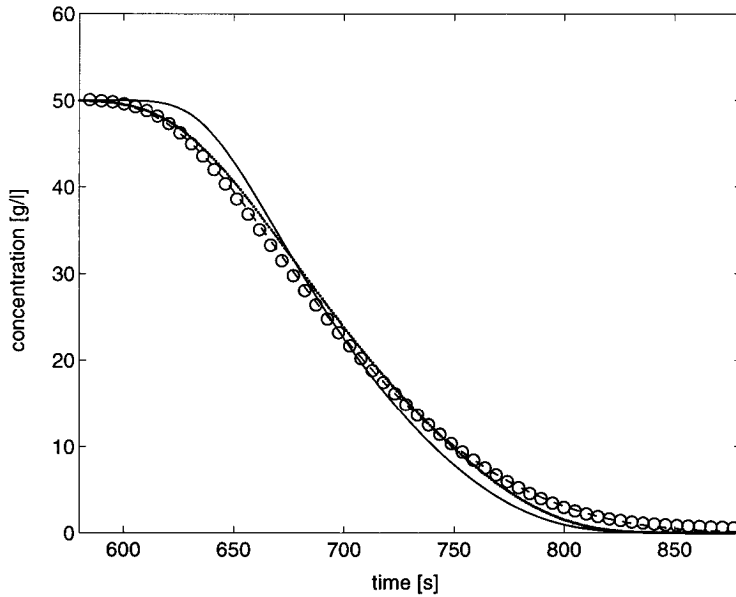
It is seen, somehow surprisingly, that the entire concentration range, from the plateau to the zero concentration, can be well described using a constant mass transfer coefficient, which is however different for each experiments. In particular, it is seen that again the mass transfer coefficient, also for the desorption process, tends to decrease as larger solute concentrations are involved. We therefore repeat here the same procedure adopted above for the adsorption process and obtain the following empirical expression for the desorption process, i.e.transport from solid to fluid:

$$k_{m,des} = A_{des} + \frac{B_{des}}{1 + C_{des}c}$$ (5.15)

where the following values for the adjustable parameters have been obtained: A_{des}=0.25, B_{des}=3.15, C_{des}=0.16.

Using the concentration dependence in Eq.5.15 for the mass transfer coefficient, the computed elution profiles shown in Figs.5.27-5.29 are obtained. Although the agreement with the experimental data is not as good as the one obtained with the fitted constant value of the mass transfer coefficient, still the obtained agreement is reasonable. In addition it appears that the so obtained values for the desorption mass transfer coefficient is clearly smaller than the one shown in Fig.5.24 and obtained by fitting the frontal analysis breakthrough curves obtained in the adsorption mode. This support the conclusion that a different value of the mass

transfer coefficient has to be postulated for the desorption and the adsorption process in order to well reproduce the measured elution profiles.

Accordingly, we modified the pore diffusion model so that the mass transfer coefficients for the desorption and the adsorption process have different values, both functions of concentrations as given by Eq.5.14 and 5.15, respectively. The experimental overloaded peak profiles can be simulated using this model as shown in Figs.5.30 and 5.31, leading to a satisfactory agreement with the experimental values. Nevertheless, a better agreement with the experimental curves can be achieved using the constant value of the mass transfer coefficient for the desorption process (instead of Eq.5.15), which has been adjusted to the tailing region of the peak, while using Eq.5.14 for the mass transfer coefficient for the adsorption process. However it is clear that this latter solution not only has no clear physical meaning but also it cannot be generalized to other operating conditions.

Fig. 5.30: Experimental and simulated peak profiles for AD; injected amount: 100 µl, injected concentration: 100 g/l, flow-rate: 0.5 ml/min. (O) Experimental data; model simulations: (—) $k_{m,ads}$=f(c), given by Eq.5.14 and $k_{m,des}$=1.4 1/s, (--) $k_{m,ads}$=f(c), given by Eq.5.14 and $k_{m,des}$=f(c), given by Eq.5.15.
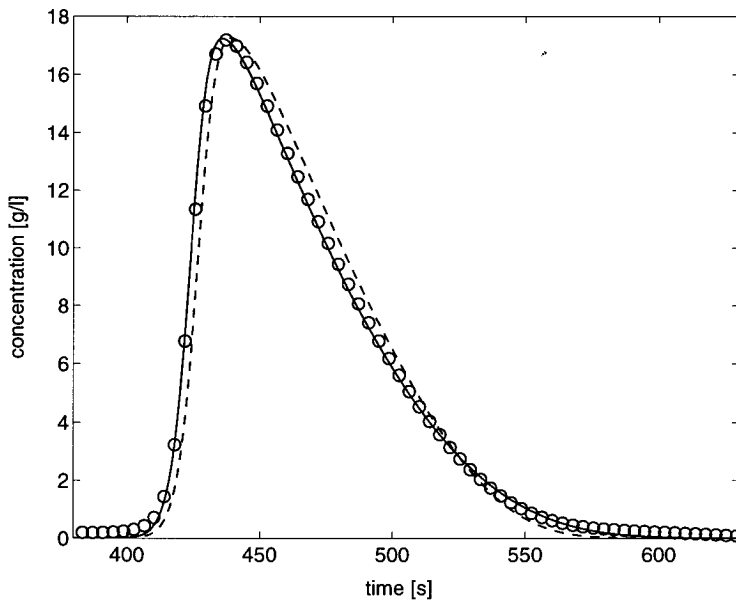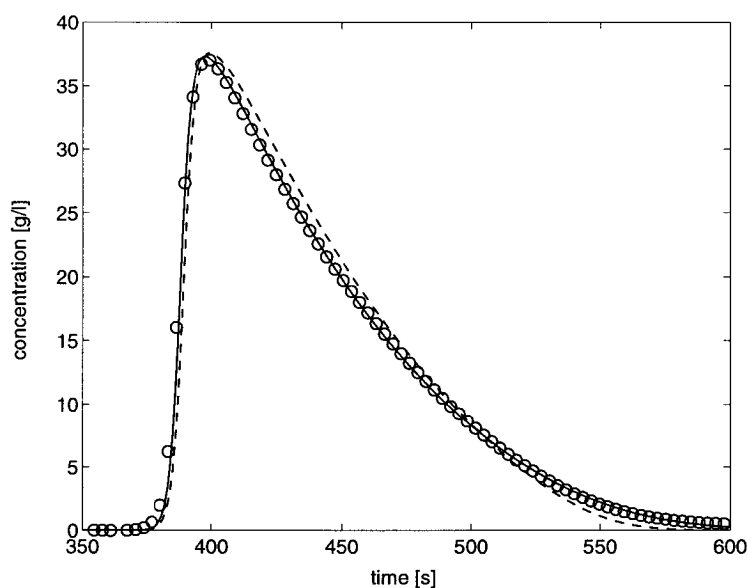
Fig. 5.31: Experimental and simulated peak profiles for AD; injected amount: 250 μl, injected concentration: 100 g/l, flow-rate: 0.5 ml/min. (O) Experimental data; model simulations: (—) $k_{m,ads}$=f(c), given by Eq.5.14 and $k_{m,des}$=0.8 1/s, (--) $k_{m,ads}$=f(c), given by Eq.5.14 and $k_{m,des}$=f(c), given by Eq.5.15.

As a possible physical explanation of the obtained results we can consider that the average pore size of the reversed phase packing material is of about 100 Å, while the dimension of the molecule size of AD is between 50 and 100 Å. Accordingly, the mass transfer of the solute molecules to the adsorption sites inside the pores is hindered by the presence of other solute molecules, due to the large dimensions of these compared to the narrow pore size [26,31]. For increasing solute concentration this effect decreases and the mass transfer coefficient reaches a constant value, due to the fact the solid phases reaches saturation and the solute adsorbed concentration does not decrease further.

In addition to this, a second more complex phenomenon can be observed on reversed phase when the desorption process takes place. The modified non-polar surface of the reversed phase, on which alkyl groups are attached, combined with the narrow pore size, can lead to a distribution of the binary eluent system deviating from its original composition in the feed. Now, the alcohol molecules of the eluent mixture can be enriched in the pore phase, since they are interacting with the surrounding adsorptions sites, while the water molecules are excluded from the pores due to their more polar character. Therefore the desorption process takes place in a rather different environment as the adsorption process, thus justifying a completely and lower value of the mass transfer coefficient. We leave this point open to further investigations needed to achieve a better understanding of the mass transport processes on reversed phase chromatography.

Conclusion

In this thesis a general procedure has been developed, which allows evaluating all the quantities involved in a reliable chromatographic model in a fast and optimal manner. The reliability of the procedure could be shown, taking into account some constraints, which arise in the pharmaceutical industry at an early development stage of a new pharmaceutical product. In particular, these constraints involve the availability of only small amounts of the mixture to be separated, and additionally no pure species are available. In addition to that, the procedure still has to satisfy convenient compromises between accuracy and time requirement. The main goal of the general procedure is the determination of the adsorption isotherms, because these are by far the most important in determining the performance of a chromatographic separation at high concentrations. For this, another condition has to be fulfilled, which is that the isotherms have to be studied on the same packing materials used in the preparative industrial process. Usually preparative packing material exhibits lower efficiency than the corresponding ones used for analytical purposes, characterized by much lower particle sizes. This restriction, along with the ones described above, requires a new way to determine the adsorption isotherms, because classical methods for such measurements are ruled out.

In this work, the peak fitting method has been used, whereby the parameters of a predefined equilibrium isotherm are estimated by fitting directly the composition values at the outlet of an analytical column packed with preparative packing material and fed with a pulse of the mixture to be separated. The procedure requires the preliminary accurate estimation of all the other parameters, which affect the behavior of the chromatographic column, such as porosities, axial dispersion and resistances to mass transfer.

In order to test the general procedure in a realistic industrial context, the production process of the ascomycin derivative AD as well as a racemic mixture of industrial interest has been considered. In particular, the purification process of AD from NP1 and NP2, and the separation process between AD and 9-EPI, has been investigated on reversed phase and on silica gel. In addition to this, a separation process of a racemic mixture on a chiral phase has been designed. As a demonstration for a complete design procedure of a separation process, here the chromatographic separation of the mixture to be separated has gone through all development stages. This includes the screening of stationary phases and solvents, the determination of the adsorption behavior of the racemic mixture with the help of the peak fitting method, and the design of a SMB process using the parameters determined before. The measurements fulfilled the constraints given above very well, because the parameters were determined in two days and only 20 mg of material were required.

The three processes involve largely different concentration ranges of the mixture to be separated and in addition, different stationary phases with specific characteristic properties. It is found that in all cases the developed procedure provides reliable estimates of the equilibrium isotherms, which have also been verified through independent measurements obtained using different techniques. An important aspect of the procedure is the possibility of collecting individual fractions of the stream leaving the column and to analyze them individually. This allows overcoming the problem of incomplete peak resolution, which derives from the use of preparative stationary phases, i.e. of chromatographic columns with low efficiency. This procedure allows reducing, with respect to the perturbation and frontal analysis method, the consumption of the amount of the mixtures to be separated of about one order of magnitude. The applicability of the general procedure could be verified explicitly, due to the application of that to a large spectrum of different separation cases as mentioned above.

In the case of reversed phase chromatography deviations between experimental and simulated concentrations in the eluted streams under overloaded conditions have been observed, which contrast with the excellent agreement between the calculated and experimental data obtained when using either silica gel or a chiral stationary phase. In particular, in the case of overloaded pulses on reversed phase the experimental curve shows a significant stronger tailing and a lower peak height than the simulated one. To analyze this phenomenum more in detail, first the role of impurities as well as the influence of "extra-column" effects on the elution profile have been investigated. As a conclusion of these investigations, for the experimental station and the operating conditions used in this work the shape of the peak profiles is not influenced through the effects mentioned above. Furthermore, it could be explicitly verified that the lumped pore diffusion model, which has been used to describe mass transfer in the chromatographic column, is sufficiently accurate for the situations examined in this work.

With the help of frontal analysis and the perturbation method the mass transfer kinetics have been investigated in detail on reversed phase, in order to see if the mass transfer changes with concentration and affects the shape of the elution profiles under overloaded conditions. It could be figured out that the mass transfer coefficient decreases significantly with solute concentration in the fluid phase. In addition to this, a different value of the mass transfer coefficient has to be postulated for the desorption and the adsorption process in order to well reproduce the measured elution profiles. Accordingly, the lumped pore diffusion model was modified so that the mass transfer coefficients for the desorption and the adsorption process have different values, both functions of concentrations. Using such a model the prediction of elution profiles on reversed phase under overloaded conditions could be improved significantly. Nevertheless, the best agreement with the experimental curves could be achieved using a constant value

of the mass transfer coefficient for the desorption process, which has been adjusted to the tailing region of the peak, and using a mass transfer coefficient as a function of the solute concentration for the adsorption process. This phenomenum has to be analyzed more in detail and at this point further investigations are needed to achieve a better understanding of the mass transport processes on reversed phase chromatography.

Notations

c_{feed}	Concentration in the feed stream (g/l)
c_i	Concentration of component i in the fluid phase (g/l)
c_i^p	Concentration of component i in the pores of the particles (g/l)
$c_{in,i}$	Inlet concentration of component i in a CST
$c_{out,i}$	Outlet concentration of component i in a CST
D	Column Diameter (cm)
D_{ax}	Axial dispersion coefficient (cm^2 s^{-1})
D_m	Molecular diffusion coefficient (cm^2 s^{-1})
D_P	Pore diffuison coefficient (cm^2 s^{-1})
D_s	Surface diffusion coefficient (cm^2 s^{-1})
D^0_s	Surface diffusion coefficient at c=0 (cm^2 s^{-1})
d_p	Diameter of the particle (cm)
H_i	Henry coefficient of component i (-)
H_i^*	Effective Henry coefficient of component i defined by Eq.2.2 (-)
$H_{bi1,i}$	Henry coefficient of component i of the first bi-Langmuir term
$H_{bi2,i}$	Henry coefficient of component i of the second bi-Langmuir term
k'_0	Retention factor (-)
K_a	Kinetic coefficient (s^{-1})
$k_{ads,i}$	Adsorption rate constant of component i
$k_{des,i}$	Desorption rate constant of component i
k_f	Film diffusion coefficient (cm s^{-1})
K_i	Equilibrium constant of component i
$k_{m,i}$	Lumped mass transfer coefficient of component i (s^{-1})
$k_{m,anal}$	Lumped mass transfer coefficient evaluated under diluted conditions (s^{-1})
K_p	Pressure drop constant (kg s^{-2})
L	Column length (cm)
m_i	Mass stream ratio in zone i (-)
p	Pressure (bar)
Q	Flow-rate (ml/s)
Q_{feed}	Feed stream (ml/s)
Q_i	Flow-rate in zone i (ml/s)
q_i	Concentration of component i in the stationary phase in (g/l)
q_i^s	Saturation capacity of component i in the stationary phase (g/l)
$q_i^{bi1,s}$	Saturation capacity of component i of the first bi-Langmuir term in the stationary phase (g/l)
$q_i^{bi2,s}$	Saturation capacity of component i of the second bi-Langmuir term in the stationary phase (g/l)
$\overline{q_i}$	Concentration of component i in the particle in (g/l)
r	Radial coordinate in the pore (cm)
R_p	Radius of the particle (cm)

t	Time (s)
t^*	Switch time (min)
$t_{r,i}$	Retention time of component i (s)
t_o	Retention time of an inert component (s)
u	Superficial velocity (cm s^{-1})
V	Volume of the empty column (cm^3)
V_{CST}	Volume of a continuous stirred tank (cm^3)
$w_{0.5}$	Width of the peak at 50% of its height (cm)
x	Axial coordinate in the column (cm)

Greek symbols

α	Selectivity (-)
β	Packing specific constant in Eq.1.6 (-)
ε	Total Porosity (-)
ε_b	Interparticle porosity (-)
ε_p	Intraparticle porosity (-)
γ	Packing specific constant in Eq.1.6 (-)
η_m	Viscosity of an eluent mixture (Pa s)

Bibliography

[1] S. Böcker; M. Mazzotti; M. Morbidelli. Development of chromatographic processes of the pharmaceutical industry. Proceedings of the seventh international conference of fundamentals of adsorption. submitted

[2] G. Guiochon; S.G. Shirazi; A.M. Katti. Fundamentals of preparative and non-linear chromatography. Boston, MA: Academic Press **1994**

[3] A. Seidel-Morgenstern; R.-M. Nicoud. Proceedings of the european meeting on the Simulated Moving Bed Process. Nancy, 6.-8.12.93, **1993**

[4] F. James; M. Sepulveda; F. Charton; I. Quinones; G. Guiochon. Determination of binary equilibrium isotherms from the individual chromatographic band profiles. Chem. Eng. Sci. **1999**, *54*, 1677-1696

[5] E.V. Dose; S. Jacobsen; G. Guiochon. Determination of isotherms from chromatographic peak shapes. Anal. Chem. **1991**, *63*, 833-839

[6] D.M Ruthven. Principles of Adsorption and Adsorption processes. Wiley, New York, **1984**

[7] L.R. Petzold. Sandia Report **1982**, SAND82-8637

[8] J.J. van Deemter; F.J. Zuiderweg; A. Klinkenberg. Longitudinal diffusion and resistance to mass transfer as causes of nonideality in chromatography. Chem. Eng. Sci. **1956**, *5*, 271-289

[9] E. Katz; K.L. Ogan; R.P.W. Scott. Peak dispersion and mobile phase velocity in liquid chromatography: the pertinent relationship for porous silica. J. Chromatogr. **1983**, *270*, 51-75

[10] E. Klesper; U. Köhler. Influence of linear velocity, column length and pressure drop in SFC: II. Plate numbers, effective plate numbers and resolutions. J. Chromatogr. Sci. **1994**, *32*, 525-533

[11] S. Böcker; M. Mazzotti; M. Morbidelli. Design of Chromatographic separations on reversed phase. Sep. Sci. Tech. submitted

[12] E. Küsters; C. Heuer; D. Wieckhausen. Purification of an ascomycin derivative with simulated moving bed chromatography. A case study. J. Chromatogr. A **2000**, *874*, 155-165

[13] C. Horvath; W. Melander. Liquid chromatography with hydrocarbon-aceous bonded phases; theory and practice of reversed phase chromatography. J. Chromatogr. Sci. **1977**, *15*, 393-404

[14] A. Vailaya; C. Horvath. Retention in reversed-phase chromatography: partition or adsorption? J. Chromatogr. A **1998**, *829*, 1-27

[15] R.C. Wilhoit; B.J. Zwolinski. Physical and thermodynamic properties of aliphatic alcohols. New York, N.Y.: American Institute of Physics, **1973**

[16] I. Quinones; A. Cavazzini; G. Guiochon. Adsorption equilibria and overloaded band profiles of basic drugs in a reversed-phase system. J. Chromatogr. **2000**, *877*, 1-11

[17] D. Tondeur; H. Kabir; L.A. Luo; J. Granger. Multicomponent adsorption equilibria from impulse response chromatography. Chem.Eng. Sci. **1996**, *51*, 3781-3797

[18] E. Francotte. Enantioselective chromatography as a powerful alternative for the preparation of drug enantiomers. J. Chromatogr. A **2001**, *906*, 379-397

[19] M. Schulte; J. Strube. Preparative enantioseparation by simulated moving bed chromatography. J. Chromatogr. A **2001**, *906*, 399-416

[20] G. Storti; M. Mazzotti; M. Morbidelli; S. Carra. Robust design of a binary countercurrent separation process. AIChE J. **93**, *39*, 471-492

[21] G. Biressi; O. Ludemann-Hombourger; M. Mazzotti; R.M. Nicoud; M. Morbidelli. Design and optimization of a Simulated Moving Bed unit: role of deviations from equilibrium theory. J. Chromatogr. A **2000**, *876*, 3-15

[22] M. Morbidelli; A. Servida; G. Storti; S. Carra. Simulation of multicomponent adsorption beds. Model analysis and numerical solution. Ind. Eng. Chem. Fundam. **1982**, *21*, 123-131

[23] K. Miyabe; G. Guiochon. Analysis of surface diffusion phenomena in reversed-phase liquid chromatography. Anal. Chem. **1999**, *71*, 889-896

[24] D.D. Do. Adsorption Analysis: Equilibria and Kinetics. Imperial College Press, London, **1998**

[25] M. Suzuki. Adsorption Engineering. Kodansha/Elsevier, Tokyo, **1990**

[26] D. Grzegorczyk; G. Carta. Frequency response of liquid-phase adsorption on polymeric adsorbents. Chem. Eng. Sci. **1997**, *52*, 1589-1608

[27] D. E. Cherrak; S. Khattabi; G. Guiochon. Adsorption behavior and prediction of the enantiomers of 3-chloro-1-phenyl-1-propanol. Influence of the mass transfer kinetics. J. Chromatogr. A **2000**, *877*, 109-122

[28] S. Khattabi; D. E. Cherrak. G. Guiochon. Study of the adsorption behavior of the enantiomers of 1-phenyl-1-propanol on a cellulose-based chiral stationary phase. J. Chromatogr. A **2000**, *877*, 95-107

[29] K. Miyabe; G. Guiochon. Kinetic study of the concentration dependence of the mass transfer rate coefficient in anion-exchange chromatography of bovine serum albumin. Biotechnol. Prog. **1999**, *15*, 740-752

[30] K. Miyabe; G. Guiochon. Determination of the lumped mass transfer rate coefficient by frontal analysis. J. Chromatogr. A **2000**, *890*, 211-223

[31] Md.M. Hossain; D.D. Do. Immobilization of enzymes in porous solids under restricted diffusion conditions. AIChE J. **1986**, *32*, 1088-1098

Curriculum vitae

Sebastian Böcker

1971	Born on 17th of June, Rheda-Wiedenbrück, Germany

1971   Born on 17th of June, Rheda-Wiedenbrück, Germany

1981 – 1990   Einstein Gymnasium, Rheda-Wiedenbrück, Germany

1991 – 1997   University of Dortmund
Diplom in Chemical Engineering

1998 – 2001   Doctoral studies at the Chemical Engineering Department,
Swiss Federal Institute of Technology (ETH), Zürich